

**Solution Structure of the 30 kDa Homodimeric Sud  
Protein from *Wolinella Succinogenes***

**Dissertation**

Zur Erlangung des Doktorgrades  
der Naturwissenschaften

**vorgelegt beim  
Fachbereich Chemische und Pharmazeutische Wissenschaften  
der Johann Wolfgang Goethe-Universität  
in Frankfurt am Main**

von

**Yi-Jan Lin**

aus Kaohsiung, Taiwan

Frankfurt am Main, 2003  
(DF1)

vom Fachbereich Chemische und Pharmazeutische Wissenschaften der  
Johann Wolfgang Goethe-Universität als Dissertation angenommen.

Dekan: Prof. Dr. J. Engels

1. Gutachter: Prof. Dr. H. Rüterjans
2. Gutachter: P.D. Dr. U. Günther

Tag der Disputation

## Acknowledgments

The work was carried out in the Institute of Biophysical Chemistry of the Johann Wolfgang Goethe-University Frankfurt am Main under the instruction of Prof. Dr. Heinz Rüterjans from October 1998 to February 2003.

First of all I would like to thank my academic advisor, Prof. Dr. Heinz Rüterjans, for his generous support and providing excellent work conditions during the past four and a half years.

In addition, I would like to thank:

Dr. Frank Löhr for his excellent measurements of all kind of NMR-spectra and discussions about NMR theory,

Dr. Oliver Klimmek (group of Prof. Kröger, Institute of Microbiology) for the sample preparation and helpful discussions about protein function,

Dr. Stefania Pfeiffer for discussions about basic NMR knowledge and AURELIA program

Dr. Christian Lücke for his concrete and useful discussions about resonance assignments,

Mr. Felician Dencea for his cooperation in the structure calculations,

Dr. Hans Wienk for his discussions and measurements of residual dipolar couplings,

Dr. Michael Nilges (Pasteur Institute, Paris) for providing the ARIA program and discussions on how to use it,

Dr. Takahisa Ikegami (Osaka University, Japan) for discussions about structure refinements and residual dipolar couplings,

Dr. Peter Güntert (Riken, Japan) for helpful discussions about structure calculations using his CYANA program,

Dr. Michael Sattler (EMBL, Heidelberg in Germany) and Dr. Michael Nilges for providing me the opportunity to participate in EMBO practical course: 'Structure determination of biological macromolecules by solution NMR' at the European Molecular Biology Laboratory (EMBL) in Heidelberg,

P.D. Dr. Ulrich Günther, Dr. Frank Löhr, Dr. Christian Lücke and Dr. Oliver Klimmek for many discussions and corrections of the manuscript,

Dr. Luis Horacio Gutierrez Gonzalez for his technical help of computers,

all members of our group for providing a nice working atmosphere,

the DFG (Deutsche Forschungsgemeinschaft) for a scholarship and the SFB (Sonderforschungsbereich) for financial support.



## Abbreviations

ADRs	ambiguous distance restraints
ARIA	Ambiguous Restraints for Iterative Assignment
COSY	Correlation Spectroscopy
CSA	Chemical Shift Anisotropy
CSI	chemical shift indices
DD	Dipole-Dipole Interaction
HSQC	Heteronuclear Single-Quantum Coherence
INEPT	Insensitive Nuclei Enhancement by Polarization Transfer
ISPA	isolated spin pair approximation
NCS	non-crystallographic symmetry
NMR	Nuclear Magnetic Resonance
NOE	Nuclear Overhauser Effect
NOESY	Nuclear Overhauser Effect and Exchange Spectroscopy
ppm	Parts per million
rdc	residual dipolar coupling
Rhod	rhodanese
RMSD	Root-Mean-Square Deviation
Sud	sulfide dehydrogenase (formerly named)
TOCSY	Total Correlation Spectroscopy
TROSY	transverse-relaxation-optimized spectroscopy

<b>1. Introduction</b>	<b>1</b>
<b>2. Theoretical Aspects</b>	<b>5</b>
2.1 Multidimensional NMR experiments	5
2.1.1. Principles of Multidimensional NMR	5
2.1.2. Resonance assignments	9
2.2 Nuclear Overhauser Enhancement (NOE)	12
2.2.1. Introduction	12
2.2.2. Relaxation Pathways	13
2.3 Residual dipolar couplings	21
2.3.1 Introduction	21
2.3.2 Alignment tensor	23
2.4 The ARIA-Program	26
2.4.1 Introduction	26
2.4.2 Ambiguous distance restraints	26
2.4.3 Target distances and limits of error	27
2.4.4 Distance target function	28
2.4.5 Removal of noise	29
2.4.6 Stereospecific assignment	30
2.4.7 NOE assignment and 3D structure determination	30
2.4.8 Calculation of symmetric multimer structures	32
2.4.8.1 Symmetry ADRs	32
2.4.8.2 Co-monomer restraints	33
<b>3. Materials and Methods</b>	<b>35</b>
3.1 Sample preparation	35
3.2 NMR spectroscopy	37
3.3 Experimental NMR restraints	41
3.4 Structure calculation	41

<b>4. Results and Discussion</b>	<b>43</b>
4.1 NMR Assignments	43
4.1.1 Backbone resonance assignments	43
4.1.2 Side chain resonance assignments	50
4.1.3 Inter-monomer NOE assignments	54
4.2 Residual dipolar couplings	56
4.3 Automatic NOE assignments and structure determination	58
4.4 Dipolar coupling data for refinement and relative orientations	59
4.5 Description of the structure	63
4.6 Structure-function relationship	66
<b>5. Summary</b>	<b>73</b>
<b>6. References</b>	<b>81</b>
<b>7. Appendices</b>	<b>85</b>

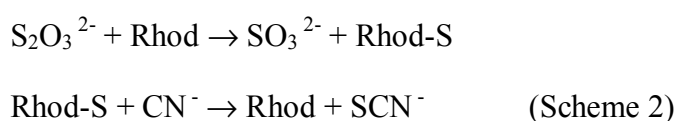
# 1 Introduction

The periplasmic Sud (formerly named: sulfide dehydrogenase) protein of *Wolinella succinogenes* which grows in the presence of polysulfide ( $S_n^{-2}$ ) as terminal electron acceptor (Klimmek et al., 1991) has previously been proposed to transfer polysulfide-sulfur to the active site of the membrane bound polysulfide reductase, which is exposed to the periplasm (Klimmek et al., 1998). The ability to perform oxidative phosphorylation with the elementary sulfur instead of oxygen is widespread among anaerobic bacteria and archaea. Most of these organisms are hyperthermophilic and belong to the Archaea family. Elementary sulfur is not well suited as a substrate for prokaryotes because of its low solubility in water. As elementary sulfur is readily converted to polysulfide in aqueous solutions of sulfide ions, polysulfide is thought to be a possible intermediate of sulfur reduction.

The Sud protein consists of two identical subunits (15.3 kDa including a C-terminal His tag of six histidine residues after cloning in *E. coli*.) and does not contain prosthetic groups or heavy metal ions. Each monomer contains a single cysteine residue, which covalently binds up to 10 polysulfide-sulfur atoms when incubated in a polysulfide solution (Klimmek *et al.*, 1999). The Cys residues are involved in the catalytic function of Sud. The replacement of Cys by Ser results in the loss of activity of sulfur transfer. The single Cys residue is obviously required for the function as a polysulfide-sulfur transferase. The sulfur transfer from Sud to the polysulfide reductase probably occurs in a complex of the two proteins (Klimmek *et al.*, 1998). So far there exists no homologous structure of Sud protein in other organisms.

Sud, similar to rhodanese of *A. vinelandii* (Bordo *et al.*, 2000), also catalyses the transfer of polysulfide-sulfur from polysulfide to the artificial acceptor cyanide

(Scheme 1). Rhodanese catalyses the transfer of a sulfur atom from suitable sulfur donors to sulfur acceptors. Rhodanese binds covalently a sulfur atom to the cysteine residue in the active site. The enzyme cycles between a ligand-free form (Rhod) and a sulfur-covalent form (Rhod-S) (Scheme 2).



The monomeric rhodanese of *A. vinelandii* consists of two similar but not identically folded  $\alpha/\beta$ , N-terminal and C-terminal domains, each of approximately 125 amino acids (Figure 1.1). Both domains contain a central parallel  $\beta$ -sheet that is formed by five strands in the N-terminal domain and by four strands in the C-terminal domain. The active-site residue, Cys230, is located in the C-terminal domain but not in the N-terminal domain and is the first residue of the 230-234 loop. The active loop forms a semicircular, cradle-like, conformation (Figure 1.2). The peculiar active-site 230-235 loop structure (Gln231, Thr232, His233, His234, and Arg235) and the vicinal positively charged residues (Arg97 and Arg169) provide a strong positive electrostatic field pointing toward the anion binding site (Cys-S<sup>-</sup>). The increased nucleophilic character of the cysteine residue is expected to be at the basis of the active cysteine reactivity.

In order to explain the function and how the polysulfide-sulfur is transferred from Sud protein to polysulfide reductase, it is essential to determine the tertiary structure of the protein. Nuclear magnetic resonance (NMR) spectroscopy provides a

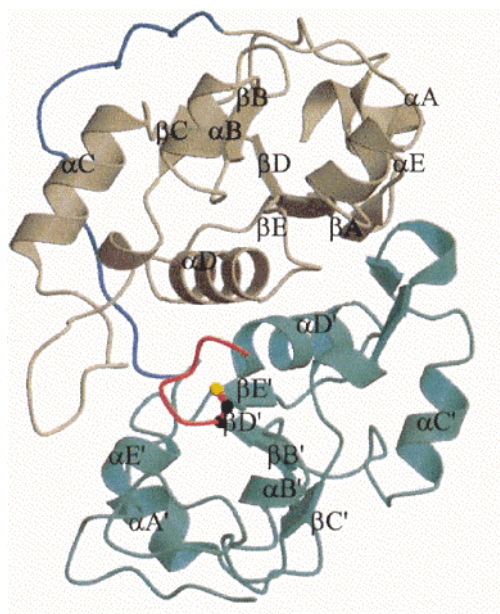


Figure 1.1. Crystal structure of *A. vinelandii* rhodanese. The N- and C-terminal domains are brown and green, respectively. The active-site loop is shown in red and the catalytic residue, Cys230, is represented in yellow.

feasible method to solve the structures of macromolecules in solution. The main structural data derived from NMR are scalar couplings and NOEs, which are translated into restraints on dihedral angles and interproton distances, respectively. The quality of the solution structure is proportional to the number of restraints used in the structure calculations. Once the assignment of the NMR spectrum has been completed, the determination of the solution structure of a protein using NMR is usually carried out in two stages. The first stage involves the collections of NOE-derived restraints. The second phase of the structure determination process involves the use of computational methods such as distance geometry and molecular dynamics calculations. At this stage, additional NMR information, including the stereospecific assignments of diastereotopic protons and hydrogen bond restraints, is used.

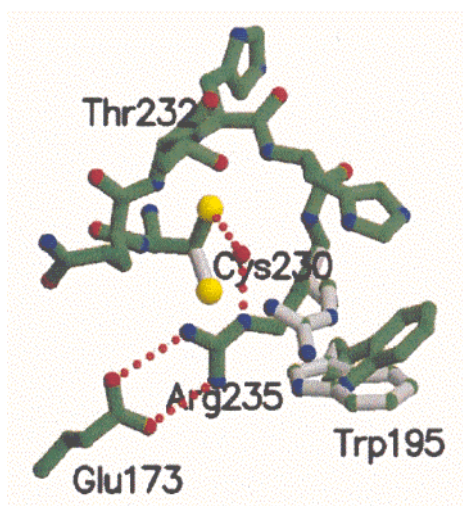


Figure 1.2. Environment of the active site of the sulfur-free rhodanese. Hydrogen bonds are shown in red dotted lines.

The main limitations to the NMR method arise from unfavourable transverse relaxation time ( $T_2$ ), from resonance overlap in large proteins, and from internal mobility and multiple conformations. Particularly for large proteins, it is difficult to obtain complete quantitative data. Structures obtained from incomplete assignments and restraints usually lack precision and may not be as precise as one where a large number of restraints is available.

The solution structure of the Sud protein has been determined using the NMR methodology. The structure-function relationship and the possible pathway of polysulfide-sulfur transfer can be derived from the determined structure.

## 2 Theoretical Aspects

### 2.1 Multidimensional NMR experiments

#### 2.1.1 Principles of Multidimensional NMR

In multidimensional heteronuclear NMR experiments a heteronuclear resonance is correlated with a proton resonance by transferring the coherence between the heteronuclear (*s*) and proton (*i*) spins. The overall sensitivity of heteronuclear correlation NMR experiments is proportional to

$$S/N \propto \gamma_{\text{ex}}\gamma_{\text{det}}^{3/2}[1 - \exp(-R_{1,\text{ex}} T_c)],$$

in which  $\gamma_{\text{ex}}$  and  $\gamma_{\text{det}}$  are the gyromagnetic ratios of each nucleus excited at the beginning of the sequence and detected at the end of the sequence, respectively;  $T_c$  is the recycle time of the experiment; and  $R_{1,\text{ex}}$  is the spin-lattice relaxation rate constant of the excited nucleus. Initially proton spin polarization is transferred to the heteronucleus, performs the desired manipulations of heteronuclear spin, and then the heteronuclear coherence finally is transferred back to proton magnetization for detection.

In order to increase the resonance resolution of a spectrum, the concept of 2D NMR is easily extended to higher dimensionality. For example, the two pulse schemes can be concatenated to yield a 3D experiment (Figure 2.1a, b, c). The signals, acquired during the time  $t_3$ , are obtained for many different  $t_1$  and  $t_2$  durations. As was the case in the 2D NOESY experiment, the data are modulated in the  $t_1$  dimension by



the frequencies of other nearby protons, while in the  $t_2$  dimension the modulation frequency is that of the  $^{15}\text{N}$  or  $^{13}\text{C}$  nucleus that is directly attached to the observed proton. In the HSQC experiment (Figure 2.1b) the INEPT pulse sequence transfers the polarization of sensitive nuclei ( $i$ ) to the insensitive nuclei ( $s$ ). The magnetization of  $s$  spin evolves for a time  $t_1$  (which is changed incrementally), then the reverse INEPT step transfers the resulting polarization of  $s$  spin back to  $i$  spin for detection. The 2D HSQC experiment is integral component of all heteronuclear 3D and 4D NMR experiments. For the  $is$  ( $i = ^1\text{H}$ , and  $s = ^{15}\text{N}$  or  $^{13}\text{C}$ ) NOESY-HSQC experiment (Figure 2.1c), the sequence until the end of time  $\tau_m$  is a homonuclear NOESY experiment with  $s$  spin decoupling during the  $t_1$  evolution period. An application of a  $180^\circ(s)$  pulse at the midpoint of  $t_1$  decouples the  $J_{is}$  coupling interaction. The  $90^\circ(i)$  pulse immediately preceding the end of time  $\tau_m$  is equivalent to the first  $90^\circ(i)$  pulse in the HSQC experiment, and the pulse sequence following the end of time  $\tau_m$  is the same as that in the HSQC experiment (Figure 2.1b). Figure 2.2 shows the advantage of 3D over 2D NMR. Figure 2.2a is a 2D spectrum and exhibits a high degree of resonance overlap, while Figure 2.2b represents a slice from the 3D spectrum and the resonance overlap is dramatically reduced compared to that in a 2D spectrum.

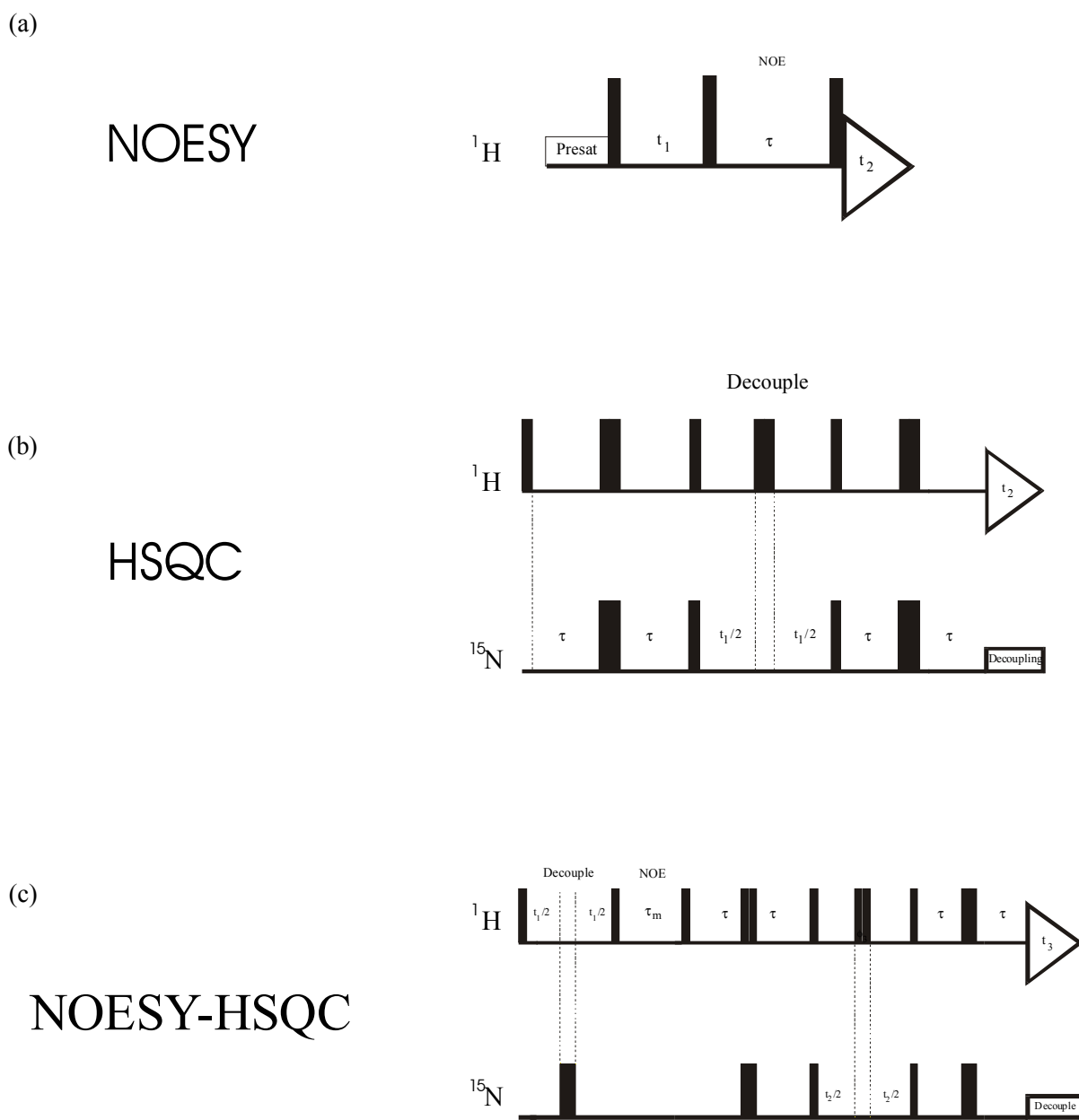


Figure 2.1. Examples of timing diagrams of 2D and 3D NMR pulse sequences. (a) 2D NOESY experiment. (b) 2D  $^{15}\text{N}$ - $^1\text{H}$  HSQC correlation experiment. (c) 3D  $^{15}\text{N}$ -separated NOESY-HSQC correlation experiment, obtained by combining a and b. Radiofrequency pulses are marked by vertical bars and have typical durations of tens of microseconds. The narrow and wide bars stand for  $90^\circ$  and  $180^\circ$  pulses, respectively. Signals are acquired during time  $t_2$  (a and b) and  $t_3$  (c). Each scheme is repeated many times by increasing  $t_1$  (and  $t_2$  for c) from 0 to  $\sim 30$  ms.

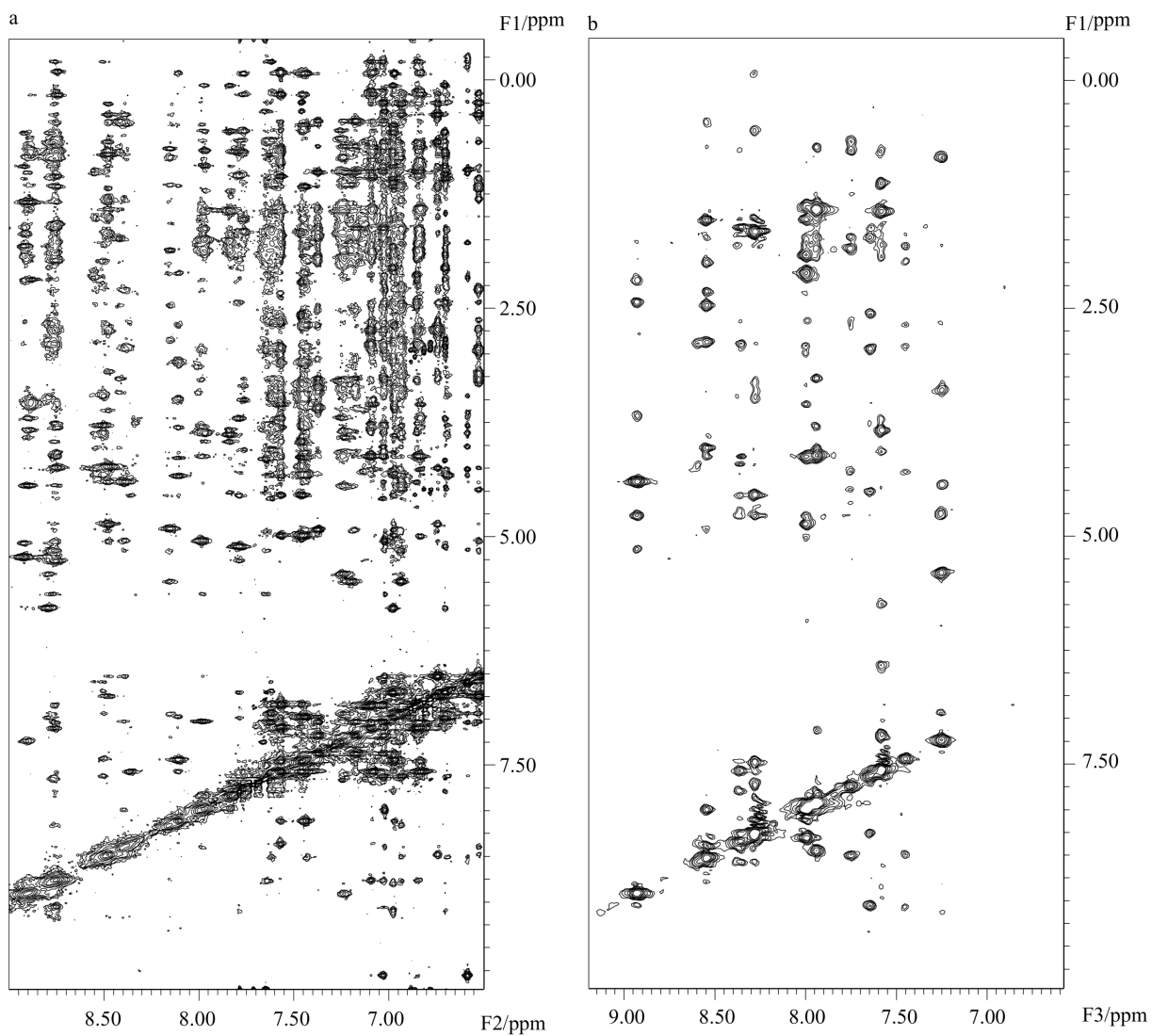


Figure 2.2. 2D spectrum (a) and one out of 128 slices through the 3D  $^{15}\text{N}$ -separated NOESY-HSQC experiment of Sud protein (b). In the 3D spectrum the resonance overlap is dramatically reduced compared to that in the 2D spectrum.

### 2.1.2 Resonance assignments

*Classical assignment strategy (Wüthrich et. al)* In homonuclear protein NMR spectroscopy, there are three essential 2D experiments: COSY, TOCSY and NOESY. But as the molecular mass of the macromolecule increases, these conventional experiments fail for large proteins because of overlap of signals. Therefore, it is necessary to employ triple-resonance experiments on  $^{15}\text{N}/^{13}\text{C}$ - or (and)  $^{15}\text{N}/^{13}\text{C}/^2\text{H}$ -labeled proteins to resolve and assign the signals of interest by extending the experiments to higher dimensions. The heteronuclear one-bond couplings,  $^1J_{\text{CH}}$  (125-160 Hz) and  $^1J_{\text{NH}}$  (~92 Hz), are much larger than  $^3J_{\text{HH}}$  (< 10 Hz) used in conventional 2D experiments, and frequently as much as 50-90% of the magnetization can be transferred from protons to their directly coupled heteronuclei. Three- and four-dimensional heteronuclear-edited NMR experiments resolve cross-peaks between  $^1\text{H}$  spins according to the chemical shift of the heteronuclei bound directly to the  $^1\text{H}$  spins. A 3D heteronuclear-edited experiment is composed of COSY, TOCSY, NOESY transfers, and INEPT transfers. The application of deuteration in combination with triple-resonance dramatically improved the spectral resolution and sensitivity owing to reduction of the number of relaxation pathways relative to similar experiments performed on fully protonated molecules.

*Triple-resonance experiments* Threedimensional heteronuclear triple-resonance experiments such as HNCACB, HN(CA)CO, HNCO, and HN(CA)N correlate backbone  $^1\text{HN}$ ,  $^{15}\text{N}$ ,  $^1\text{H}\alpha$ ,  $^{13}\text{C}\alpha$ , and  $^{13}\text{CO}$  (and side-chain  $^1\text{H}\beta$  and  $^{13}\text{C}\beta$ ) spins using one-bond and two-bond scalar coupling interactions. These experiments constitute a sequential resonance assignment strategy. At least two and often more independent pathways can be found to support a given sequential assignment, without any

knowledge of the spin-system type. The 3D triple-resonance experiments yield very well-resolved spectra compared to the classical sequential backbone resonance assignment strategy based on the observation of characteristic short-range NOEs in NOESY spectra. The experiments which correlate  $^{13}\text{C}$ - $^{13}\text{C}$  are used in the assignment of aliphatic  $^1\text{H}$  and  $^{13}\text{C}$  resonances of  $^{13}\text{C}$ -labeled proteins. These experiments utilize magnetization transfer via the  $^1J_{\text{CH}}$  ( $\sim 140$  Hz) and  $^1J_{\text{CC}}$  (30-40 Hz) couplings. For large proteins the magnetization transfer via  $^1J_{\text{CH}}$  and  $^1J_{\text{CC}}$  is significantly more efficient.

In order to obtain spectra of large molecules with reduced signal line width, TROSY (transverse-relaxation-optimized spectroscopy), has been introduced (Pervushin et al., 1997). In the TROSY approach the dipole-dipole (DD) and chemical shift anisotropy (CSA) interactions in a  $^{15}\text{N}$ - $^1\text{H}$  pair can be used to select the narrowest line of the quartet for a very large proteins via compensation of dipole-dipole and chemical shift anisotropy interactions. In a 2D correlation experiment (Wider et al., 1999) (Figure 2.3), a multiplet is observed without decoupling. To improve the resolution, the multiplet can be collapsed into a single line using broadband decoupling. In the TROSY approach the heteronuclear N-H splitting is not decoupled. In Figure 2.3b each individual multiplet component has different transverse relaxation times and hence, different line width. Especially for large proteins studied at higher magnetic field, the differential line width broadening of each component is more significant and deteriorates the averaged signal. TROSY actually takes advantage of CSA relaxation at higher field to cancel field-independent dipolar relaxation. Instead of decoupling, the TROSY experiment uses a phase cycling to cancel the three broader components and keep only the sharpest one.

The TROSY approach has been applied in different triple-resonance

experiments used to study the 30 kDa Sud protein.

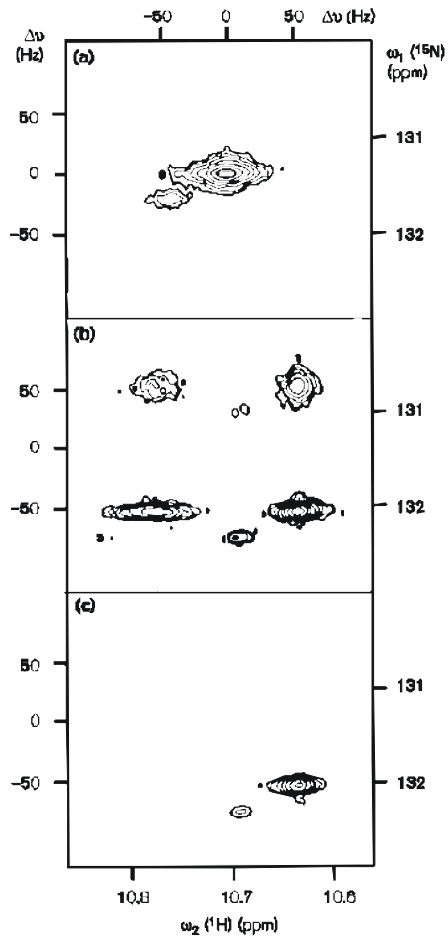


Figure 2.3. One  $^{15}\text{N}$ - $^1\text{H}$  cross peak from different types of  $^{15}\text{N}$ - $^1\text{H}$  correlation spectra. (a) Conventional broad-band decoupled  $^{15}\text{N}$ - $^1\text{H}$  HSQC spectrum. (b) same as (a), but without decoupling during  $t$  and  $t_2$  (Figure 2b). (c) A TROSY spectrum without decoupling using the sharp component in the lower right of (b) by phase cycling.

## 2.2 Nuclear Overhauser Enhancement

### 2.2.1 Introduction

The nOe represents a change in the intensity of a NMR resonance when the transitions of another one are saturated and a new equilibrium is established.

Dipolar interaction is usually the dominant relaxation mechanism for spin  $\frac{1}{2}$  nuclei with other spins. In a case of double resonance, irradiation of one set of spins by a  $B_2$  field can cause intensity changes of signals of other spins. This change in intensity results from the fact that the  $T_1$  relaxation of one of the pair of spins is partly caused by the spins being irradiated. For two-spin dipoles,  $i$  and  $s$ , between which the spatial distance is less than 5 Å, if the  $s$ -resonance is irradiated by a  $B_2$  field (so as not to perturb the  $i$  spin) for a lengthy period of time  $t \gg 1/\rho_i, 1/\rho_s$ , ( $\rho_i$  and  $\rho_s$  are autorelaxation rate constants or the spin-lattice relaxation rate constants,  $R_{1i}, R_{1s}$  in the Bloch terminology for  $i$  and  $s$  spin, respectively) and then the populations across the  $s$  spin transitions are equalized and the  $i$  spin magnetization evolves to a value,  $I_Z^{ss}$ . In this situation, the  $s$  spins are said to be saturated. The NOE  $\eta_i(s)$  at nucleus  $i$  when nucleus  $s$  is saturated is

$$\eta_i(s) = (I_Z^{ss} - I_Z^0) / I_Z^0$$

or

$$\eta_i(s) = \sigma_{is}^{\text{NOE}} \gamma_s / \rho_i \gamma_i \quad [2.1]$$

where the rate constant  $\sigma_{is}$  is the cross-relaxation rate constant and represents the net cross relaxation, and  $\rho_i$  represents the autorelaxation rate constant for spin  $i$  and describes the total relaxation for nucleus  $i$ .  $I_Z^{ss}$  is the resulting total longitudinal

magnetization of the enhanced  $i$ -signal and  $I_Z^0$  is the initial longitudinal magnetization observed at thermal equilibrium without perturbing the system. From this definition, the NOE will be positive if the new intensity is larger than the unperturbed intensity and negative if it is less.

### 2.2.2 Relaxation Pathways

The NOE changes the intensities of the signals. The intensity is proportional to the population difference of the two energy levels between which the nuclear resonance transition occurs. Figure 2.4 shows the energy level scheme and populations for a two-spin system  $i$  and  $s$ .

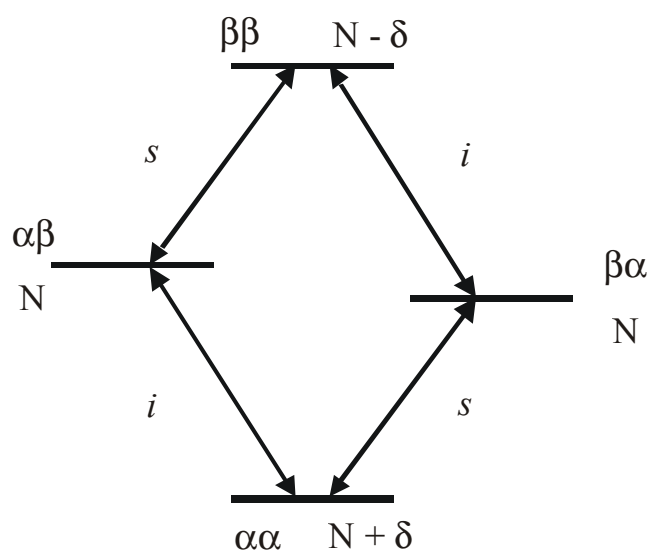


Figure 2.4. Energy level and population of a homonuclear AX system.



Here  $i$  and  $s$  may be protons – as in our examples - or they may be nuclei of different species. We assume that they are not  $J$ -coupled, i.e.  $J_{is} = 0$ . There are four energy levels,  $\alpha\alpha$ ,  $\alpha\beta$ ,  $\beta\alpha$  and  $\beta\beta$  states. At thermal equilibrium a Boltzmann distribution is set up. For simplicity we will assume that the difference in energy between states  $\beta\alpha$  and  $\alpha\beta$  is negligible, so that these states have equal populations. The populations for each state are  $N + \delta$ ,  $N$ ,  $N$  and  $N - \delta$ , respectively. The state  $\alpha\alpha$ , being of lower energy, contains an excess  $\delta$  of nuclei, while  $\beta\beta$  will be deficient by an equal amount  $\delta$ . The single quantum transitions between states  $\alpha\alpha$  and  $\beta\alpha$  and between states  $\alpha\beta$  and  $\beta\beta$  are transitions of  $s$  nuclei, while those between  $\alpha\alpha$  and  $\alpha\beta$  and between  $\beta\alpha$  and  $\beta\beta$  are those of  $i$  nuclei. Because we have assumed no  $J$ -coupling, the two transitions of nucleus  $i$  have exactly equal energy, as do those of nucleus  $s$ ; the unperturbed spectrum contains two singlets of equal intensity, while the transitions between  $\beta\alpha$  and  $\alpha\beta$  and between  $\alpha\alpha$  and  $\beta\beta$  are not observed.

The NOE experiment, which involves continuously saturating a transition of one nucleus ( $s$ , for example), disturbs the population differences which no longer correspond to the equilibrium situation. The disturbed system tries to restore the equilibrium by relaxation that occurs predominantly via dipole-dipole interaction. Hence the NOE and the dipole-dipole relaxation mechanism are intimately connected.

Figure 2.5 shows all possible and theoretically allowed relaxation pathways. The rate constant for the various processes will be designated  $W$ . The four  $W_1$  correspond to the single quantum transitions that constitute the spin-lattice relaxation processes ( $T_1$ ).  $W_0$  and  $W_2$  correspond to zero and double quantum transitions, respectively. They cannot be excited by electromagnetic radiation. They are spectroscopically forbidden and cannot be observed in the NMR spectrum. But they are allowed in relaxation.  $W_0$  and  $W_2$  are determined almost entirely by dipole-dipole

relaxation.

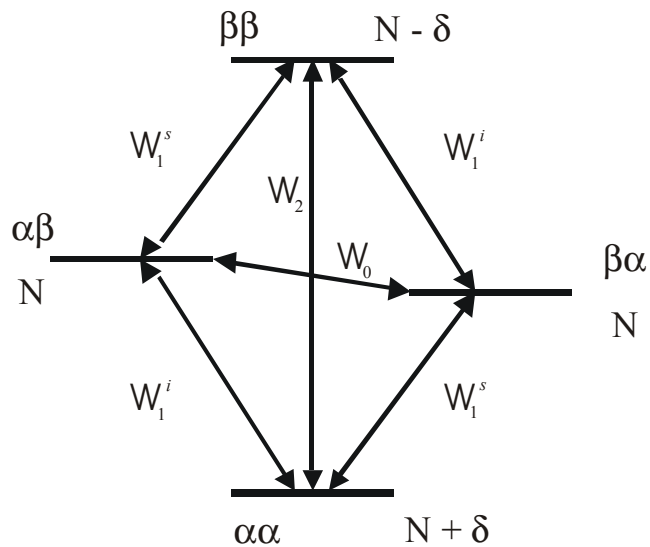


Figure 2.5. Connections between the energy levels of an AX system, which may be involved in relaxation.

For the initial condition at equilibrium, the population differences between states can be summarized as follows:

*i* transitions:

$$\alpha\alpha - \alpha\beta \} \text{ --- } \delta$$

$$\beta\alpha - \beta\beta \} \text{ --- } \delta$$

*s* transitions:

$$\alpha\alpha - \beta\alpha \} \text{ --- } \delta$$

$$\alpha\beta - \beta\beta \} \text{ --- } \delta$$

$\Delta m = 0$  transition:

$$\beta\alpha - \alpha\beta \} \text{ --- } 0$$

$\Delta m = 2$  transition:

$$\alpha\alpha - \beta\beta \} \text{ --- } 2\delta \quad [2.2]$$

If  $s$ -transitions are saturated (Figure 2.6), levels 1 and 3 become equally populated, as also do levels 2 and 4.

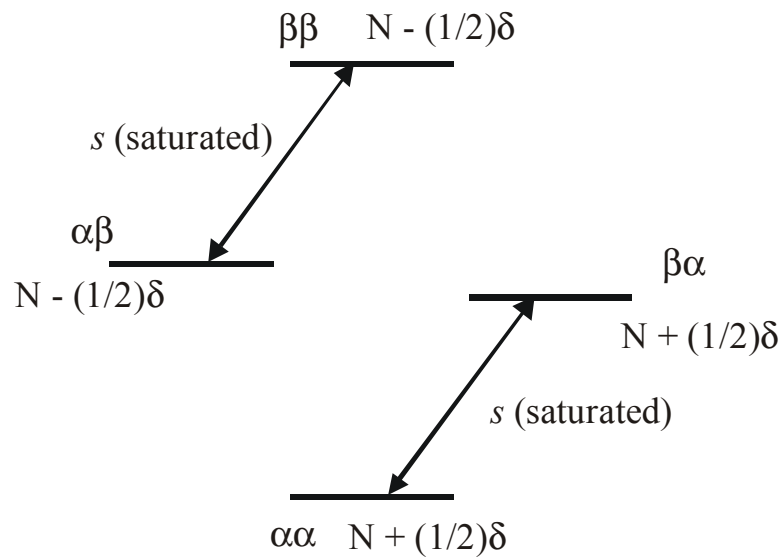


Figure 2.6 Populations of the energy levels immediately after the saturation of the  $s$  transitions.

The new population differences are:

$i$  transitions:

$$\alpha\alpha - \alpha\beta \} \text{ --- } \delta$$

$$\beta\alpha - \beta\beta \} \text{ --- } \delta$$

$s$  transitions:

$$\alpha\alpha-\beta\alpha \} \text{---} 0$$

$$\alpha\beta-\beta\beta \} \text{---} 0$$

$\Delta m = 0$  transition:

$$\beta\alpha-\alpha\beta \} \text{---} \delta$$

$\Delta m = 2$  transition:

$$\alpha\alpha-\beta\beta \} \text{---} \delta \quad [2.3]$$

The system is no longer at equilibrium. The relaxation pathway  $W_{1s}$  is irrelevant, because the population differences across those transitions are fixed by the saturation of the resonance.  $W_{1i}$  is irrelevant as well, because the population difference across each  $i$  transition before and after saturating  $s$  is the same. If only single quantum transitions are active as relaxation pathways, saturating  $s$  does not affect the intensity of  $i$ , or in other words there is no NOE at  $i$  due to  $s$ .

The population difference between states  $\alpha\beta$  and  $\beta\alpha$  is now  $\delta$ , whereas at equilibrium it was 0.  $W_0$  tries to transfer population from the state  $\beta\alpha$  to the state  $\alpha\beta$  to restore a population difference of 0. This reduces the population differences between  $\alpha\alpha$  and  $\alpha\beta$  and between  $\beta\alpha$  and  $\beta\beta$  which are related to the  $i$  signal intensity. This is synonymous with a decrease in  $i$  signal intensity. This tendency is counteracted by  $W_{1i}$ , since the  $i$  transitions were already at equilibrium, so the net result will depend on the balance of  $W_{1i}$  and  $W_0$ . If  $W_0$  is dominant, saturating  $s$  decreases intensity of signal  $i$ , or in other words there is negative NOE at  $i$  due to  $s$ .

The population difference  $\alpha\alpha-\beta\beta$  is now  $\delta$ , whereas at equilibrium it was  $2\delta$ .  $W_2$  tries to increase the population of the  $\alpha\alpha$  state at the expense of the population of the  $\beta\beta$  state and restore a population difference of  $2\delta$ . This causes an increase in the

population differences between  $\alpha\alpha$  and  $\alpha\beta$  and between  $\beta\alpha$  and  $\beta\beta$  states thereby tending to increase the  $i$  signal intensity. This tendency is counteracted by  $W_{1i}$  as well. If  $W_2$  is the dominant relaxation pathway, then saturating  $s$  increases the intensity of signals due to  $i$ , or in other words there a positive NOE at  $i$  due to  $s$  will be observed.

The combination of these two opposing relaxation mechanisms determines whether the intensity increases or decreases. For large proteins the molecules tumble slowly (long  $\tau_C$ ) which generates a small fluctuating magnetic field. When the frequency of the small fluctuating field is the same as that of  $s$  (for example),  $s$  will relax to  $\alpha$  state from  $\beta$  state and release energy to the local fluctuating field to make  $i$  excite to  $\beta$  state from  $\alpha$  state ( $W_0$ ). The relaxation pathway  $W_1$  via releasing energy to lattice is irrelevant. The small fluctuating field tends to be unable to contain frequencies close to the sum of the Larmor frequencies  $\nu_i$  and  $\nu_s$  and therefore cannot induce  $W_2$  transition. Therefore in large molecules with long correlation time  $\tau_C$ ,  $W_0$  predominates, and one observes a negative NOE. Here  $\tau_C$  characterizes the mean waiting time between one move and the next (by vibration, rotation or translation). Conversely the small molecules tumble faster, which generates a larger fluctuating field. Therefore in small molecules with short correlation time  $\tau_C$ ,  $W_2$  predominates, and one observes a positive NOE. From the close connection between dipole-dipole relaxation and NOE it explains why NOE depends on the distance between nuclei, since the dipolar coupling decreases in inverse proportion to the sixth power of the distance.

The interaction that gives rise to the NOE is the dipolar coupling between two nuclei. The rapid reorientation of the dipolar interaction is a suitable source of fluctuating field to stimulate longitudinal relaxation. In a system of two spins separated by a distance  $r_{is}$ , the relaxation rates via dipolar coupling are:

$$W_{1i} = (3/2) q \tau_C / (1 + \omega_i^2 \tau_C^2)$$

$$W_{1s} = (3/2) q \tau_C / (1 + \omega_s^2 \tau_C^2)$$

$$W_0 = q \tau_C / (1 + (\omega_i - \omega_s)^2 \tau_C^2)$$

$$W_2 = 6 q \tau_C / (1 + (\omega_i + \omega_s)^2 \tau_C^2)$$

with:

$$q = (1/10) \gamma_i^2 \gamma_s^2 (h / 2\pi)^2 (1 / r_{is}^6) \quad [2.4]$$

Examining equation [2.1], we identify  $\sigma_{is} = W_2 - W_0$ ,  $\rho_i = 2 W_i + W_2 + W_0$  and substitute into [2.1]. The result obtained is:

$$\eta_i(s) = (\gamma_s / \gamma_i) (W_2 - W_0) / (2 W_i + W_2 + W_0) . \quad [2.5]$$

For small molecules in non-viscous solution  $W_2$  is dominant and then  $\eta > 0$ , one can observe positive NOE as for macromolecules or in very viscous solution  $W_0$  is dominant and then  $\eta < 0$ ; negative NOEs are observed. If  $W_2$  and  $W_0$  balance, the NOE disappears. These observations indicate that relaxation is related to molecular motion. For a homonuclear spin system, the cross-relaxation rate constant  $\sigma_{is}$  is given by:

$$\sigma_{is} = W_2 - W_0$$

$$\begin{aligned}
&= (1/10) \gamma_i^2 \gamma_s^2 (h / 2 \pi)^2 (1/r_{is}^6) [6\tau_C / (1 + (\omega_i + \omega_s)^2 \tau_C^2) - \tau_C / (1 + (\omega_i - \omega_s)^2 \tau_C^2)] \\
&= (1/10) \gamma_H^4 (h / 2 \pi)^2 (1/r_{is}^6) [6\tau_C / (1 + 4\omega_0^2 \tau_C^2) - \tau_C] \quad [2.6]
\end{aligned}$$

and the NOE enhancement is given by:

$$\begin{aligned}
\eta_i(s) &= (\gamma_s / \gamma_i) (W_2 - W_0) / (2 W_{1i} + W_2 + W_0) \\
&= [-1 + 6 / (1 + 4\omega_0^2 \tau_C^2)] / [1 + 3 / (1 + \omega_0^2 \tau_C^2) + 6 / (1 + 4\omega_0^2 \tau_C^2)] \quad [2.7]
\end{aligned}$$

The cross-relaxation rate constant is proportional to the inverse sixth power of the distance between the two dipolar interacting spins, but  $\eta_i(s)$  does not depend on the distance  $r_{is}$  between two spins. The  $r^{-6}$  dependence of  $\sigma_{is}$  is used in NOESY experiments. Signal intensities can be directly translated into distances in proteins. The large density of protons in proteins yields a network of distances which is the basis for structure determination.

## 2.3 Residual dipolar couplings

### 2.3.1 Introduction

Internuclear magnetic dipole couplings contain long-range structural information, but in isotropic solution, they average to zero. However, their effect on nuclear spin relaxation leads to measurable nuclear Overhauser effects (NOEs), which are the main basis for the macromolecular structure determination by NMR. Because the NOE-derived distance restraints are not sufficient to determine the relative orientation of structural elements with few connecting NOEs available, residual dipolar couplings are used.

The applicability of the residual dipolar coupling depends on the magnitude of the degree of alignment of the molecule in the magnetic field. For most diamagnetic proteins, the magnetic susceptibility is dominated by aromatic residues as well as the susceptibility anisotropy of the peptide bonds. Since the magnetic susceptibility anisotropy tensors of these contributions are normally not colinear, the net value of the magnetic susceptibility is usually small. If many aromatic groups are stacked on each other in such a way that their magnetic susceptibility contributions are additive, like in the case of nucleic acids and protein-nucleic acid complexes, larger residual dipolar couplings are obtained.

Residual dipole couplings arise from small degrees of alignment of molecules at high magnetic field using very dilute liquid crystalline phases. The mechanism of induced orientation is assumed to be based on collision of the non-spherically shaped protein with the planar bilayer-like surfaces of the oriented bicells (Figure 2.7).



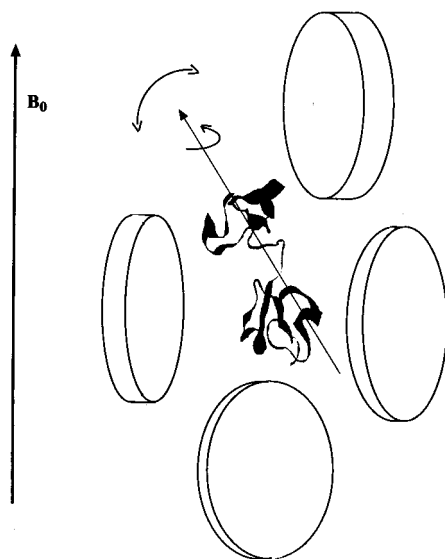


Figure 2.7. Protein molecules being oriented by collisions with field oriented lipid bilayer disks (bicelles).

Several different liquid crystal media can be used to partially align the molecules with respect to the magnetic field, including phospholipid bicells composed of mixtures (about 3:1) of DMPC/DHPC (dimyristoyl phosphatidylcholin/dihexanoyl phosphatidylcholin) or DIODPC/CHAPSO, filamentous phages, or purple membrane fragments in aqueous solution. In these media it is possible to measure residual dipolar couplings for a variety of different fixed-distance internuclear vector types, including one-bond  $^{15}\text{N}-^1\text{H}$ ,  $^{13}\text{C}\alpha-^1\text{H}\alpha$ ,  $^{13}\text{C}\alpha-^{13}\text{CO}$  vectors.

The general expression for the residual dipolar coupling  $D^{\text{AB}}(\theta, \phi)$  between two directly coupled spin-1/2 nuclei A and B can be simplified to the form

$$D^{AB}(\theta, \phi) = D^{AB}_a \{ (3\cos^2\theta - 1) + (3/2)R(\sin^2\theta\cos 2\phi) \}$$

$$\text{with } D^{AB}_a = -(B_0^2 h / 60 k T \pi^2) S \gamma_A \gamma_B \langle r_{AB}^{-3} \rangle x_a ; R = D^{AB}_r / D^{AB}_a \quad [2.8]$$

where  $D^{AB}_a$  and  $D^{AB}_r$  represent the axial and rhombic components of the molecular alignment tensor,  $\mathbf{D}$ , defined as  $1/3[D^{AB}_{zz} - (D^{AB}_{xx} + D^{AB}_{yy})/2]$  and  $1/3(D^{AB}_{xx} - D^{AB}_{yy})$ , respectively, with  $|D^{AB}_{zz}| > |D^{AB}_{yy}| \geq |D^{AB}_{xx}|$ ;  $R$  is the rhombicity of this tensor and always positive;  $\theta$  is the angle between the A-B interatomic vectors and the  $z$  axis of the tensor; and  $\phi$  is the angle which describes the position of the projection of the A-B interatomic vector on the  $x$ - $y$  plane, relative to the  $x$  axis (Figure 2.8).  $D^{AB}_a$  contains various constants, including the gyromagnetic ratios of two nuclei,  $\gamma_A$  and  $\gamma_B$ , the inverse cube of the internuclear distance  $\langle r_{AB}^{-3} \rangle$ , where  $\langle \rangle$  brackets indicate vibration averaging, the generalized order parameter  $S$ , the magnetic field strength  $B_0$ , and the axial component of the magnetic susceptibility tensor  $x_a$ . Values of  $S^2$  obtained from  $^{15}\text{N}$  or  $^{13}\text{C}$  relaxation experiments typically are from 0.7 to 0.9 for the structured regions in proteins,  $S$  usually is ranging between 0.85 and 0.95.

### 2.3.2 Estimate for alignment tensor

The extreme  $D^{AB}$  values correspond to orientations of A-B vectors closest to the  $z$  and  $y$  principle axes of the alignment tensor, so that with the condition that  $D^{AB}_{zz} + D^{AB}_{yy} + D^{AB}_{xx} = 0$ , the relation between  $D^{AB}_{zz}$ ,  $D^{AB}_{yy}$  and  $D^{AB}_{xx}$  is given by :

Molecular alignment tensor frame (x,y,z)

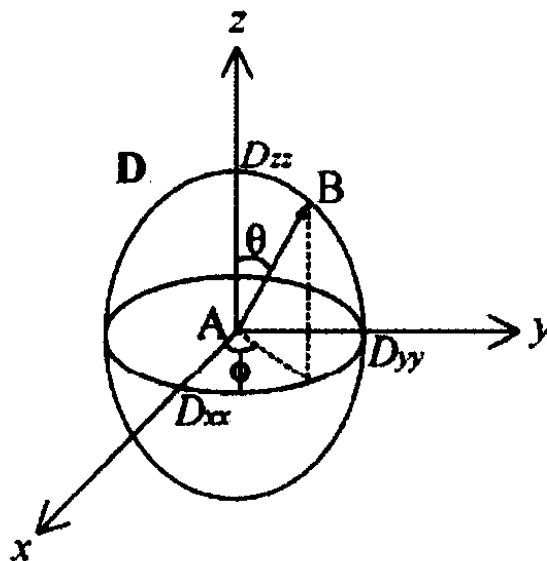


Figure 2.8. A schematic representation of the molecular alignment tensor  $D$  ( $x,y,z$ ). The tensor for a dipolar pair A-B is indicated. The axial ( $D_a$ ) and rhombic ( $D_r$ ) components of the alignment tensor,  $D$ , are defined as  $1/3[D_{zz} - (D_{xx} + D_{yy})/2]$  and  $1/3(D_{xx} - D_{yy})$ , respectively. The principal axis values (i.e.,  $D_{xx}$ ,  $D_{yy}$  and  $D_{zz}$ ) of the alignment tensor are indicated in the alignment frame.

$$\begin{aligned}
 D_{zz}^{AB} &= 2 D_a^{AB} \\
 D_{yy}^{AB} &= - D_a^{AB}(1 + 1.5 R) \\
 D_{xx}^{AB} &= - D_a^{AB}(1 - 1.5 R)
 \end{aligned}
 \tag{2.9}$$

The largest extreme value of dipolar coupling is therefore  $2D_a^{AB}$  under the condition  $|D_{zz}^{AB}| > |D_{yy}^{AB}| \geq |D_{xx}^{AB}|$ . The other extreme value can be used for the estimate of the rhombicity  $R$  when  $D_a^{AB}$  is available. If several sets of residual dipolar couplings are available, all observed one-bond and two-bond dipolar couplings can be

normalized to, for example, the N-H dipolar coupling, by multiplying the observed A-B dipolar coupling by  $(\gamma_N\gamma_H\langle r_{NH}^{-3}\rangle) / (\gamma_A\gamma_B\langle r_{AB}^{-3}\rangle)$ . The normalized values of  $D_{zz}^{AB}$  and  $D_{yy}^{AB}$  are obtained by averaging all high and low extreme values of normalized values, respectively.

## **2.4 ARIA Program**

### **2.4.1 Introduction**

ARIA (Ambiguous Restraints for Iterative Assignment) is a program for automatic NOEs assignment and structure calculation from NMR data. In particular, the method uses ambiguous distance restraints (ADRs) to resolve the assignment of ambiguous NOEs that arise from peak overlaps or peaks consisting of intra- and inter-molecular NOE peaks in a symmetric multimer.

### **2.4.2 Ambiguous distance restraints**

One of the major bottlenecks in the determination of solution NMR structures of proteins is the assignment of ambiguous NOEs. In NMR spectra of biological macromolecules, several protons often have the same chemical shift. An NOE cross peak involving these protons can not be directly converted into a distance restraint between two atoms. Furthermore, because of limited spectral dispersion, a NOESY cross peak may in fact arise as a sum of two or more distinct NOEs. Therefore, even after the proton chemical shifts have been completely assigned, the task of assigning the ambiguous NOEs remains. Many critical ambiguous long-range NOE interactions can only be interpreted on the basis of a structural model. Structure calculations are therefore usually performed in an iterative way, using preliminary structures based on a few unambiguous NOEs to further assign more ambiguous and unambiguous NOEs. ARIA is a fully automated iterative assignment method based on the use of ADRs. With the isolated spin pair approximation (ISPA), an ambiguous NOE depends simply

on the sum of inverse sixth powers of individual proton-proton distances:

$$\text{NOE} \propto \sum_{a=1}^{N_{\delta}} d_a^{-6} \quad [2.10]$$

where  $N_{\delta}$  indicates the number of possible assignments of a peak, given a chemical shift tolerance  $\delta$ .

The ambiguous distance restraint (ADR) can be derived by defining an effective  $D$ , which contains contributions from distances between all pairs of protons that are possible assignments of the NOE

$$D \equiv \left( \sum_{a=1}^{N_{\delta}} d_a^{-6} \right)^{-1/6} \quad [2.11]$$

Prior to the introduction of ADRs, ambiguous data were generally not used in NMR structure calculation for the simple reason that there was no easy way to specify the direct use of ambiguous data in the calculation. However, it is simple to see that ambiguous information can be used to give unambiguous results.

### 2.4.3 Target distances and error bounds

The calibration step used in ARIA gives an error estimate of the measured distance. Lower and upper limits are derived by error estimates in  $d^{\text{obs}}$ :

$$\begin{aligned}
L &= d^{\text{obs}} - \Delta^- \\
U &= d^{\text{obs}} + \Delta^+
\end{aligned}
\tag{2.12}$$

where  $\Delta$  is error estimate. Empirically,  $\Delta^+ = \Delta^- = 0.125 (d^{\text{obs}})^2$  is a good starting point for the automatic calibration in ARIA.

#### 2.4.4 Distance target function

During the structure calculation, the distances measured in the structures are restrained to upper and lower limits. The energy of a single distance restraint is

$$E_{\text{NOE}} = k_{\text{NOE}} \begin{cases} (L - D)^2 & \text{if } D < L \\ 0 & \text{if } L \leq D \leq U \\ (D - U)^2 & \text{if } U < D \leq U + \sigma \\ \alpha + \beta (D - U) + \gamma (D - U)^{-1} & \text{if } D > U + \sigma \end{cases}
\tag{2.13}$$

where  $k_{\text{NOE}}$  is the energy constant,  $D$  is the distance measured in the current ensemble of structures or a  $(\sum d^{-6})^{-1/6}$  distance such as in Eq. [2.11], and  $U$  and  $L$  are upper and lower bounds, Eq. [2.12], respectively. The parameter  $\sigma$  determines the distance at which the potential switches from harmonic to asymptotic behavior,  $\beta$  is the asymptotic slope of the potential, and the coefficients  $\alpha$  and  $\gamma$  are determined such that the potential is continuous and differentiable at  $U + \sigma$ . If  $D$  is between  $L$  and  $U$ , the energy is zero. Values of  $\sigma = 1.0 \text{ \AA}$ ,  $\beta = 2.0$  seem to be good for a global convergence of the calculation, while  $\sigma = 0.5 \text{ \AA}$ ,  $\beta = 0.1$  are better for distinguishing noise peaks from real data.

### 2.4.5 Removal of noise

It is never safe to assume that an experimental list of restraints is completely free of errors. Structural consistency is often taken as the final criterion to evaluate distance restraints. The error bounds are set wide enough that all experimental data is geometrically consistent, and the calculation attempts to find structures that do not violate any of the bounds, i.e. the final value of the energy or target function is zero.

In building three-dimensional structures from NOE data, most noise peaks will be inconsistent with each other and real peaks. If structures are calculated with restraints from both real and noise peaks, the latter will preferentially be violated in the calculated structures. The violations due to incorrect restraints will be present systematically rather than randomly. A violation analysis is performed as follows: calculate the fraction  $R_{vio}$  of structures in which a particular restraint is violated in calculated structures by more than a threshold  $v_{tol}$ :

$$R_{vio} = 1/S_{conv} \sum_S \Theta(D - U - v_{tol}) \quad [2.14]$$

$\Theta(x)$  is the Heaviside step function,  $S$  is the number of converged structures, and  $U$  is the upper distance limit. If  $R_{vio}$  exceeds a threshold (typically 50%), the restraint is either removed or set up to  $[0.0 \dots 6.0 \text{ \AA}]$  for the lower and upper limits.

Peaks incompatible with all the other restraints in a calculated structure can also simply be a consequence of error bounds set too narrowly.



#### **2.4.6 Stereospecific assignment**

ARIA performed a floating chirality procedure, instead of using pseudoatoms, to treat nonstereospecifically assigned methylene or isopropyl groups in the calculation of protein structures from NMR data. If these assignments are missing, pseudoatoms are usually introduced to replace the methylene or isopropyl protons. Consequently, the corresponding experimental distance constraints must be widened because of pseudoatom corrections. The protocol makes use of two strategies to induce the proper conformation of the prochiral centers: explicit atom 'swapping' following an evaluation of the NOE energy term, and atom 'floating' by reducing the angle and improper force constants that enforce a defined chirality at the prochiral center. In the present version of ARIA, floating is not performed by swapping atom positions, but by swapping the chemical shift assignments during the calculations. A problem arises in that the coordinates may not be consistent with the input restraints, since the chemical shift assignments may change during the calculation.

#### **2.4.7 NOE assignment and 3D structure determination**

ARIA performs simultaneously the assignment of NOE peaks and a concomitant structure calculation. The input files include the amino acid sequence of the corresponding protein, a list of assigned chemical shifts, uninterpreted or partly assigned 2D, 3D or 4D NOE peak lists. Additionally, torsion angles, J-couplings, residual dipolar couplings, intermolecular NOE restraints, hydrogen bonds or disulfide bridges can be added as restraints as well.

ARIA performs 9 iterations (iteration 0...iteration 8). In general, the starting

structures for ARIA in the iteration 0 have random torsion angles. The random structures can be replaced by preliminary structures calculated from manually assigned restraints if these are available. In the following iterations, some structures are refined, and some are calculated ab initio with random torsion angles. A calculation with eight iterations with 20 structures per iteration generally gives satisfactory results. The iterative NOE assignment strategy in ARIA is illustrated in Figure 2.9.

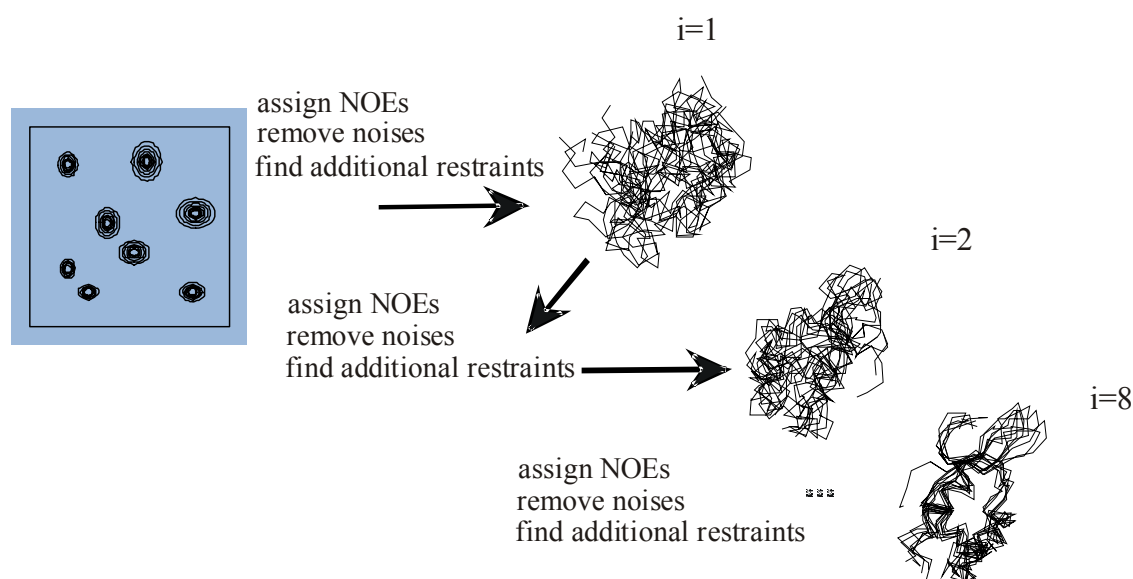


Figure 2.9. Illustration of iterative NOE assignments and structure calculations in ARIA.

## 2.4.8 Calculation of symmetric multimer structures

Many biologically important proteins form symmetric oligomers. Symmetric oligomers present a special difficulty for structure determination by NMR, since all symmetry-related protons will have the same magnetic environment and therefore will be degenerated in chemical shift; only one monomer is 'seen' in the spectra. This is referred to as symmetry degeneracy. Dispersion degeneracy (peak overlap) and symmetry degeneracy are quite distinct. Dispersion degeneracy can be improved with better resolved spectra, but symmetry degeneracy cannot. In NOESY spectra of multimers, there are three different kinds of NOE peaks: (i) 'intra-monomer', those arising solely from dipolar coupling between protons within the same monomer; (ii) 'inter-monomer', between protons on different monomers; and (iii) 'co-monomer', describing NOEs which consist of *both* correlations between protons on the same monomers *and* between protons on the different monomers. In the case of symmetric multimers it is impossible to distinguish between intra-, inter-, and co-monomer NOE signals (Figure 2.10).

### 2.4.8.1 Symmetry ADRs

Eq. [2.11] is valid for both dispersion degeneracy and symmetry degeneracy. One NOE peak may have contributions from intramonomer, from intermonomer or from both, intra- and intermonomer NOEs. But it is impossible to distinguish from which contribution the volume has. The introduction of ambiguous restraint makes it possible to deal with the NOE peaks containing symmetry degeneracy. For example,

in Figure 2.10 the volume,  $V$ , of the cross peak has contributions from three NOEs (volumes  $V_1$ ,  $V_2$ , and  $V_3$ , respectively and they could be derived from intra-, inter- or comonomer NOEs). It means

$$V = V_1 + V_2 + V_3$$
$$D = (d_1^{-6} + d_2^{-6} + d_3^{-6})^{-1/6} \quad [2.15]$$

Therefore Eq. [2.11] is valid for symmetry degeneracy as well.

#### 2.4.8.2 Co-monomer restraints

For NOEs close to the symmetry axis of the oligomer, it is difficult to exclude the intra-monomer contribution even with asymmetric labelling experiments. It is then useful to enforce that both intra- and inter-monomer contributions are present in an NOE. This is achieved by introducing a co-monomer constraint, which is an upper limit of typically 5-6 Å on all inter-and intra-monomer contributions to the NOE.

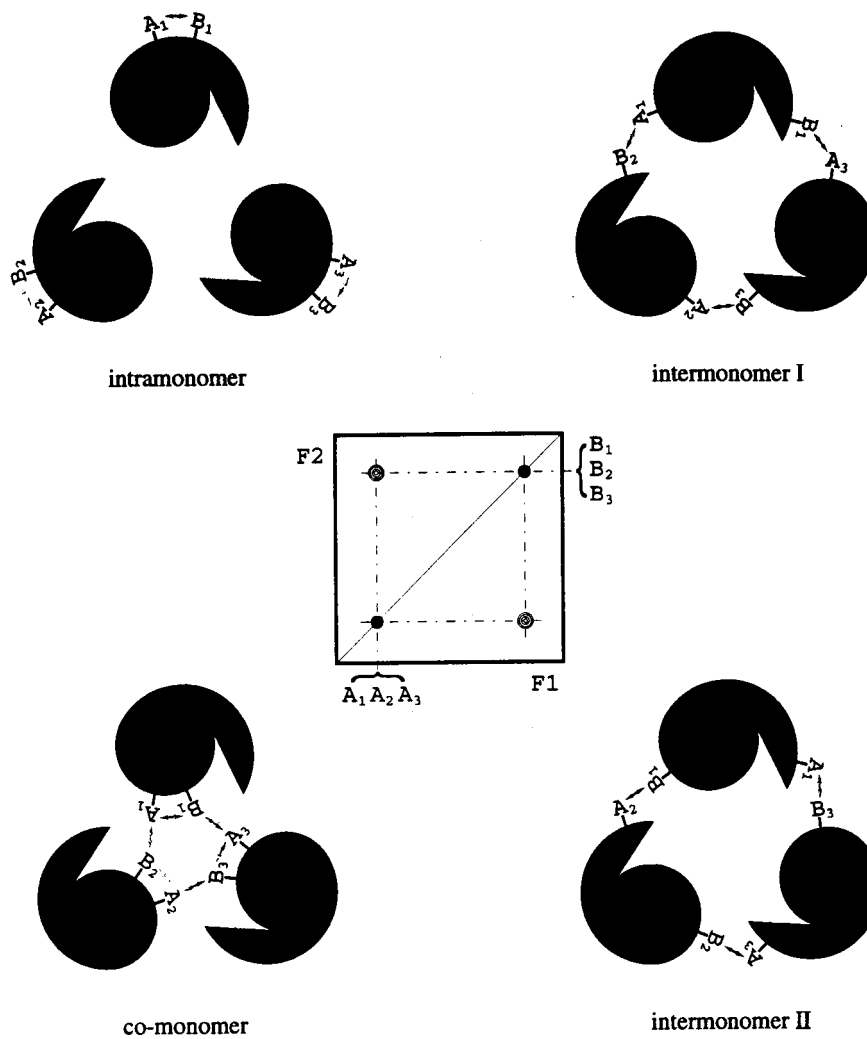


Figure 2.10. Intra-, inter-, and comonomer NOEs. Symmetry-related protons (e.g.,  $A_1, A_2$ , and  $A_3$ ) occur at the same position of the NOESY diagonal; hence, it is not possible to distinguish the class of an NOE peak.

## 3 Materials and Methods

### 3.1 Sample preparation

Expression and purification of recombinant Sud protein from *Escherichia coli* was carried out using a similar protocol to that previously described (Klimmek et al., 1998). Uniform  $^{15}\text{N}$  and  $^{15}\text{N}/^{13}\text{C}$  labeling was achieved by growing bacteria on isotope enriched minimal medium using  $^{15}\text{N}$  ammonium chloride (Martek) and  $^{13}\text{C}_3$  enriched glycerol (Martek) as main nitrogen and carbon source, respectively. For protein samples labelled with  $^2\text{H}/^{15}\text{N}/^{13}\text{C}$ , the bacteria were grown on Celtone<sup>®</sup>-dCN (Martek, deuteration degree: 97 %). NMR samples of purified protein (0.6 - 1.2 mM dimer) were prepared in 50 mM sodium phosphate at pH 7.6, 1 mM polysulfide ( $\text{S}_n^{-2}$ ), 13 mM sulfide, and 5% v/v  $\text{D}_2\text{O}$ . For the measurement of residual dipolar couplings, the isotropic sample contained 0.55 mM dimer protein in 50 mM sodium phosphate at pH 7.6, 1 mM polysulfide ( $\text{S}_n^{-2}$ ), 13 mM sulfide, and 10% v/v  $\text{D}_2\text{O}$ . The anisotropic sample contained 0.48mM dimer protein in the same buffer solution as that of the isotropic sample except the alignment media, C8E5/n-octanol, has been added (Rückert et al., 2000). The molar ratio of C8E5 to n-octanol was 0.87 and the C8E5/water ratio was 6% w/v. To prepare asymmetrically labeled sample for the measurement of inter-monomer NOEs mixed Sud-dimers were prepared from isolated Sud-His<sub>6</sub>-dimer (unlabeled) and isolated  $^{15}\text{N}$ -labeled Sud-His<sub>6</sub>-dimer. These dimers were mixed in equal amounts at a very low concentration (each species 10 nM) in an anaerobic buffer containing 50 mM potassium phosphate and 10% (v/v) glycerol, pH 8.0. To induce monomerisation of the isolated dimers 0.02% (w/v) sodium dodecylsulfate was added. The mixture was stirred for 48 h at room temperature under anaerobic conditions. For initiation of dimerisation and protein recovery the whole

mixture was applied to a 10 ml-Ni-nitrilotriacetic agarose (Qiagen) column equilibrated with 50 mM potassium phosphate and 10% (v/v) glycerol, pH 8.0. The column was rinsed extensively with the same buffer (0.5l) to remove the SDS, then the protein was eluted with this buffer containing additional 0.2 M imidazole. The eluted Sud-protein was concentrated up to 30 g/l by pressure dialysis using a 10-kDa filter and imidazole was removed by repeated dilution und concentration (five times) of the protein with a buffer containing 50 mM potassium phosphate, pH 7.65. The same procedure was also performed for the  $^{13}\text{C}$ -labeled-unlabeled Sud-dimers. Mixed Sud-dimers were prepared from isolated Sud-His<sub>6</sub>-dimer (unlabeled) und isolated  $^{13}\text{C}$ -labeled Sud-His<sub>6</sub>-dimer in D<sub>2</sub>O. The protein was loaded with sulfur before dissolving in the described buffer. Sample tubes were flushed with nitrogen while filling and subsequently widely sealed afterwards in order to exclude oxygen from the sample volume. Under these conditions, it can be assumed that the protein remains sulfur-loaded during the NMR experiments.

## 3.2 NMR spectroscopy

NMR data were acquired at 300 K using Bruker DMX-600 and DRX-800 NMR spectrometers equipped with xyz-gradient  $^1\text{H}$ ,  $^{15}\text{N}$ ,  $^{13}\text{C}$  triple resonance probe heads. The sensitivity and resolution of triple resonance experiments was improved by employing the TROSY technology (Pervushin et al., 1997; Salzman et al., 1999). The software packages XWINNMR and AURELIA (Bruker Analytische Messtechnik GmbH, Karlsruhe) were used for data processing and data analysis, respectively. 2D and 3D Spectra were processed using XWINNMR and 4D spectra using nmrPine (Delaglio et al., 1995).  $^1\text{H}$  chemical shifts were referred to internal DSS (2,2-dimethyl-2-silapentane-5-sulfonate sodium salt) at 0.00 ppm.  $^{15}\text{N}$  and  $^{13}\text{C}$  chemical shifts were calibrated indirectly using the appropriate gyromagnetic ratios (Wishart et al., 1995).

*Backbone resonance assignment* Backbone sequential resonance assignments were obtained using TROSY-based 3D triple-resonance HNCACB (Grzesiek et al., 1992), HNCO (Ikzra et al., 1990; Grzesiek et al., 1992), HN(CA)CO (Clubb et al., 1992), and HNCAN (Löhr et al., submitted) experiments using  $^2\text{H}/^{15}\text{N}/^{13}\text{C}$  protein samples as well as HNCO (Ikzra et al., 1990; Grzesiek et al., 1992), HNCA (Ikzra et al., 1990; Grzesiek et al., 1992), and HCACO (Ikzra et al., 1990; Palmer et al., 1992) experiments using  $^1\text{H}/^{15}\text{N}/^{13}\text{C}$  protein samples.  $^{15}\text{N}$ ,  $^1\text{HN}$ ,  $^{13}\text{CO}$ ,  $^{13}\text{C}\alpha$ , and  $^{13}\text{C}\beta$  chemical shifts of the protonated protein were confirmed using 2D [ $^1\text{H}$ ,  $^{15}\text{N}$ ]-HSQC, and 3D HNCA, HNCO, and H(C)CH-COSY experiments.  $^1\text{H}\alpha$  chemical shifts were obtained from a 3D HCACO experiment.

*Aliphatic side chain resonance assignment*  $^{13}\text{C}$  side chain assignments were based on the 3D CC(CO)NH and CC(CA)NH experiments (FarmerII and Venters, 1995) with a



$^{13}\text{C}$  spin-lock time of 21 ms and 17 ms, respectively on the same sample.  $^1\text{H}\alpha$  chemical shifts were obtained from a 3D HCACO experiment and  $^1\text{H}$  side chain resonances were assigned using 3D  $^{13}\text{C}$ -separated H(C)CH-COSY and H(C)CH-TOCSY experiments with a  $^{13}\text{C}$  spin-lock time of 17 ms on a uniformly  $^{15}\text{N}/^{13}\text{C}$  labeled sample of Sud in 95%  $\text{H}_2\text{O}/5\%$   $\text{D}_2\text{O}$ .

*Aromatic resonance assignment* The resonances of aromatic protons were obtained via a 2D homonuclear NOESY with a mixing time of 70 ms, a 2D homonuclear TOCSY with 44 ms  $^1\text{H}$  spin-lock time on an unlabeled sample in  $\text{D}_2\text{O}$  and a 3D  $^{13}\text{C}$ -separated NOESY HSQC experiment with a mixing time of 70 ms employing a constant-time [ $^{13}\text{C}$ ,  $^1\text{H}$ ]-TROSY evolution period (Pervushin, et al., 1998) optimized for aromatic carbons on a  $^{15}\text{N}/^{13}\text{C}$  labeled sample in  $\text{H}_2\text{O}$ . The resonance assignment of aromatic protons was mainly based on the NOE correlations between aromatic proton and  $\text{H}\beta$  protons of intra-residue in 2D and 3D NOESY, while the TOCSY spectrum provides all aromatic resonances within a spin system.

*Stereospecific resonance assignment* Stereospecific assignments of isopropyl groups of Val and Leu residues were determined by using a biosynthetic approach (Neri et al., 1989) on the basis of the  $^{13}\text{C}$ - $^{13}\text{C}$  one-bond coupling with 2D  $J$ -coupled  $^{13}\text{C}$  HSQC and 2D CT  $^{13}\text{C}$  HSQC experiments on a 10%  $^{13}\text{C}$ -labeled sample. In the  $J$ -coupled  $^1\text{H}/^{13}\text{C}$  HSQC the *pro-R* methyl group and the adjacent  $>\text{CH}$ - group originate from the same pyruvate molecule and hence generate a doublet due to the one-bond  $^{13}\text{C}$ - $^{13}\text{C}$  coupling, while *pro-S* methyl groups a singlet. In the CT  $^1\text{H}/^{13}\text{C}$  HSQC *pro-R* and *pro-S* methyl group show positive and negative peaks, respectively.

*NOE assignment* NOE assignments and distance restraints of NH-NH were obtained from a 4D  $^{15}\text{N}/^{15}\text{N}$ -separated NOESY (Venters, et al., 1995, Grzesiek, et al., 1995) with a mixing time of 300 ms on a uniformly  $^2\text{H}/^{15}\text{N}$  labeled protein in  $\text{H}_2\text{O}$ . NOE-based distance restraints were derived from a 3D  $^{13}\text{C}$ -separated NOESY-HSQC with a mixing time of 80 ms using a uniformly  $^{13}\text{C}/^{15}\text{N}$  labeled protein in  $\text{D}_2\text{O}$ , a 3D  $^{15}\text{N}$ -separated NOESY-HSQC with a mixing time of 75 ms recorded with a uniformly  $^{15}\text{N}$  labeled protein in  $\text{H}_2\text{O}$ , a 3D constant-time methyl  $^{13}\text{C}$ -separated NOESY-HSQC with a mixing time of 100 ms on a uniformly labeled  $^{13}\text{C}/^{15}\text{N}$  protein in  $\text{H}_2\text{O}$ , and a 2D homonuclear [aromatic proton,  $^1\text{H}$ ]-NOESY with a mixing time of 70 ms on a sample in  $\text{D}_2\text{O}$ , using ARIA (Nilges et al., 1998) for automated iterative NOE assignments, distance calibration from NOE peaks and structure calculations. The NOE-derived distance restraints were classified as unambiguous and ambiguous distance restraints. The 3D methyl  $^{13}\text{C}$ -resolved NOESY HSQC provides correlations between protons and methyl groups, while the 2D [aromatic proton,  $^1\text{H}$ ]-NOESY provides many long range NOEs between aromatic protons and surrounding protons.

*Inter-monomer NOE assignment* To determine NOEs across the dimer interface, a 3D  $^{15}\text{N}$ -separated NOESY HSQC experiment with a mixing time of 120 ms on a heterodimer sample containing one  $^2\text{H}/^{15}\text{N}$ -labeled monomer and one unlabeled monomer (Ferentz, et al., 1997) in  $\text{H}_2\text{O}$  and a 4D constant-time J-resolved  $^{13}\text{C}$ -separated NOESY experiment (Melacini et al., 2000) with a mixing time of 150 ms on a sample containing one  $^{13}\text{C}/^{15}\text{N}$ -labeled monomer and one unlabeled monomer were recorded. The former experiment yields NOEs between the amide protons of the  $^2\text{H}/^{15}\text{N}$ -labeled monomer and the carbon-bound protons of the unlabeled monomer. The latter one allows the separation of inter- and intramolecular NOEs along the J-

resolved dimension. The intramolecular NOEs between  $^{13}\text{C}$ -bound protons appear at  $\pm J_{\text{CH}}/2$  Hz, while intermolecular NOEs between  $^{13}\text{C}$ - and  $^{12}\text{C}$ -bound protons appear at zero frequency offset because they are not  $J$ -modulated.

*Residual dipolar coupling* A generalized version of the [ $^{15}\text{N}$ - $^1\text{H}$ ]-TROSY experiment (Andersson et. al., 1998) (Lerche et al., 1999) was used for the measurement of  $^1J_{\text{NH}}$  scalar coupling and  $(^1J_{\text{NH}} + D^{\text{NH}})$  coupling on a non-orientated and orientated sample, respectively.

*Other restraints* Slowly exchanging amide protons were identified by recording 2D  $^1\text{H}$ - $^{15}\text{N}$  HSQC experiments one day and five days after transferring the protein into  $\text{D}_2\text{O}$  solution. This information combined with the strong NH to sequential  $\text{H}\alpha$  connectivities and to  $\text{H}\alpha$  of the other  $\beta$  strand connectivities allows the identification of  $\beta$  strands and hydrogen bonds between  $\beta$  strands. The amide protons located in the five-stranded parallel  $\beta$  sheet remained unexchanged five days after the addition of  $\text{D}_2\text{O}$ . The backbone amide protons involved in hydrogen bonds were measured as well using  $^{\text{h}3}J_{\text{NCO}}$  coupling experiment. The  $\phi$  and  $\psi$  angle constraints were obtained using the program TALOS (Cornilescu et al., 1999) which predicts backbone torsion angles from chemical shifts and amino acid sequence similarities.

### 3.3 Experimental NMR restraints

The cross-peak volumes were determined using the Bruker AURELIA program. The NOESY cross-peak volumes were converted into distances based on the use of ambiguous distance restraints (ADRs) that were treated using the  $r^{-6}$  sum protocol described by Nilges (1993). All experimental unambiguous intermonomer distance restraints and all NH-NH distance restraints derived from 4D spectrum were set to 6 Å for upper bounds and 2 Å for lower bounds. Hydrogen bond restraints were defined by 1.8-2.3 Å for the H-O distance and 2.7-3.2 Å for the N-O distance. Residual dipolar coupling restraints  $D^{\text{NH}}$  were derived via measuring the coupling difference between  $(^1J_{\text{NH}} + D^{\text{NH}})$  coupling and  $^1J_{\text{NH}}$  scalar coupling.

### 3.4 Structure calculation

The dimer structure of Sud was calculated *de novo* by using the simulated annealing protocol of ARIA that is based on the use of ADRs (ambiguous distance restraints). The ambiguous distance restraints, including those that have both intra- and inter-monomer contributions, were treated with a target function that computes an effective distance  $D = (\sum r^{-6})^{-1/6}$ , which contains contributions from distances between all pairs of protons that are possible assignments of the NOE, as described by Nilges (1993). In addition, a combination of the non-crystallographic symmetry (NCS) restraints (Brünger, 1992) and distance symmetry restraints (Nilges, 1993) was applied during the structure calculation. The former serves to minimize the atomic r.m.s. difference between the two monomers, thus making the two monomers identical, while the latter restrains the two monomers in a symmetrical arrangement.

Symmetry of the dimer was obtained by forcing the distance between the C $\alpha$  of residue a in the monomer A and C $\alpha$  of residue b in the monomer B to be equal to that between C $\alpha$  of residue a in the monomer B and C $\alpha$  of residue b in the monomer A, and so on. All non-stereospecifically assigned prochiral groups, except manually assigned isopropyl groups, were treated with a floating assignment approach (Folmer *et al.*, 1995). The polysulfide-binding Sud structure was additionally calculated by attaching five or ten polysulfide sulfur atoms to the cysteine residue of each monomer. 20 out of 200 calculated structures were selected on the basis of lowest distance, dihedral angle and residual dipolar coupling restraint violations. Since there is no NOE information available between the polysulfide and the Sud protein, the orientation of the polysulfide was derived only from simulated annealing. The simulated annealing protocol in ARIA consisted of four stages: a high temperature stage at 10000 K with 25000 MD steps, a first cooling stage from 10000 K to 2000 K with 25000 MD steps, a second cooling stage from 2000 K to 1000 K with 21000 MD steps, and a third cooling stage from 1000 K to 50 K with 18000 MD steps.

Nine iterations (iteration0 ~ iteration8) were performed by ARIA for automatic NOE assignment and structure calculation. To utilize residual dipolar coupling refinement in the structure calculation, the values of  $D_a^{AB}$  and  $R$  must be determined from experimental data (Clare, *et al.*, 1998), where  $D_a^{AB}$  and  $R$  represent the axial component and the rhombicity of the molecular alignment tensor, respectively. The geometric content of the residual dipolar couplings is incorporated into the simulated annealing protocol by including the term  $E_{\text{dipolar}} = k_{\text{dipolar}} (\delta_{\text{calc}} - \delta_{\text{obs}})^2$ , where  $k_{\text{dipolar}}$  is a force constant and  $\delta_{\text{calc}}$  and  $\delta_{\text{obs}}$  are the calculated and observed values of the residual dipolar couplings, respectively.

## 4 RESULTS AND DISCUSSION

### 4.1 NMR Assignments

#### 4.1.1 Backbone resonance assignment

The backbone resonances of  $^1\text{HN}$ ,  $^{15}\text{N}$ ,  $^1\text{H}\alpha$ ,  $^{13}\text{C}\alpha$ , and  $^{13}\text{CO}$  (and side-chain  $^1\text{H}\beta$  and  $^{13}\text{C}\beta$ ) were assigned using combinations of different TROSY-based triple-resonance experiments (Table 4.1). For example, the HNCACB experiment (Figure 4.1) correlates the amide  $^1\text{H}$  and  $^{15}\text{N}$  resonances of one residue with  $^{13}\text{C}\alpha$  and  $^{13}\text{C}\beta$  chemical shifts of intra- and its preceding residues. The  $\text{C}\beta$  chemical shifts of Thr and Ser are significantly shifted to lower fields (60~70 ppm) compared to the  $\text{C}\beta$  chemical shifts of the other amino acids, therefore Thr and Ser residues are often used as starting residues to initiate the sequential resonance assignment. The HN(CA)N experiment (Löhr et al., 2000) correlates N,N-connectivities between a protonated amide group and amides of the preceding and following residues (Figure 4.2). Hence the sequential backbone resonance assignment across proline residues can be achieved. Each monomer of the Sud protein contains 8 proline residues which  $^{15}\text{N}$  resonances could be assigned with this method.

The resonance assignments were complete for the all backbone  $^{15}\text{N}$  and  $^1\text{HN}$  (except residues A1, D2, K90-A95),  $^{13}\text{C}\alpha$  (except residues A1, K90-R94),  $^{13}\text{CO}$  (except residues A1, K90-R94),  $^{13}\text{C}\beta$  (except residues A1, K90-A95), and  $^1\text{H}\alpha$  (except residues A1, K90-R94, G116, S131) nuclei. The correlation signals of the residues A1, D2, M3, G78, K90-A95, as well as S131 are absent in 2D [ $^1\text{H}$ ,  $^{15}\text{N}$ ]-HSQC (Figure 4.3) due to fast exchange of the corresponding amide protons with the solvent protons. Fast chemical exchange is also likely to be the reason for the absence

Table 4.1

TROSSY-Based Triple-Resonance Experiments Used for Backbone Sequential Resonance Assignment of Sud Protein

Experiment	Correlations observed	solvent	Labeling		Spectrometer
			$^{15}\text{N}$	$^{13}\text{C}$ $^2\text{H}$	
HNCACB	$\text{C}\alpha(i-1)$ , $\text{C}\beta(i-1)/\text{NH}(i)$ , $\text{N}(i)/\text{C}\alpha(i)$ , $\text{C}\beta(i)$	H <sub>2</sub> O	+	+	800
HN(CA)CO	$\text{NH}(i)$ , $\text{N}(i)/\text{CO}(i)$ , $\text{CO}(i-1)$	H <sub>2</sub> O	+	+	800
HNCO	$\text{NH}(i)$ , $\text{N}(i)/\text{CO}(i-1)$	H <sub>2</sub> O	+	+	800
HN(CA)N	$\text{NH}(i)$ , $\text{N}(i)/\text{N}(i+1)/\text{N}(i-1)$	H <sub>2</sub> O	+	+	800
HNCA	$\text{NH}(i)$ , $\text{N}(i)$ , $\text{C}\alpha(i)$	H <sub>2</sub> O	+	-	800
HNCO	$\text{NH}(i)$ , $\text{N}(i)/\text{CO}(i-1)$	H <sub>2</sub> O	+	-	800
HCACO	$\text{C}\alpha(i)$ , $\text{H}\alpha(i)$ , $\text{CO}(i)$	H <sub>2</sub> O	+	-	800

Table 4.2

Experiments Used for Aliphatic Side-Chain Resonance Assignment of Sud Protein

Experiment	Correlations observed	solvent	Labeling		Spectrometer
			$^{15}\text{N}$	$^{13}\text{C}$ $^2\text{H}$	
CC(CO)NH	$\text{NH}(i)$ , $\text{N}(i)/\text{aliphatic C}(i-1)$	H <sub>2</sub> O	+	+	600
CC(CA)NH	$\text{NH}(i)$ , $\text{N}(i)/\text{aliphatic C}(i)$	H <sub>2</sub> O	+	+	600
H(C)CH-COSY	aliphatic $\text{C}(i)$ , aliphatic coupled $\text{H}(i)$	D <sub>2</sub> O	+	-	600
H(C)CH-TOCSY	aliphatic $\text{C}(i)/\text{aliphatic H}(i)$	D <sub>2</sub> O	+	-	600

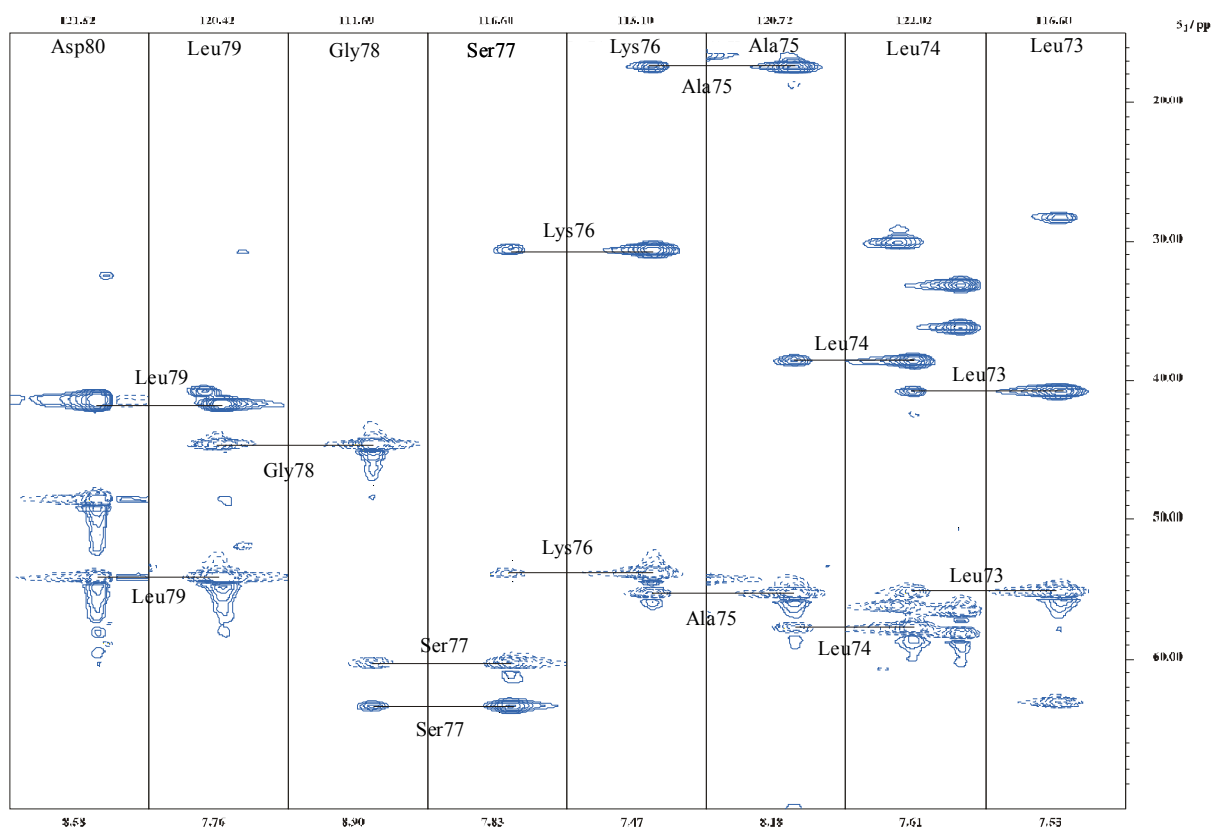


Figure 4.1. Sequential backbone resonance connectivities in the region of Asp80-Leu73 of the Sud protein in a TROSY-based HNCACB spectrum. The peaks with dashed and solid line indicate  $\text{C}\alpha$  and  $\text{C}\beta$ , respectively. Every slice contains  $\text{C}\alpha$  and  $\text{C}\beta$  chemical shifts of intra and preceding residues.

of information within the segment K90-A95. In addition, the sequence of A92-A93-R94-A95-A96 complicates the resonance assignments.  $^{15}\text{N}$ ,  $^1\text{HN}$ ,  $^{13}\text{CO}$ ,  $^{13}\text{C}\alpha$ , and  $^{13}\text{C}\beta$  chemical shifts of the deuterated protein were confirmed using 2D [ $^1\text{H}$ ,  $^{15}\text{N}$ ]-HSQC, and 3D HNCA, HNCOC, H(C)CH-TOCSY and H(C)CH-COSY experiments with a protonated sample.  $^1\text{H}\alpha$  chemical shifts were obtained from a 3D HCACO experiment.



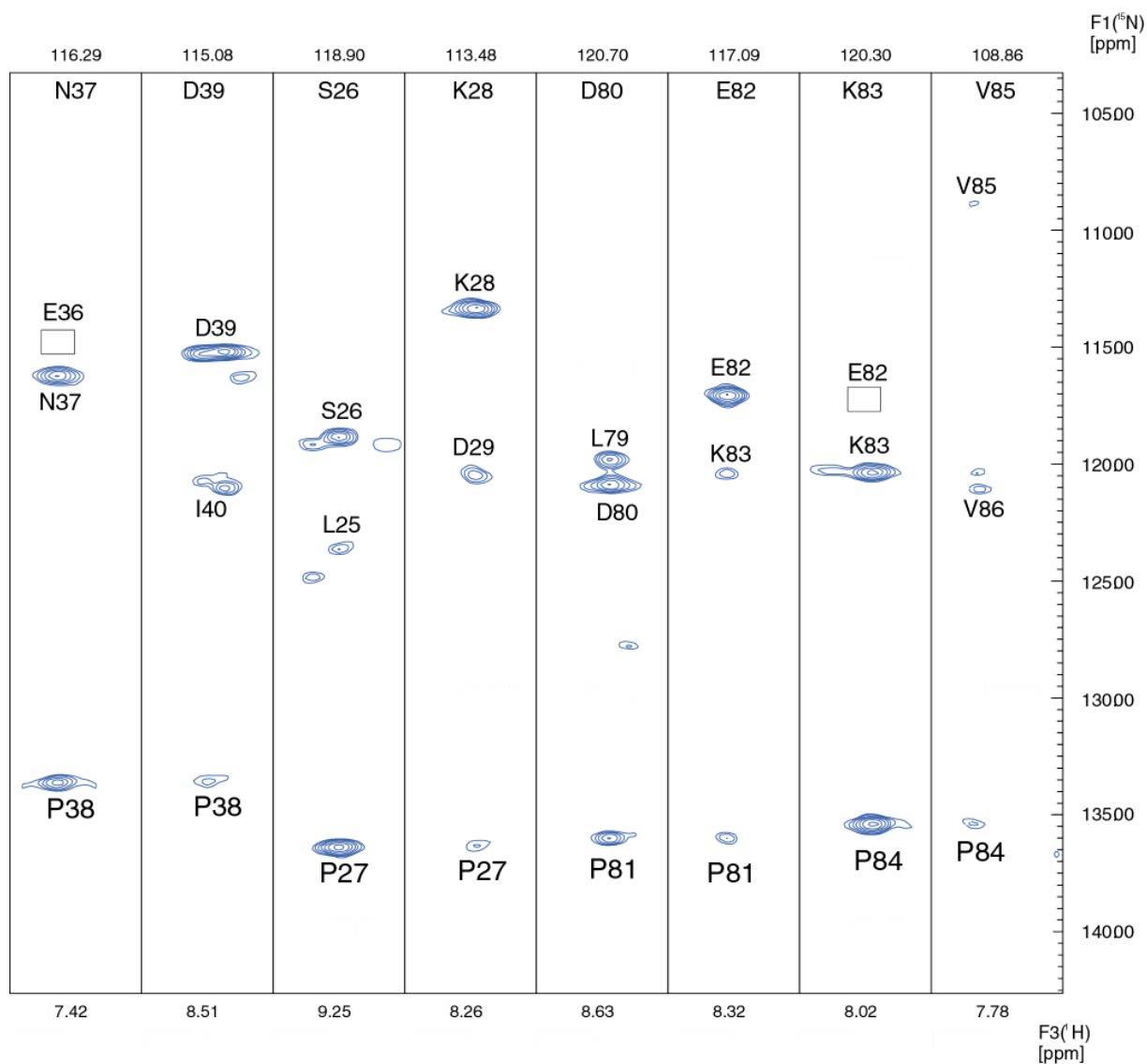


Figure 4.2. Sections of F1/F3 slices from a HN(CA)N spectrum of the Sud protein. The correlations of N, NH of intraresidue with N of preceding and following residues allow the assignment of the  $^{15}\text{N}$  resonances of prolines. As examples, the nitrogens of prolines 38, 27, 81 and 84 are assigned. Each monomer of Sud protein contains 8 proline residues, all of which nitrogens could be assigned with the HN(CA)N technique.

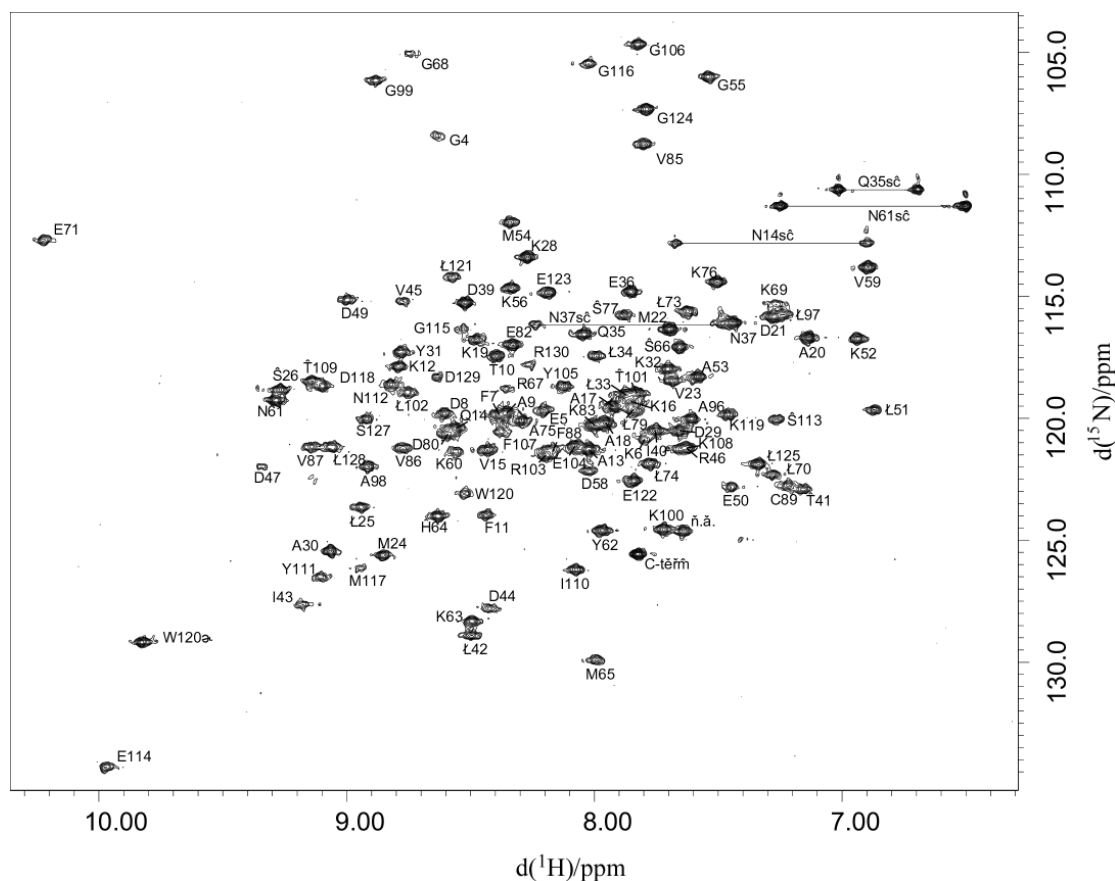


Figure 4.3. 2D- $[^1\text{H}, ^{15}\text{N}]$ -HSQC spectrum of Sud at 0.5 mM concentration. Cross peaks are assigned using the sequence position of corresponding residues. Observed side chain amide moieties are connected by horizontal bars.

The  $[^1\text{H}, ^{15}\text{N}]$ -HSQC spectrum of the Sud dimer showed good dispersion of  $^1\text{H}$  and  $^{15}\text{N}$  resonances (Figure 4.3). The assignments are available for 123 amino acids with 8 residues unassigned. The overall quality of the spectra was not always comparable to the shown  $[^1\text{H}, ^{15}\text{N}]$ -HSQC. Frequently, a second set of signals (from amino acid 20 to 130) appeared a few days after preparation of the sample which could be also combined in an almost complete sequential resonance assignment (Figure 4.4).

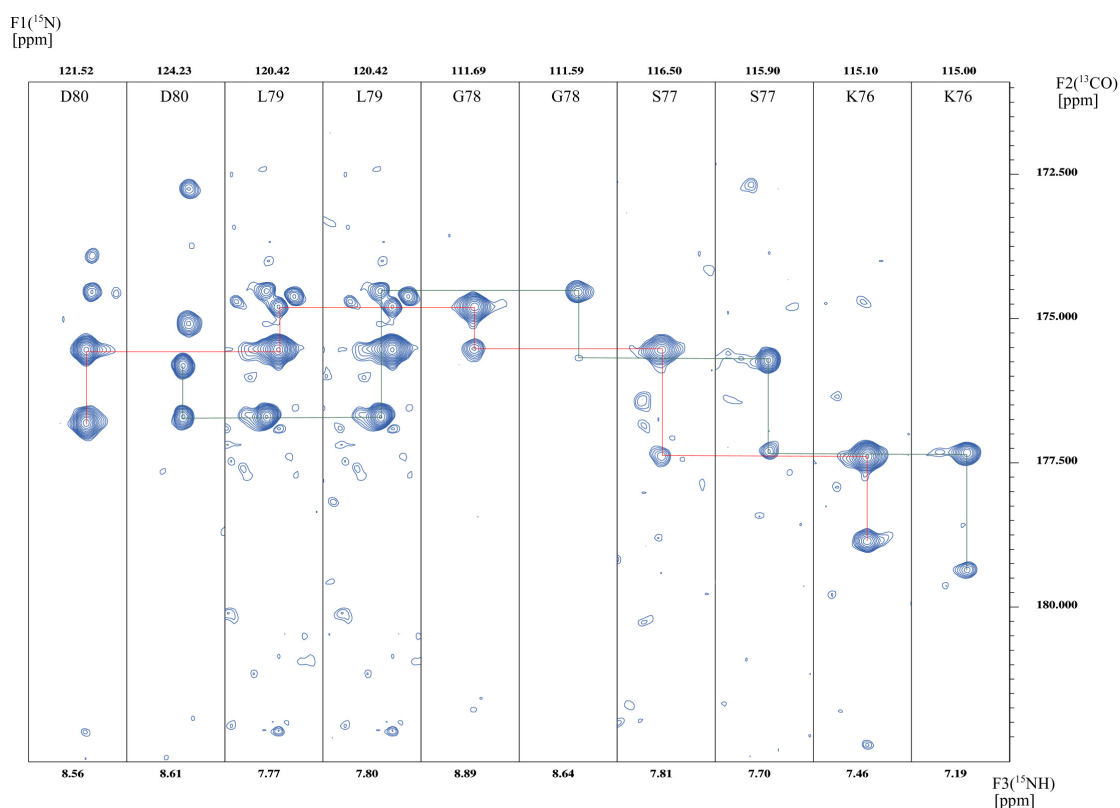


Figure 4.4 Two different assignment connectivities in the same region from D80-K76 in the TROSY-based HN(CA)CO spectrum on a sample with 1mM Sud dimer concentration. This experiment correlates <sup>1</sup>H, <sup>15</sup>N and CO resonances of one residue and CO resonance of its preceding residue.

The additional resonance signals complicated the interpretation of the spectra. With only very few exceptions, the two sets of signals show very similar chemical shifts compared to the first assignment. But the line width of the additional signals is not significantly increased. The intensities of the additional signals increased over the time, therefore this phenomenon may be attributed to different conformations at higher sample concentrations (Figure 4.5). The line width of additional signals is not significantly increased.

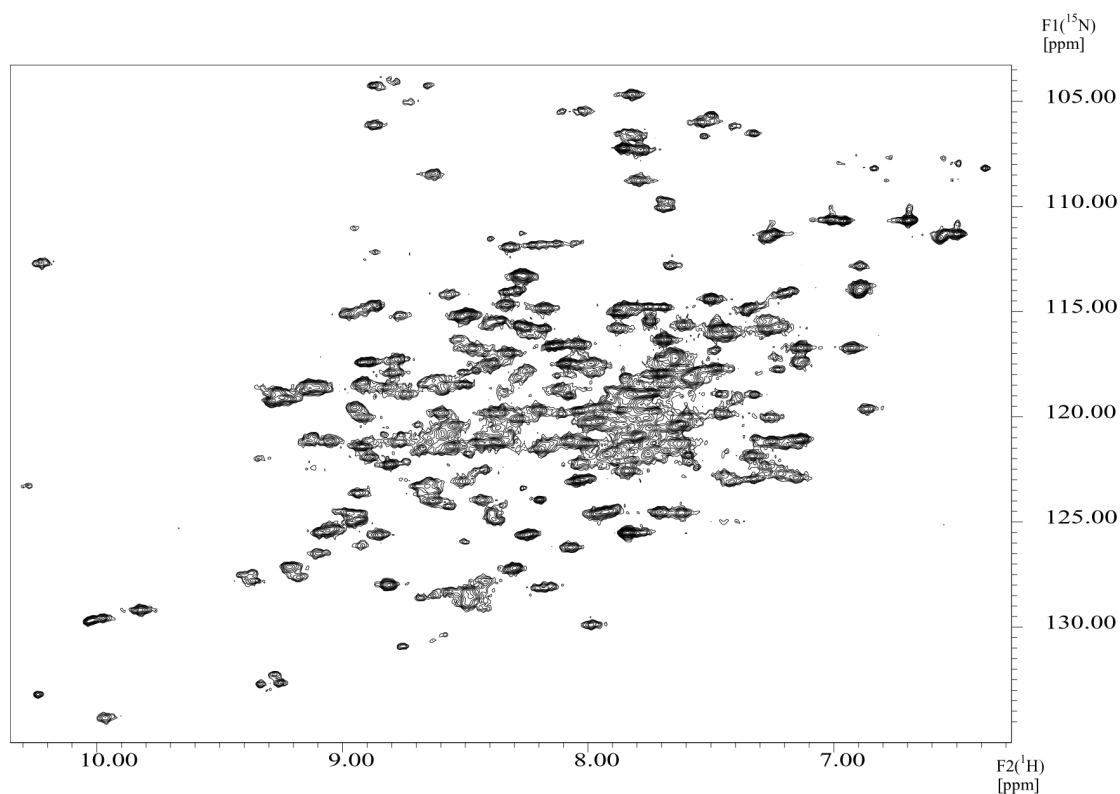


Figure 4.5 2D- $^1\text{H}$ ,  $^{15}\text{N}$ -HSQC spectrum of the Sud dimer at higher concentration (1mM dimer). Many additional signals appear at this higher concentration compared to the spectrum (Figure 4.3) of Sud at lower concentration (0.5 mM dimer).

However, protein samples remained unchanged with much longer time at lower sample concentrations ( $\leq 0.5$  mM dimer) (Figure 4.3). In addition, traces of oxygen influence the buffer in which Sud is dissolved. It decreases the amount of dissolved sulfur within the buffer and the yellow color of the sample fades out. Subsequently, the polysulfide sulfur chain bound to the single cysteine of each monomer of Sud will be shortened which might lead to the observation of different species of protein molecules within the sample.

The CSI program by Wishart et al. (1997) was used to determine consensus

chemical shift indices for all assigned residues (Figure 4.3). The data revealed an  $\alpha/\beta$ -protein with six  $\alpha$ -helices and six  $\beta$ -strands which are likely to be parallel in this case. Here, it appeared that the  $^{13}\text{C}\beta$  chemical shifts were not very informative with regard to the secondary structure elements, especially for the identification of the  $\beta$ -strands. Therefore, the consensus CSI for Sud was based on the  $^{13}\text{C}\alpha$ ,  $^1\text{H}\alpha$  and  $^{13}\text{CO}$  chemical shifts. The obtained secondary structure was consistent with results obtained from a secondary structure prediction using the amino acid sequence of Sud (<http://www.embl-heidelberg.de/predictprotein/> ; Fisher et al., 1999). Figure 4.6 shows the plots of CSI corresponding to the two different assignments of the deuterated sample (Figure 4.6 a and b). The first assignment of the protonated sample (Figure 4.6 c) shows different secondary structure predictions.

#### **4.1.2 Side chain resonance assignment**

Using the known backbone chemical shifts as a starting point, the majority of side chain  $^1\text{H}$  and  $^{13}\text{C}$  resonances could be assigned by a combination of one  $\text{CC}(\text{CO})\text{NH}$  (Figure 4.7) and one  $\text{CC}(\text{CA})\text{NH}$  experiments for aliphatic  $^{13}\text{C}$  resonance assignment as well as one  $\text{H}(\text{C})\text{CH-COSY}$  and one  $\text{H}(\text{C})\text{CH-TCOSY}$  (Figure 4.8) experiments for aliphatic proton resonance assignment. The  $\text{CC}(\text{CO})\text{NH}$  experiment correlates the amide  $^1\text{H}$  and  $^{15}\text{N}$  resonances of one residue with all aliphatic  $^{13}\text{C}$  spins of the preceding residue, while the  $\text{H}(\text{C})\text{CH-TCOSY}$  experiment correlates the given resonances of aliphatic  $^{13}\text{C}$  and its attached proton with all proton resonances within the same spin system. Table 4.2 lists the experiments used for the aliphatic side-chain resonance assignments.

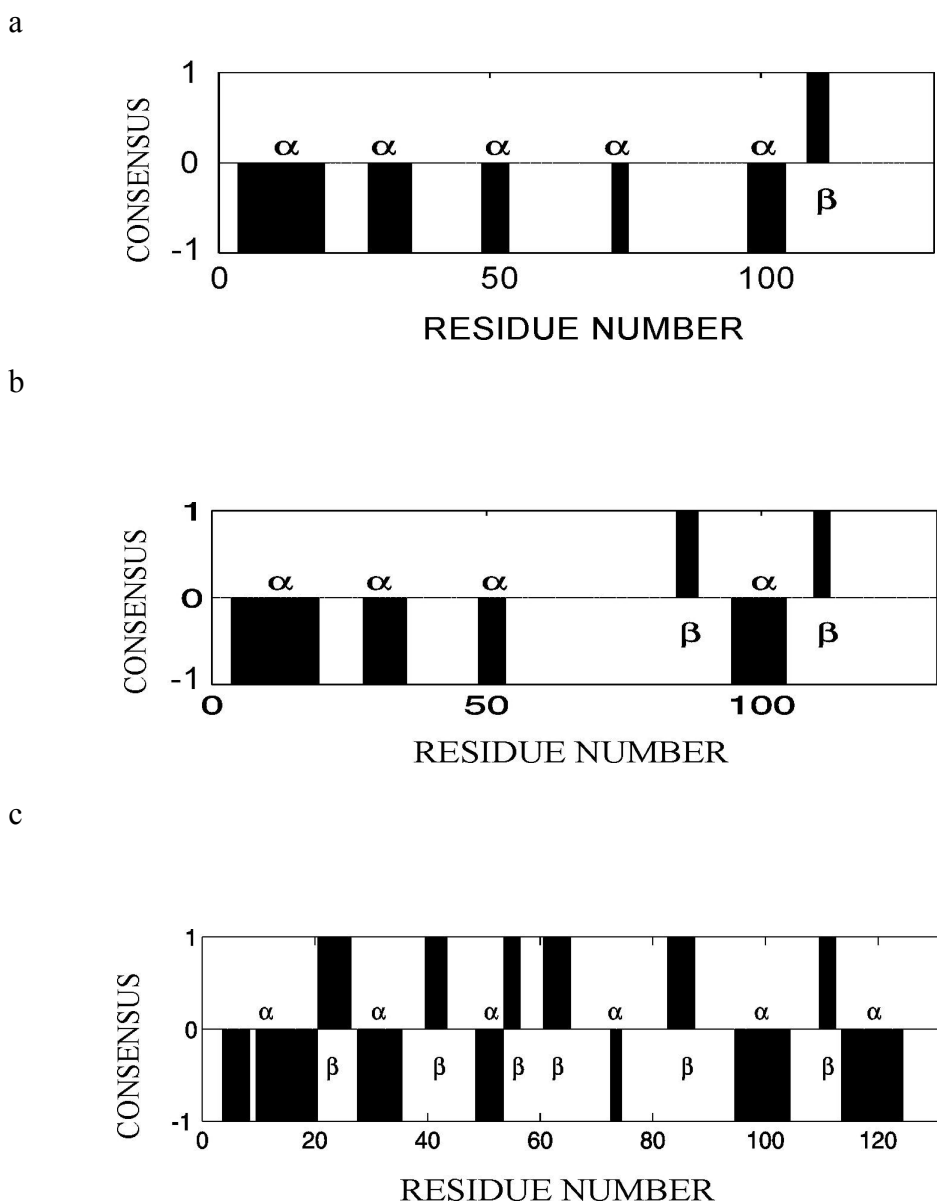


Figure 4.6 Consensus chemical shift indices derived from the  $^{13}\text{C}\alpha$ ,  $^{13}\text{C}\beta$  and  $^{13}\text{CO}$  resonances (a and b for the first and second sets of assignments, respectively) of the deuterated Sud sample and  $^{13}\text{C}\alpha$ ,  $^1\text{H}\alpha$  and  $^{13}\text{CO}$  (c) chemical shifts (for the first set of assignment) of the protonated sample, respectively.

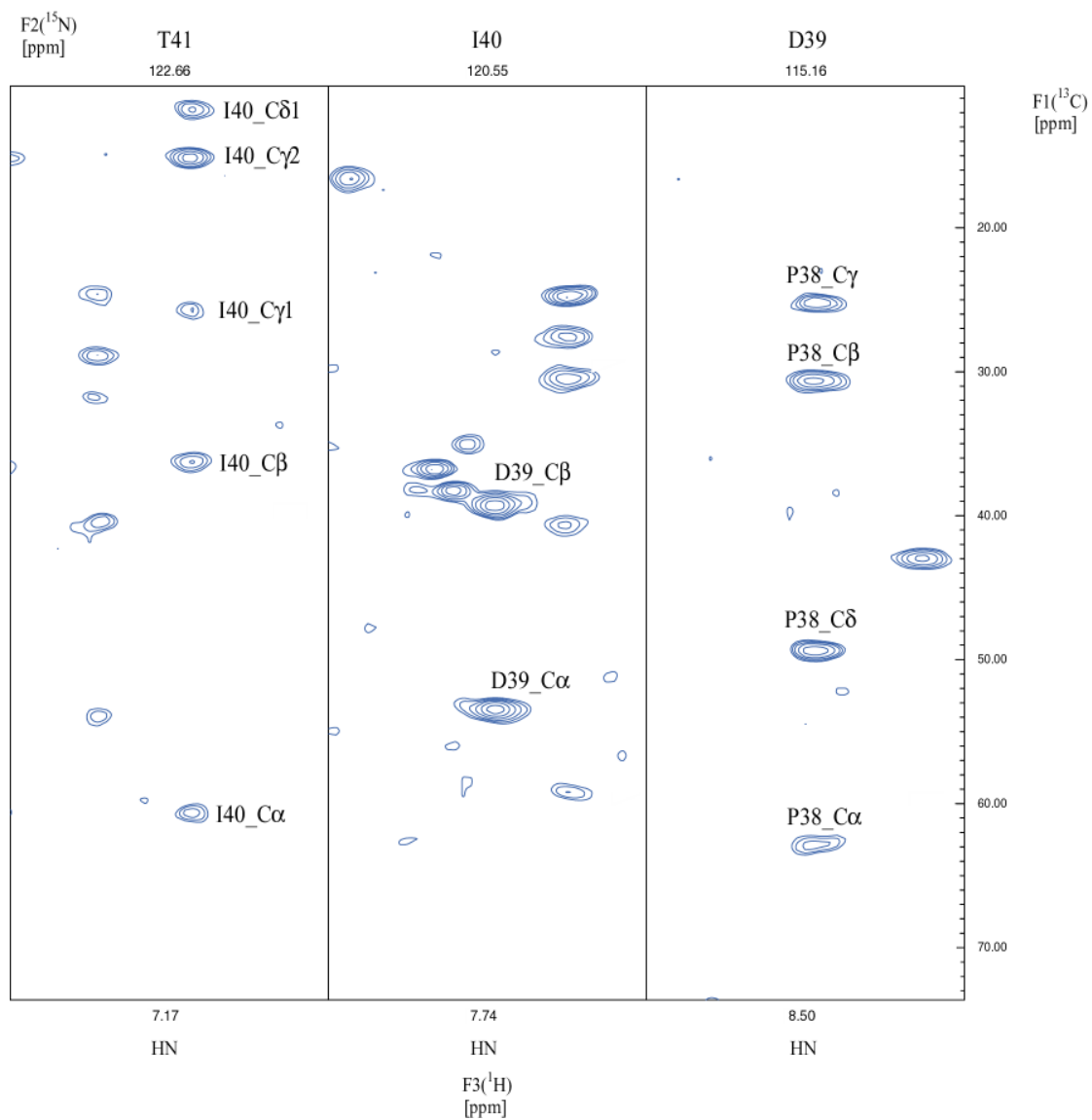


Figure 4.7. Selected regions from F1(<sup>13</sup>C)-F3(<sup>1</sup>HN) slices of a CC(CO)NH spectrum of <sup>2</sup>H/<sup>15</sup>N/<sup>13</sup>C-labeled Sud protein. This experiment correlates <sup>15</sup>N and <sup>1</sup>HN of Thr41, I40 and D39 with all aliphatic <sup>13</sup>C spins of their preceding residues.

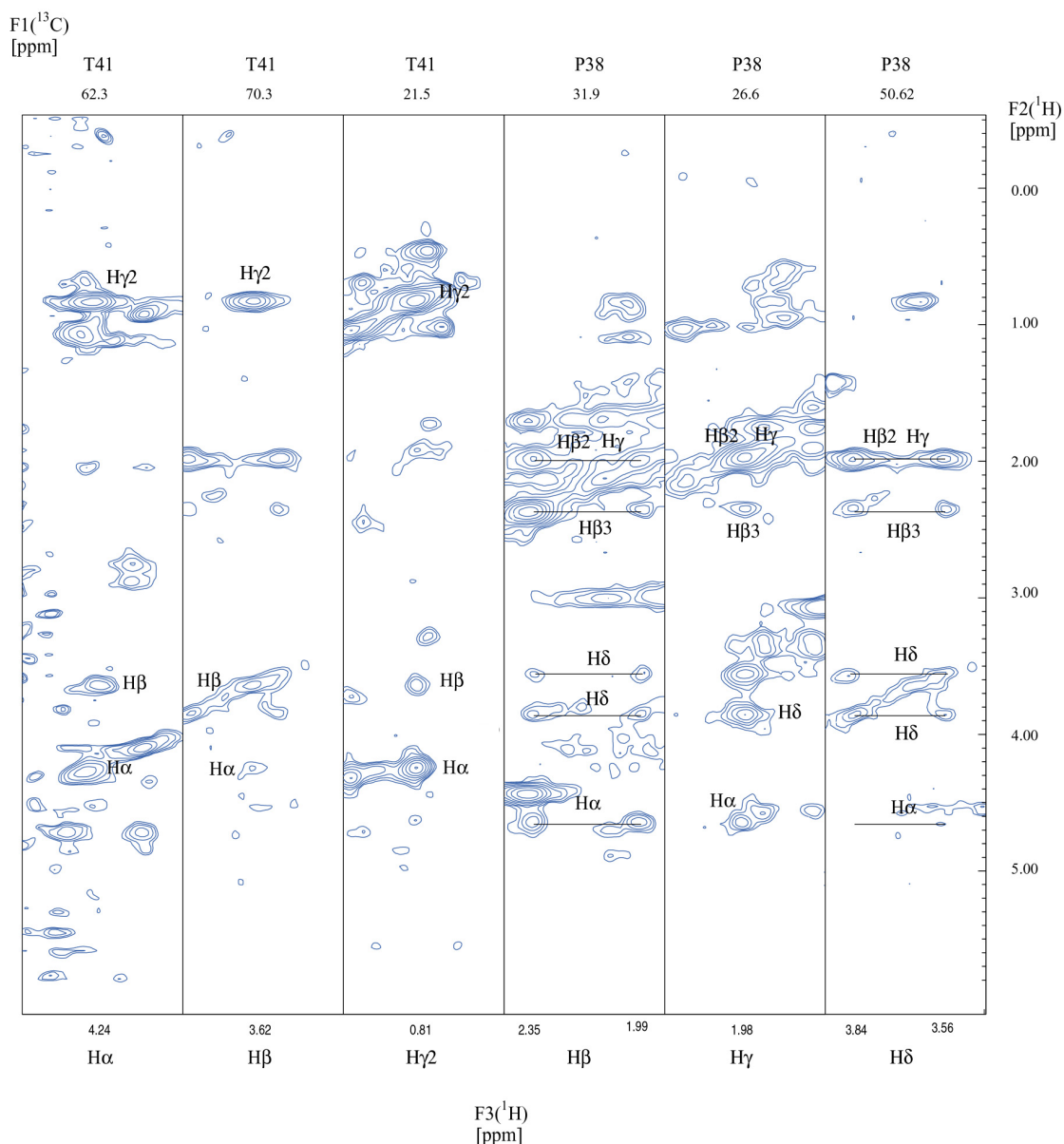


Figure 4.8. Selected regions from F1(<sup>13</sup>C) slices of a H(C)CH-TOCSY spectrum of <sup>13</sup>C-labeled Sud protein, showing correlations originating from <sup>1</sup>Hα, <sup>1</sup>Hβ, and <sup>1</sup>Hγ2 of Thr41 and <sup>1</sup>Hβ, <sup>1</sup>Hγ and <sup>1</sup>Hδ of Pro38.

Altogether, about 74% of the all protons were assigned. Stereospecific assignments of nearly all isopropyl groups from 21 Val and Leu residues were obtained, except Leu73. Most aromatic proton resonances were assigned except Hζ of Phe 88 and Phe 107 as well as the labil protons in the aromatic rings. Many aliphatic



proton resonances were missing because of the heavy overlap of signals in the 3D H(C)CH-COSY and H(C)CH-TOCSY spectra and some missing labile side chain protons which are not always observable. The Sud dimer protein contains 17 Lys, 14 Leu and one His tag for each monomer. It complicated the resonance assignments. The conventional 3D  $^{15}\text{N}$ -separated TOCSY HSQC failed because of the large molecular weight (30 kDa) of the dimer protein, which caused broad lines, and made the resonance assignments of side chains more difficult. Appendix A.1 and Appendix A.2 list the all assigned and missing chemical shifts, respectively. The resonances of the segment K90-R94 were not assigned because amide protons were not observed.

#### **4.1.3 Inter-monomer NOE assignments**

A total of 8 inter-monomer NOEs were unambiguously assigned using an asymmetrically labeled sample (see Materials and Methods). Due to the low concentration of the asymmetrically labeled sample, only few inter-monomer NOEs are available. The experimentally assigned resonances in contact regions between the two monomers involve mainly residues F7, D8, T10 and F11 of one monomer and A75 and Y105 of the other monomer. Figure 4.9 shows the slices from a  $^{15}\text{N}$ -resolved NOESY HSQC spectrum, in which the intermonomer NOEs were observed.

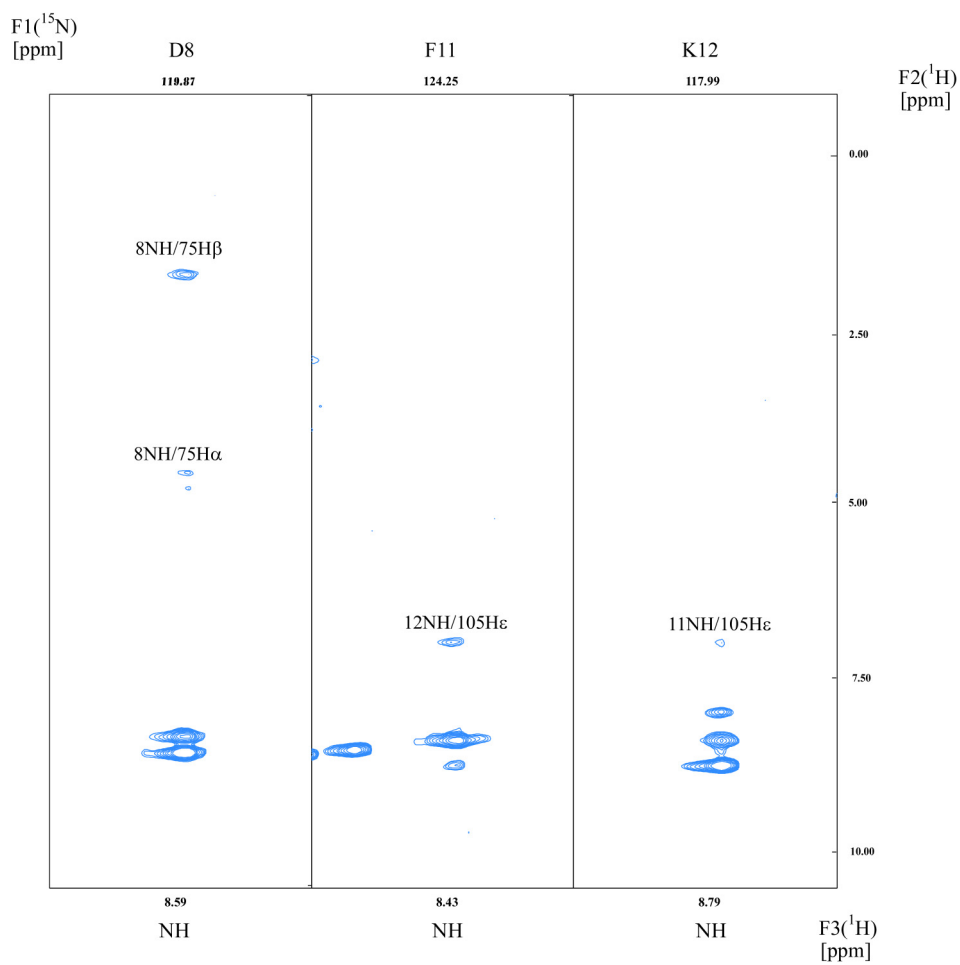


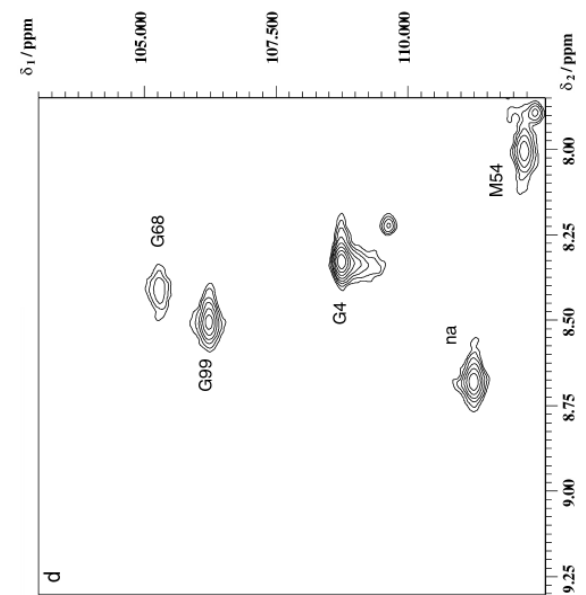
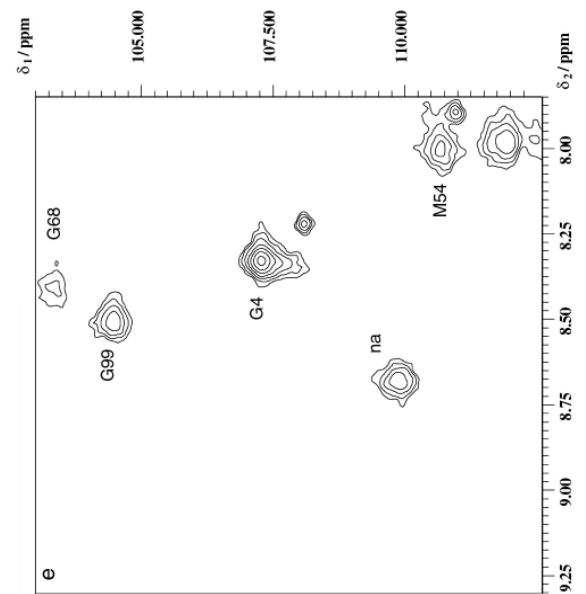
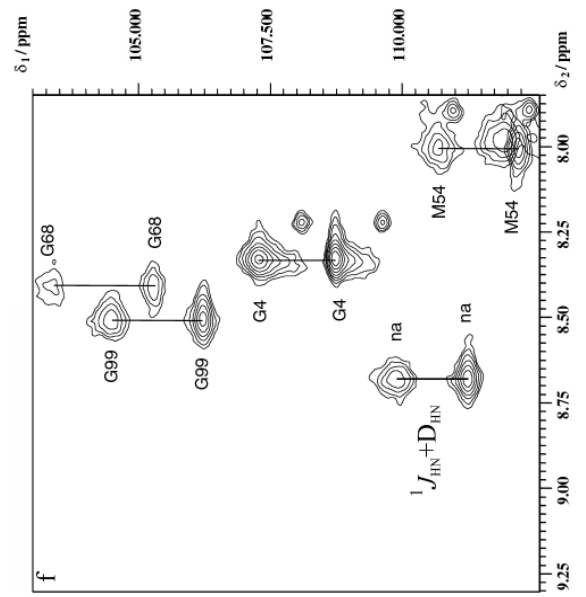
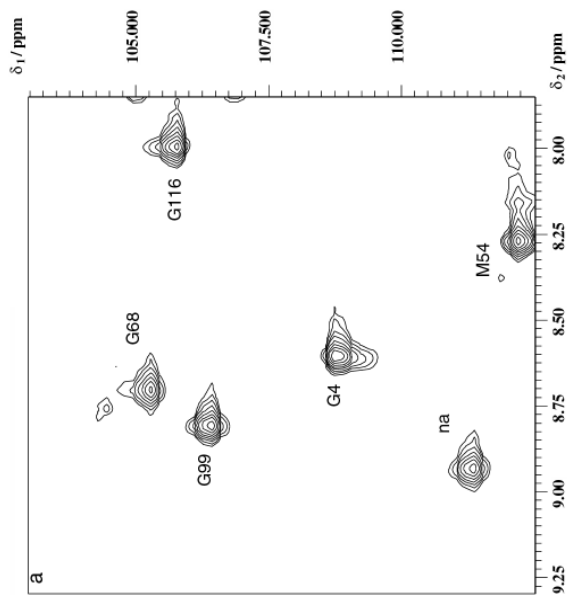
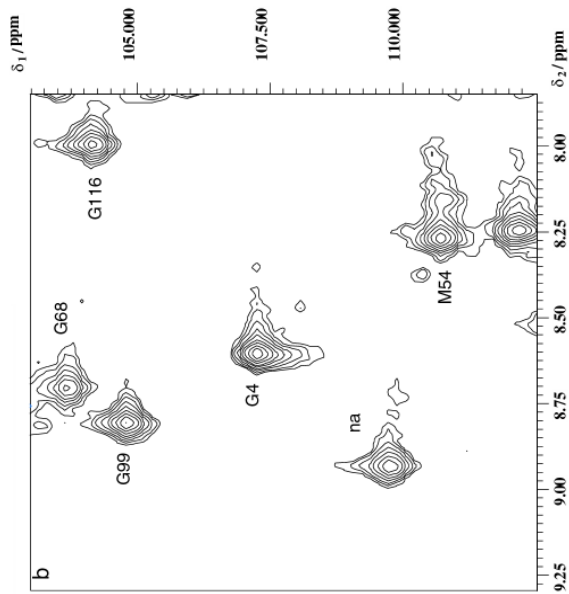
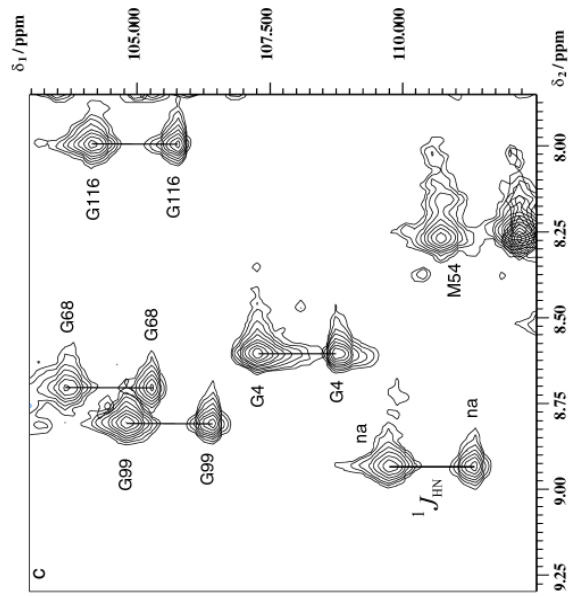
Figure 4.9. Selected regions of  $F2(^1\text{H})$ – $F3(^1\text{HN})$  slices at  $F1(^{15}\text{N})$  chemical shifts from a  $^{15}\text{N}$ -edited NOESY HSQC spectrum of Sud protein sample containing one  $^2\text{H}/^{15}\text{N}$ -labeled monomer and one unlabeled monomer. This experiment correlates NOEs between  $^1\text{HN}$  of one labeled monomer and  $^1\text{H}$  of another unlabeled monomer to provide inter-monomer NOEs.

## 4.2 Residual dipolar couplings

A total of 85 residual dipolar couplings were measured using a generalized version of the TROSY experiment on a non-orientated and orientated sample, respectively. Due to the overlap of the signals, it was impossible to measure all residual dipolar couplings. The generalized TROSY allows the editing of all four multiplet components of an HSQC cross peak recorded without heteronuclear decoupling. The four components can be edited in different subspectra by phase cycling and  $B_0$  gradients. Figure 4.10 shows subspectra using a non-orientated sample (a, b and c) and a orientated sample (d, e and f). The two subspectra show TROSY (a and d) and semi-TROSY signals (b and e). Figure 4.10c shows the difference in  $^{15}\text{N}$  frequency between the two subspectra a and b and provides  $^1J_{\text{NH}}$  couplings. Similarly, Figure 4.10f shows the difference in  $^{15}\text{N}$  frequency between the two subspectra d and e and provides the sum of  $(^1J_{\text{NH}} + D^{\text{NH}})$ . The values of residual dipolar coupling restraints  $D^{\text{NH}}$  were derived via measuring the coupling difference between  $(^1J_{\text{NH}} + D^{\text{NH}})$  coupling and  $^1J_{\text{NH}}$  scalar coupling.

---

Figure 4.10. Selected regions of generalized TROSY subspectra without heteronuclear decoupling. (a) and (b) show high and low field components in  $^{15}\text{N}$  frequency out of four components of  $^{15}\text{N}$ - $^1\text{H}$  cross peaks of amide groups using a non-orientated sample, while (d) and (e) using a oriented sample. The differences in  $^{15}\text{N}$  frequency between the two subspectra (a) and (b) as well as (d) and (e) provide the  $^1J_{\text{NH}}$  coupling (c) and the sum of  $(^1J_{\text{NH}} + D^{\text{NH}})$  (f), respectively.



### 4.3 Automatic NOE assignment and structure determination

The dimer structure was calculated *de novo* in a first iteration using 167 predefined  $\phi$  and  $\psi$  angle constraints derived from the TALOS program, 250 sequential, medium, and long range backbone-backbone and backbone-side chain NH–NH distance restraints derived from a 4D  $^{15}\text{N}/^{15}\text{N}$ -separated NOESY, 2\*17 hydrogen bond restraints between parallel  $\beta$ -strands, and 8 experimental inter-monomer restraints as additional restraints for each monomer, but no residual dipolar coupling restraints. After 9 iterative NOE assignments and structure calculations, NOE distance restraints were derived from ARIA. The unambiguous inter-monomer NOEs were searched in the spectra. Altogether, 1082 ambiguous and 4294 unambiguous NOEs, including 216 unambiguous intermonomer NOEs, were obtained with the ARIA program. These NOE-derived distance restraints and the restraints used in iteration 0, together with 158 N-H residual dipolar coupling restraints (for both monomers) used in the refinement of the relative orientation of the two monomers, were employed as input to generate an ensemble of 20 best structures with lowest energy and fewest dipolar coupling violations out of 200 calculated structures.

## 4.4 Dipolar coupling data for refinement and relative orientation

*Comparison of structures refined with and without residual dipolar coupling restraints* The structural statistics for the final 20 simulated annealing structures of Sud are summarized in Table 4.3. The ribbon representations and the best-fit superpositions of the backbone atoms for the polysulfide free structures refined with and without residual dipolar coupling (rdc) restraints are shown in Figure 4.11a,b. Incorporation of residual dipolar coupling restraints improves the relative orientation of the two monomers significantly. The rdc-refined structure shows a more compact form compared to the structure without rdc refinement. The r.m.s.d. values for all backbone heavy atoms drop from 0.97 to 0.66 for the rdc-refined ensemble (Table 4.3). The rdc-refined structures were generally better defined, with increased overall precision (Figure 4.11b). In addition, the secondary structure elements (seven helices and seven  $\beta$ -strands) of the two monomers in the rdc-refined ensemble are consistent with each other in terms of both length and sequence location, while in the ensemble without rdc restraints the secondary structure elements show minor differences, such as E71-S77 (helix) and A93-R94 (helical turn) in one monomer corresponding to E71-L74 (helix) and A93-R94 (random coil) in another monomer.

Comparing the monomer structures between the two ensembles with and without residual dipolar coupling restraints, the core regions (residues 21-129) are nearly superimposable (Figure 4.11c). Between the two ensembles the r.m.s.d. value of the core region is 0.59 for the backbone atoms, but only 0.49 if excluding the segment between residues 90-94 (Table 4.3), which belongs to the loop 89-95. The secondary structure elements are similar, except that residues P27-E36 (helix) and S66-L70 (random coil) in rdc-refined ensemble show an apparent difference

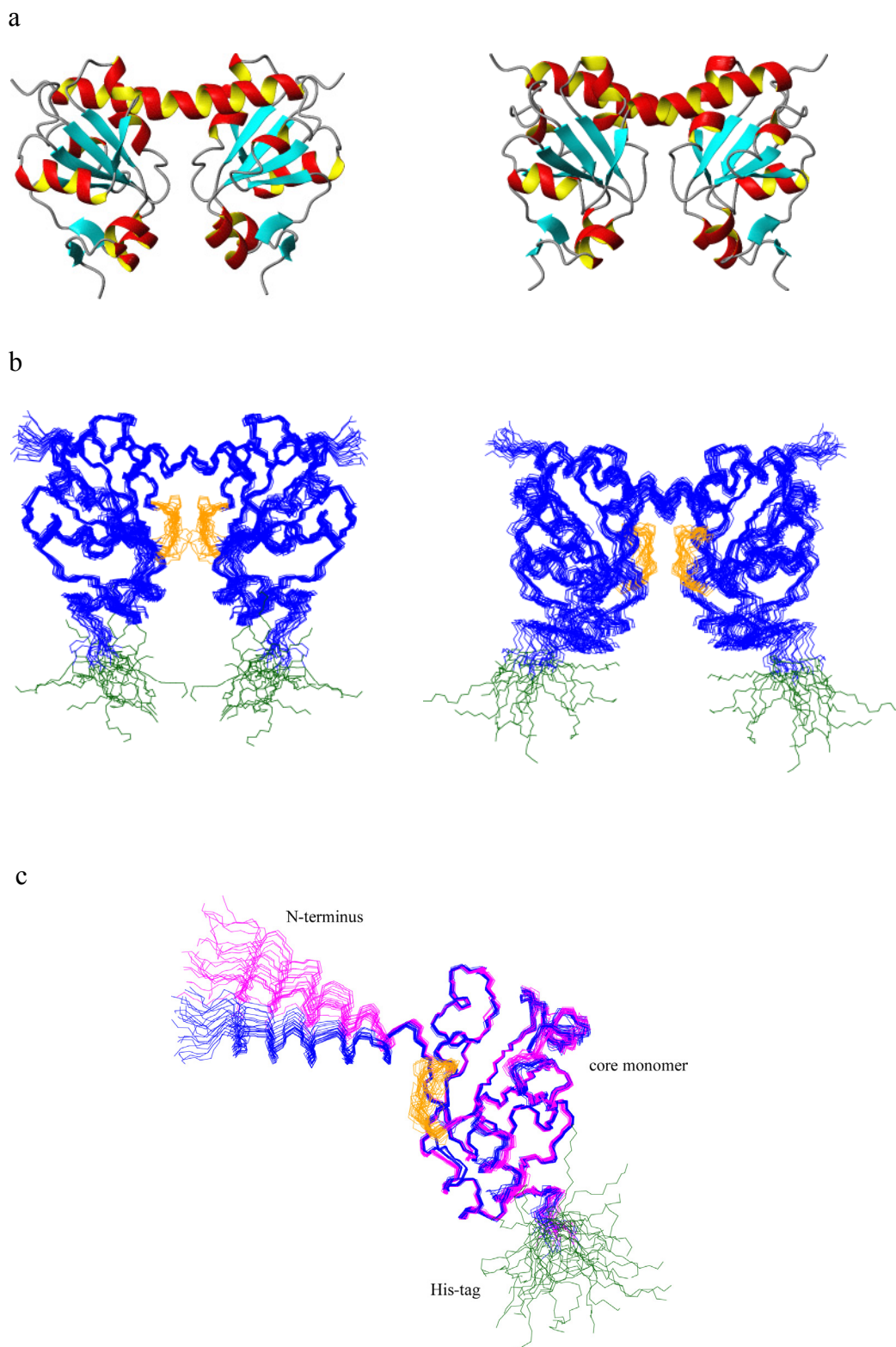


Figure 4.11. The structure of the Sud protein. (a) The ribbon representation of the polysulfide-free Sud structure refined with (left) and without (right) residual dipolar coupling restraints. The relative

orientation between the two monomers apparently changes. The His-tag is not shown here. (b) 20 best conformers with backbone atoms superimposed. The poorly defined segment, residues 90-94, and the His-tag are shown in dark orange and dark green, respectively. The ensemble refined with residual dipolar coupling restraints (left) shows better convergence. (c) Superposition of core regions of both ensembles with (blue) and without (magenta) residual dipolar coupling restraints. The core regions (residues 21-129) are nearly identical. The N-terminus of the blue ensemble converges better and shows an orientation different from that of the magenta ensemble.

compared with residues A30-E34 (helix) and R67- K69 (helix) in the ensemble without rdc refinement. This indicates that the monomer structures of the two ensembles are quite similar. The main difference of the dimer structures is the relative orientation between the two monomers. These results show that residual dipolar coupling restraints improve not only the precision of the structures, but also the relative orientation of the two monomers.

*Comparison of rdc-refined Sud structures with and without polysulfide* The rdc-refined structures bound with polysulfide (Sud-[S]<sub>5</sub><sup>-</sup> and Sud-[S]<sub>10</sub><sup>-</sup>) are highly similar to the rdc-refined ligand-free Sud structure. The location and length of secondary structure elements are identical for these three protein forms, except for the N-terminal helix. Some of the structures show a shorter helical range from residue F7 to D21, whereas in the other ones it is slightly longer from G4 to D21. This is due to missing sequential and medium-range NOEs for residues A1, D2 and M3. The rdc-refined tertiary structures with and without polysulfide are well superimposable. Table 4.3 summarizes the r.m.s.d. values of the protein backbone atoms. The r.m.s.d. values between Sud and Sud-[S]<sub>5</sub><sup>-</sup> are 0.76 for the backbone atoms and 1.07 for the heavy atoms (Table 4.3). Excluding the segment between residues 90-94, the r.m.s.d. values



drop down to 0.64 and 0.95 for the backbone and heavy atoms, respectively, thus evidencing the close structural similarity between the two ensembles.

For the structures with ten polysulfide sulfur atoms bound, only seven best structures with lowest energy and without residual dipolar coupling violation larger than 1 Hz were collected. Due to the longer chain of the polysulfide, which causes a worse convergence in the structure calculation. The segment between residues 90-94 is poorly defined due to the lack of experimental restraints. NOE restraints are missing in this segment, since no proton resonances could be assigned. The structural quality of the structure ensembles was examined with the program PROCHECK\_NMR (Laskowski *et al.*, 1996). The Ramachandran plot statistics for all ensembles are listed in Table 4.3. Considering that this analysis includes the poorly defined segment between residues 90-94, the result is quite satisfactory.

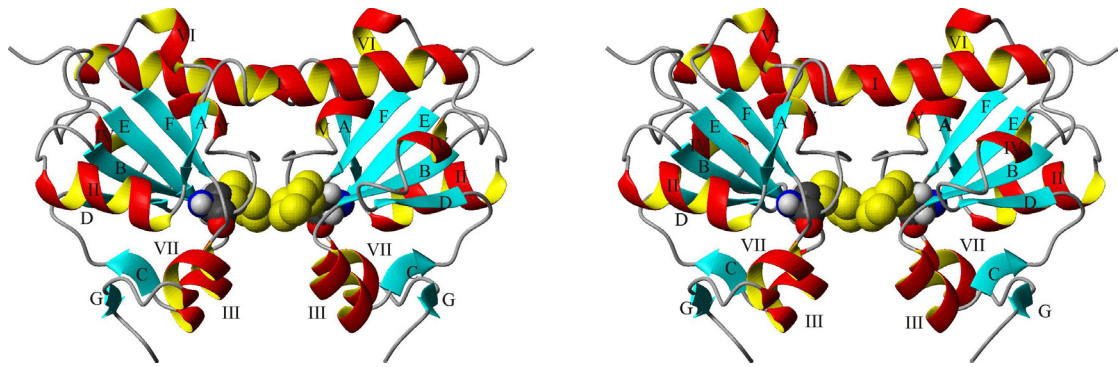
## 4.5 Description of the structure

Figure 4.12 shows a ribbon representation of the solution structure of the Sud dimer. The protein is an  $\alpha/\beta$ -protein with dimensions  $60 \text{ \AA} \times 30 \text{ \AA} \times 40 \text{ \AA}$  and has a twofold symmetry. Each monomer contains seven helices (helix I through helix VII) and seven  $\beta$ -strands ( $\beta$ A- $\beta$ G), of which  $\beta$ A,  $\beta$ B,  $\beta$ D,  $\beta$ E and  $\beta$ F form a five-stranded parallel  $\beta$ -sheet, while  $\beta$ C and  $\beta$ G form a two-stranded antiparallel  $\beta$ -sheet. The  $\beta$ -strands are formed by residues 23-25 ( $\beta$ A), 41-45 ( $\beta$ B), 56-57 ( $\beta$ C), 62-65 ( $\beta$ D), 85-88 ( $\beta$ E), 110-113 ( $\beta$ F), and 127-128 ( $\beta$ G) within each subunit. Helices are observed at residues 4-21 (I), 27-36 (II), 48-54 (III), 71-74 (IV), 96-99 (V), 101-104 (VI), and 117-122 (VII). The two polysulfide chains bound to the cysteine of each monomer point in opposite directions. The S $\gamma$  distance from the two cysteines in each monomer is between  $8.8 \sim 12.6 \text{ \AA}$  in the rdc-refined ensemble, but  $11.7 \sim 17.9 \text{ \AA}$  in the ensemble without rdc refinement.

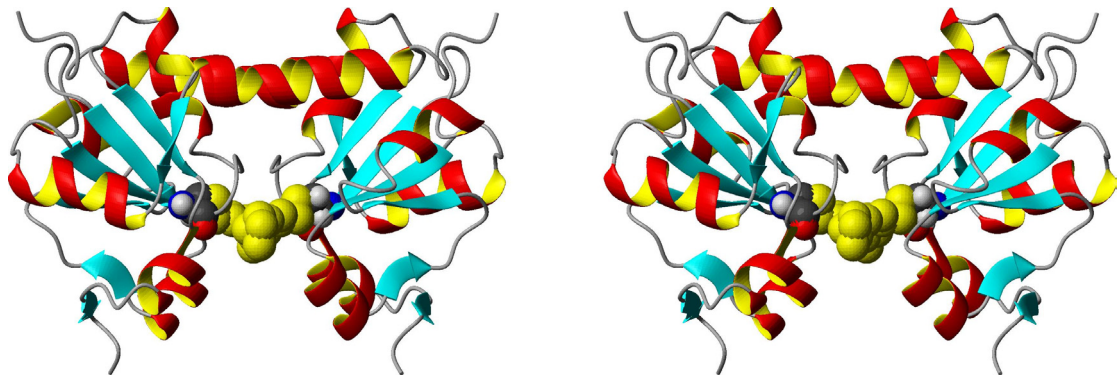
In Figure 4.12c, the two helices I are parallel to each other. An interaction between the two helices I is not observed. The helix I (N-terminus) interacts with helix V' (Figure 4.12a) to form a four-helix bundle by packing helix I and helix V' as well as helix I' and helix V together. In addition, helix I and helix IV' are packed together. These helix packings between two subunits stabilize the dimer structure.

Based on the intermonomer NOEs assigned by ARIA, the residues participating in the interaction between the two monomers are mainly F7, F11 and V15, located at the hydrophobic side of helix I, as well as L74, A75, L79, L97 and Y105. Hence, mainly hydrophobic interactions are involved in stabilizing the dimer structure. For example, the aromatic side-chains of F7' and F11' interact with Y105 and the methyl groups of L74, while F11' and V15' interact with L97. Due to the interactions with

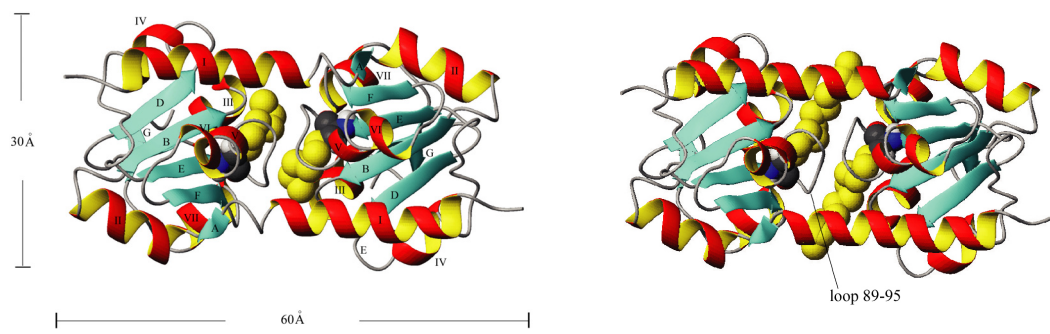
a



b



c



aromatic rings, the H $\delta$  resonances of L74 and L79 are shifted to higher field between +0.2 and -0.1 ppm.

---

Figure 4.12. Ribbon representation of the Sud protein structure. Panels a and b show stereo view of the complexes with five (a) and ten (b) polysulfide sulfur atoms refined with residual dipolar coupling restraints, respectively. The twofold axis of the symmetry is parallel to the plane of the paper. The helices I of each monomer are parallel to each other. The two polysulfide chains located at each monomer point in opposite directions. (c) presents the top view of (a) and (b) on the left and right hand side, respectively. The active-site loop between residues 89-95 shows a semicircular conformation and the polysulfide chains with ten sulfur atoms (right) extends to the protein surface.

## 4.6 Structure-function relationship

Sud protein would serve as a sulfur transferase, transferring sulfur from aqueous polysulfide to the active site of polysulfide reductase, which is exposed to the periplasmic side of the cytoplasmic membrane of *W. succinogenes*. It consists of two identical subunits, each with a single cysteine residue. Each cysteine binds up to 10 polysulfide-sulfur atoms, but mainly to five atoms. Replacement of the single cysteine by serine in the Sud monomer caused a complete loss of activity.

The active-site environment of Sud illustrates the similarity to that in rhodanese (Bordo, *et al.* 2000). The active-site loops of 13 out of 20 best structures adopt a semicircular, cradle-like, conformation, similar to Rhodanese. Figure 4.13 (13 structures) represents the environment of the active site Cys89-[S]<sub>5</sub><sup>-</sup>, in which cysteine binds five polysulfide-sulfur atoms. The side chains are dispersed due to the absence of NOEs. The catalytic Cys is located at the first residue of the 89 to 95 loop, connecting the βE strand to helix V (Figure 4.12a). The C89, R46, E50, T91 as well as R67, R94, K90 in Sud correspond to C230, R235, E173, T232 as well as W195, H234, Q231 in rhodanese, respectively. The positively charged R94 and K90 in Sud correspond to the positively charged H234, Q231 in rhodanese and in a similar way R67 by W195, respectively. The positively charged side chains of R46, R67 and R94 of Sud protein interact and stabilize the negatively charged polysulfide, while the negative charge of the side chain of E50 interacts with R46 (Figure 4.14). Residue R67 may be flexible and hence may be able to interact with polysulfide molecules of different length up to ten sulfur atoms. The mutation of one of the three arginines leads to a loss of sulfur-transfer activity (data not yet published). The amino acid

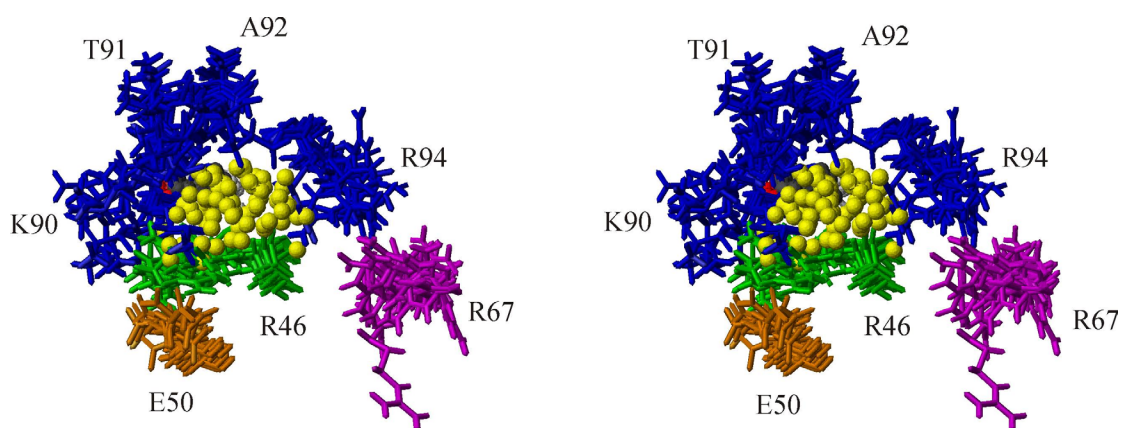


Figure 4.13. Stereo view of the 13-member representative ensemble of the active-site environment for the Sud protein bound with five polysulfide sulfur atoms. The polysulfide side chain is shown in yellow. The lack of the NOEs involved in these residues results in the dispersion of the side chains.

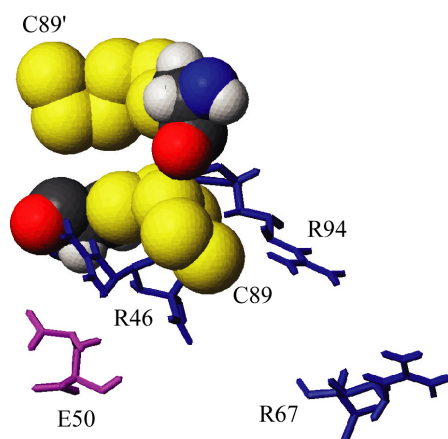


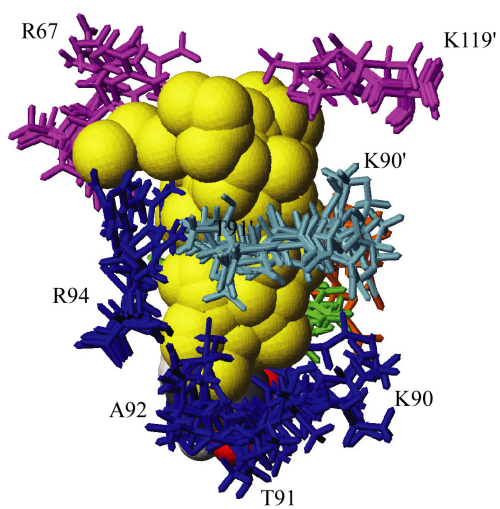
Figure 4.14. Interaction between the polysulfide and functionally important Arg residues. The positively charged R46, R67, and R94 (blue) interact with negatively charged polysulfide (yellow). C89' is also shown to emphasize the relative position to C89.

sequence alignment of rhodanese from *A. vinelandii*, *P. aeruginosa* and Sud from *W. succinogenes* shows that C89, R46, E50, R67, T91 and R94 in Sud are conserved in the other two proteins as well (data not shown).

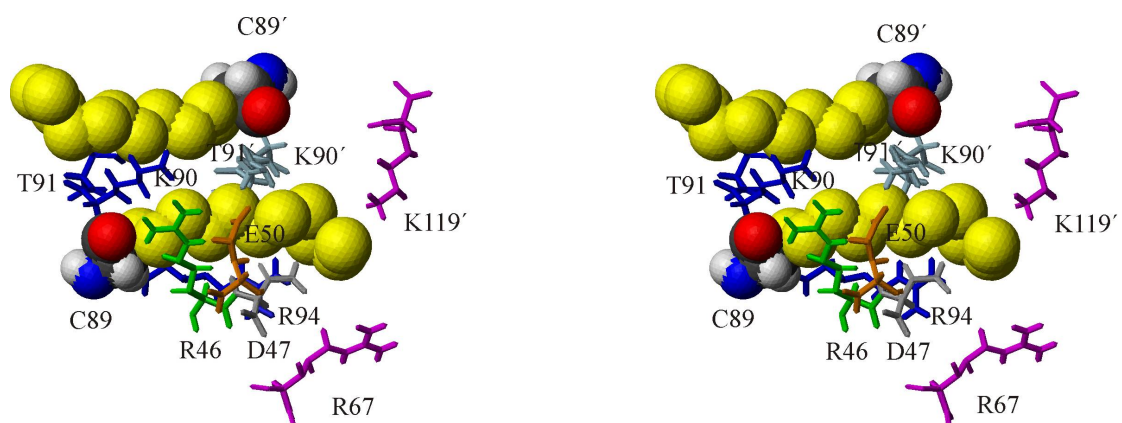
In order to understand the pathway of polysulfide or sulfur atom(s) transfer, the structure bound with 10 polysulfide sulfur atoms were calculated. Residues R46, D47, E50, K90, T91, A92, R94, K90', T91' and K119' form a channel and surround the C89-bound polysulfide (Figure 4.15), which allows a precise positioning of the extending polysulfide from the inside of the protein to residues R67 and K119' which are located at the surface of the Sud protein (Figure 4.16). According to the shifts of resonance peaks when comparing the HSQC spectra of Sud and Sud-polysulfide reductase samples, respectively, residues R67 and K119' are possible partners for the interaction with polysulfide reductase. This indicates that a polysulfide-sulfur atom(s) transfer may occur from Sud to the active site of polysulfide reductase via residues R67 and K119'. T91 corresponds to T232 located at the active-site loop in rhodanese and may play a role in forming a certain conformation to keep the polysulfide (Figure 4.15c).

K90, T91 and R94 participating in the interaction with the active center are located in the segment 90-94, in which resonances could not be assigned. This may be due to the flexibility of this segment. The same problem occurred for R46, R67 and C89. Neither  $^1\text{H}$  (except  $\text{H}\alpha$  of R46, R67 and C89) nor  $^{13}\text{C}$  resonances (except  $\text{C}\beta$  and  $\text{C}\delta$  of R46) of corresponding backbones and side chains were assigned, even in the well resolved 3D CC(CO)NH, CC(CA)NH experiments. This result may indicate the flexibility of these residues.

a



b



c

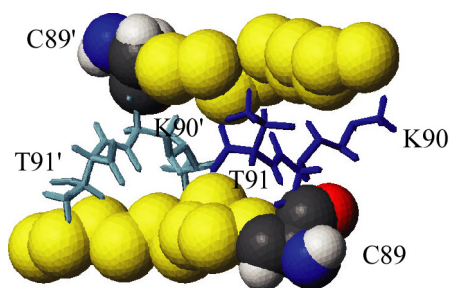




Figure 4.15. (a) Side chain orientations of residues that surround the polysulfide chain. The ensemble consists of seven structures. Residues R46 (green) and E50 (dark orange) are on the back side. (b) As in (a) but stereo viewed from a different direction and only one structure is shown. C89' is also shown to emphasize the relative position to C89. (c) T91 and K90 of one monomer form a conformation to hold the polysulfide chain of another monomer.

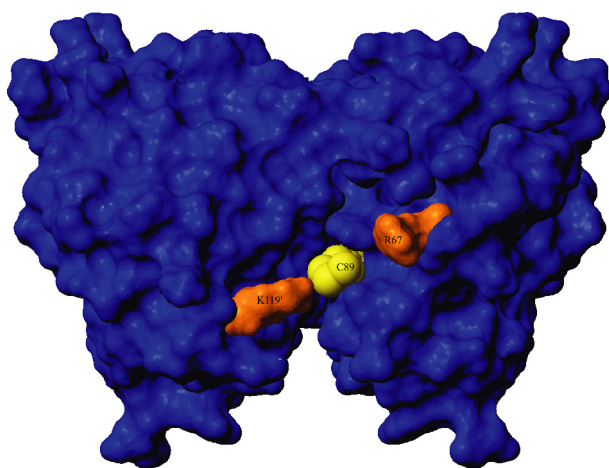


Figure 4.16. Surface diagram of the Sud protein bound to ten polysulfide sulfur atoms. The polysulfide (yellow) exposes from inside the protein to the surface. The positively charged residues R67 and K119' (dark orange) interact with the negatively charged polysulfide and may also contact with polysulfide reductase, which indicates that the polysulfide or sulfur atom(s) may be transferred from Sud to polysulfide reductase via residues R67 and K119'.

Table 4.3  
*Structural statistics of the solution structure ensembles of Sud*

	without rdc-refined	rdc-refined	rdc-refined bound with [S] <sub>5</sub> <sup>-</sup>
Restrains statistics			
NOE-derived distance restraints	5376	5376	5376
Intramonomer unambiguous	4078	4078	4078
Intermonomer unambiguous	216	216	216
ambiguous	1082	1082	1082
Hydrogen bonds	34*2	34*2	34*2
Dihedral angle restraints	334	334	334
Residual dipolar coupling restraints	158	158	158
Restrict Violations *			
NOE violations			
0.20 – 0.23 Å	0	4	4
0.23 – 0.28 Å	0	0	2
Dihedral angle violations			
5.0 – 5.7 degree	0	10	6
5.7 – 6.6 degree	0	0	2
Residual dipolar coupling violations			
> 1 Hz	--	0	0
R.m.s.d. (Å) <sup>d</sup> from mean structures			
Backbone atoms (residues 3-129)	0.99	0.76	0.72
All heavy atoms (residues 3-129)	1.40	1.28	1.28
Backbone atoms (residues 3-89; 95-129)	0.97	0.66	0.60
All heavy atoms (residues 3-89; 95-129)	1.37	1.14	1.14
Ramachandran plot analysis (%)			
most favored regions	84.2	81.4	81.2
additionally allowed regions	14.5	16.3	16.0
generously allowed regions	0.40	1.20	1.50
disallowed regions	0.90	1.10	1.40

Sud with <i>versus</i> without rdc-refined, r.m.s.d. (Å) <sup>a,m</sup>	
Backbone atoms (residues 21-129)	0.59
All heavy atoms (residues 21-129)	1.19
Backbone atoms (residues 21-89; 95-129)	0.49
All heavy atoms (residues 21-89; 95-129)	1.07

Refined Sud <i>versus</i> refined Sud-[S] <sub>5</sub> <sup>-</sup> , r.m.s.d. (Å) <sup>a,d</sup>	
Backbone atoms (residues 3-129)	0.76
All heavy atoms (residues 3-129)	1.30
Backbone atoms (residues 3-89; 95-129)	0.64
All heavy atoms (residues 3-89; 95-129)	1.15

---

<sup>a</sup> All 20 structures of one ensemble superimposed to all 20 structures of another ensemble.

<sup>d</sup> The r.m.s.d. values were calculated for dimer structures.

<sup>m</sup> The r.m.s.d. values were calculated for monomer structures.

\* The number of violation represents the total number of restraint violations from 20 structures.

## 5 Summary

Periplasmic Sud protein encoded by the *Wolinella succinogenes* catalyses the transfer of bound polysulfide-sulfur to the active site of the membrane bound polysulfide reductase. The homodimeric protein consists of 131 residues per monomer, each with one cysteine residue in the active site. Polysulfide-sulfur is covalently bound to the catalytic Cys residues of the Sud protein. In order to understand the structure-function relationship of this protein, the features of its solution structure determined by heteronuclear multidimensional NMR techniques are reported here. The first step of structure determination leads to resonance assignments using  $^{15}\text{N}/^{13}\text{C}/^2\text{H}$ - and  $^{15}\text{N}/^{13}\text{C}$ -labeled protein. The sequential backbone and side chain resonance assignments have been successfully completed.

Structure calculations were carried out using the ARIA program package. The structure is based on 2688 NOE-derived distance restraints, 68 backbone hydrogen bond restraints derived from 34 slow-exchanging backbone amide protons and 334 torsion angle restraints obtained from the TALOS program as well as 158 residual dipolar coupling restraints for the refinement of relative vector orientations. The three-dimensional structure of the Sud protein was determined with an averaged root-mean-square deviation of 0.72 Å and 1.28 Å for the backbone and heavy atoms, respectively, excluding the terminal residues. Without the poorly defined segment between residues 90-94 the average r.m.s.d. value drops down to 0.6 Å and 1.14 Å. The ensemble refined with residual dipolar coupling (rdc) restraints shows good convergence. The r.m.s.d. value for the backbone heavy atoms, excluding residues 90-94, drops down from 0.97 to 0.66 for the rdc-refined ensemble. The relative orientation of the two monomers in the protein structures refined with residual dipolar coupling restraints are also different from those without residual dipolar coupling

restraints.

The structure determination of the dimeric protein has been hampered by the high molecular mass (30 kDa), severe peak degeneracy, and by the small number of experimental intermonomer NOEs (relative orientation problem of two monomers). For the resonance assignments of aliphatic side chain, many resonances were ambiguously assigned because of severe overlap of signals. The Sud dimer protein contains 17 Lys, 14 Leu and one His tag for each monomer. It complicated the resonance assignments. The conventional 3D  $^{15}\text{N}$ -separated TOCSY HSQC experiment failed because of the large molecular weight which results in line broadening and hence made the resonance assignments of side chains more difficult.

The determined structure contains a five-stranded parallel  $\beta$ -sheet enclosing a hydrophobic core, a two-stranded anti-parallel  $\beta$ -sheet and seven  $\alpha$ -helices. The dimer structure is stabilized predominantly by hydrophobic residues.

Sud catalyses the transfer of the polysulfide-sulfur to cyanide, similar to rhodanese encoded by *Azotobacter vinelandii* (Bordo *et al.*, 2000). The two proteins are similar in the active site environment primarily owing to the main-chain conformation of the active-site loop with the cysteine residue and with respect to the surrounding positively charged residues. The active-site loop (residues 89-95) in the Sud protein appears to be flexible, reflected by few assigned proton resonances of residues 90-94 in the active site. Despite their similarity in function and their similar structure in active site, the amino acid sequences and the folds of the two proteins are remarkably different. The negatively charged polysulfide interacts with positively charged R46, R67, and R94 and hence may be stabilized in structure. The mutation of one of the three arginines that are also conserved in rhodanese from *A. vinelandii* leads to a loss of sulfur-transfer activity. The polysulfide chain extends from inside of

Sud protein to outside, where Sud may form contacts with polysulfide reductase. These contacts provide the possible polysulfide-sulfur transfer from Sud protein to the active site of polysulfide reductase.

## 5. Zusammenfassung

Das periplasmische Sud-Protein aus *Wolinella succinogenes* überträgt den gebundenen Polysulfidschwefel in das aktive Zentrum der membrangebundenen Polysulfidreduktase. Das homodimere Protein enthält 131 Aminosäurereste pro Monomer. Im aktiven Zentrum des Monomers ist eine freie Cysteingruppe angeordnet. Das Polysulfid ist kovalent an dieses katalytische Cystein des Sud-Proteins gebunden. Für das Verständnis der Struktur und Funktion dieses Proteins wurde die Lösungsstruktur mit heteronuclearer, multidimensionaler NMR-Spektroskopie ermittelt. Im ersten Schritt der Strukturbestimmung wurden die  $^{15}\text{N}$ ,  $^{13}\text{C}$ - und  $^1\text{H}$ -Resonanzen der in den stabilen Isotopen angereicherten Proteinspezies zugeordnet.

Die Rückgratresonanzen der  $^1\text{HN}$ ,  $^{15}\text{N}$ ,  $^1\text{H}\alpha$ ,  $^{13}\text{C}\alpha$ , und  $^{13}\text{CO}$ -Atome (sowie der  $^1\text{H}\beta$ - und  $^{13}\text{C}\beta$ -Seitenkettenatome) wurden mit Hilfe verschiedener Tripleresonanz-Experimente zugeordnet. Unter anderem wurden HNCACB-, HN(CA)CO-, HNCO-, HN(CA)N-, HNCA-, HNCO-, und HCACO-Experimente verwendet. Die sequenzielle Zuordnung der Resonanzen des Proteinerückgrats war annähernd vollständig, mit Ausnahme der Resonanzen der Reste 90-94. Aus CC(CO)NH- und CC(CA)NH-Experimenten für aliphatische  $^{13}\text{C}$  Resonanzen und H(C)CH-COSY- und H(C)CH-TOCSY-Experimenten für aliphatische Protonresonanzen wurden die Seitengruppenatome ( $^1\text{H}$  und  $^{13}\text{C}$ ) zugeordnet. Mit Hilfe eines zwei-dimensionalen homonuklearen NOESY-Spektrums und eines zwei-dimensionalen homonuklearen TOCSY-Spektrums einer unmarkierten Probe in  $\text{D}_2\text{O}$  ließen sich die Resonanzen von aromatischen Protonen zuordnen. Stereospezifische Zuordnungen der Isopropylgruppen von Val- und Leu-Resten wurden mit Hilfe einer biosynthetischen

Methode bestimmt.

Insgesamt wurden 74% aller Protonenresonanzen zugeordnet. Die fehlenden Seitenkettenuordnungen liegen vor allem in Seitenketten langer Aminosäurereste. Stereospezifische Zuordnungen konnten von 20 Isopropylgruppen von 21 Val- und Leu-Resten bestimmt werden. Für die meisten aromatischen Aminosäuren wurden auch die labilen Protonen der aromatischen Ringe zugeordnet.

Um die NOE-Signale zwischen den Untereinheiten des Dimers zuzuordnen, wurde ein drei-dimensionales  $^{15}\text{N}$ -editiertes NOESY-HSQC-Experiment einer Mischung aus Untereinheiten von  $^2\text{H}/^{15}\text{N}$ -markierten und nicht isotopenmarkierten Monomeren (Ferentz, et al., 1997) und ein vier-dimensionales  $J$ -editiertes  $^1\text{H}$ - $^{13}\text{C}$ -NOESY Experiment (Melacini et al., 2000) einer Probe aus  $^{13}\text{C}$ - $^1\text{H}$  und nicht markierten Untereinheiten aufgenommen. Das erste Experiment lieferte 3 NOE-Signale zwischen den Amidprotonen von der  $^2\text{H}/^{15}\text{N}$ -markierten Untereinheit zu den C-gebundenen Protonen der unmarkierten Untereinheit. Das letztere lieferte 5 weitere NOESY-Signale, wobei dieses Experiment eine klare Trennung von inter- and intramolekularen NOEs ermöglichte. Insgesamt konnten 8 NOE-Signale zwischen den beiden Untereinheiten des Dimers bestimmt werden. Diese Signale lagen im Kontaktbereich zwischen den Untereinheiten, wobei die Aminosäurereste F7, D8, T10 und F11 einer Untereinheit und A75 and Y105 der anderen Untereinheit beteiligt waren.

Die Struktur stützt sich auf 2688 aus NOE-Werten abgeleiteten Abstandsparemtern, auf Wasserstoffbrücken, die aus 34 langsam austauschenden Rückgrat-Amidprotonenresonanzen abgeleitet wurden sowie auf 334 Torsionswinkel, die mit Hilfe des TALOS-Programm erhalten wurden. Für die Verfeinerung der Struktur wurden auch 158 residuale dipolare Kopplungsparameter (RDC) verwandt.



Die drei-dimensionale Struktur des Sud-Proteins wurde mit einem gemittelten RMSD-Wert von 0,72 Å und 1,28 Å für die Rückgrat- und schweren Atome bestimmt, wobei die terminalen Reste auszunehmen sind. Ohne das nur schlecht definierte Segment der Reste 90 bis 95 würde der mittlere RMSD-Wert auf 0,6 Å und 1,14 Å absinken. Das Ensemble der Strukturen, das mit den residualen dipolaren Kopplungen verfeinert wurde, zeigt eine gute Konvergenz. Die entsprechenden RMSD-Werte, wenn man die Werte für die Reste 90 bis 94 ausnimmt, sinken durch die RDC-Verfeinerung auf 0,97 und 0,66 Å. Die relative Orientierung der beiden Monomeren in der Proteinstruktur, die mit den residualen dipolaren Kopplungsparametern verfeinert wurden, sind auch unterschiedlich zu denen, die ohne die residualen dipolaren Kopplungsparameter bestimmt wurden.

Die Struktur des dimeren Sud-Proteins wurde aus den beschriebenen Abstands-, RDC- und Winkelparametern mit Hilfe des ARIA-Programmpakets berechnet. Um der ambivalenten Zuordnungsmöglichkeit von NOESY-Signalen innerhalb einer Untereinheit bzw. zwischen den Untereinheiten Rechnung zu tragen, wurde eine ADR-Funktion (ambiguous distance restraints), welche beide Möglichkeiten berücksichtigt, verwendet. Die Strukturbestimmung des dimeren Proteins wurde erheblich behindert, nicht nur durch das hohe Molekulargewicht (30 kDa) und die dadurch bedingte Überlappung von Signalen sondern auch durch die nur geringe Anzahl von experimentellen intermonomer auftretenden NOE-Werten. Somit war die relative Orientierung der beiden Monomeren zueinander unsicher. Einige der Resonanzen der aliphatischen Seitenketten konnten wegen der ausgeprägten Signalüberlappung nicht zugeordnet werden. Das dimere Sud-Protein enthält 17 Lysin-, 14 Leucinreste und 1 Histidin-Tag für jede Untereinheit. Diese Häufigkeit komplizierte die Resonanzzuordnung. Auch das konventionelle 3D-<sup>15</sup>N-getrennte

TOCSY-HSQC-Experiment versagte, weil die Linienbreiten wegen des hohen Molekulargewichts zu groß waren.

Die Lösungsstruktur enthält ein fünfsträngiges paralleles  $\beta$ -Faltblatt, das eine hydrophobe Region enthält sowie ein zweisträngiges antiparalleles  $\beta$ -Faltblatt und sieben  $\alpha$ -Helices. Die dimere Struktur wird hauptsächlich durch hydrophobe Reste stabilisiert. Da das Sud-Protein auch den Transfer des Polysulfidschwefels zu Cyanid katalysiert, erschien eine Ähnlichkeit zum Protein Rhodanese aus *Azotobacter vinelandii* gegeben. Die beiden Proteine sind im aktiven Zentrum sehr ähnlich, besonders in der Konformation der Schlaufe des aktiven Zentrums mit dem freien Cystein und im Hinblick auf die umgebenden positiv geladenen Reste. Die Schlaufe des aktiven Zentrums (Reste 89-95) im Sud-Protein erscheinen flexibel. Diese Flexibilität wiederum verhindert die Möglichkeit der Zuordnung von Protonenresonanzen der Reste 90-94. Trotz dieser Ähnlichkeit in der Funktion und dem aktiven Zentrum sind die Aminosäuresequenzen und die Sekundärstrukturelemente der beiden Proteine bemerkenswert unterschiedlich. Die negativ geladene Polysulfidkette wechselwirkt mit den positiv geladenen Resten R46, R67 und R94 und wird dadurch in der Struktur stabilisiert. Der Austausch einer der 3 Argininreste, die auch in der Rhodanese von *Azotobacter vinelandii* konserviert sind, führt zum Verlust der Aktivität des Schwefeltransfers.

Um den Mechanismus des Polysulfidschwefeltransfers zu verstehen, wurden die mit 10 Polysulfidschwefelatomen gebundene Strukturen berechnet. Die Reste R46, D47, E50, K90, T91, A92, R94 bilden mit den Resten K90', T91' und K119' der anderen Untereinheit (') einen Kanal und umgeben die an das Cystein 89 gebundene Polysulfidkette. Diese Anordnung erlaubt es der Polysulfidkette sich vom Inneren des Sud-Proteins zu den weiter außen liegenden Resten R67 and K119' zu erstrecken. Aus

Resonanzverschiebungen in HSQC-Spektren läßt sich schließen, daß die Reste R67 und K119' wahrscheinliche Kandidaten für die für den Schwefeltransfer relevanten Wechselwirkungen mit der Polysulfidreduktase darstellen. Auuserdem könnte T91, welches in der Schlaufe des aktiven Zentrums liegt, für die Stabilisierung der Polysulfidkette eine Rolle spielen.

## 6 References

- Andersson, P., Annila, A., and Otting, G. (1998) *J. Magn. Reson.* **133**, 364-367.
- Arndt, J. W., Hao, B., Ramakrishnan, V., Cheng, T., Chan, S. I., and Chan, M. K. (2002) *Structure*, **10**, 215-224.
- A. E Derome: *Modern NMR Techniques for Chemistry Research*. Pergamon Press, Oxford, 1987.
- Andersson, P., Annila, A., and Otting, G. (1998) *J. Magn. Reson.* **133**, 364-367
- Bax, A. and Grzesiek, S. (1993) *Acc. Chem. Res.*, **26** 131-138.
- Bordo, D., Deriu, D., Colnaghi, R., Carpen, A., Pagani, S. and Bolognesi, M. (2000) *J. Mol. Biol.* **298**, 691-704.
- Brünger, A. T. (1992) *X-PLOR. A System for X-ray Crystallography and NMR*. Yale University Press, New Haven.
- Clore, G. M., Gronenborn, A. M., and Bax, A. (1998) *J. Magn. Reson.* **133**, 216-221.
- Clore, G. M., Gronenborn, A. M., and Bax, A. (1998) *J. Magn. Reson.* **133**, 216-221.
- Clubb, R. T., Thanabal, V., and Wagner, G. (1992) *J. Magn. Reson.* **97**, 213-217.
- Cornilescu, G., Delaglio, F., Bax, A. (1999) *J. Biomol. NMR*, **13**, 289-302.
- Correspondence. (1997) *nature structural biology* volume 4 number 12, 979-983.
- David S. Wishart and Brian D. Sykes. (1994) *J. Biomol. NMR*, **4**, 171-180.
- Delaglio, F., Grzesiek, S., Vuister, G. W., Zhu, G., Pfeifer, J., and Bax, A. (1995) *J. Biomol. NMR*, **6**, 277-293.
- Dotsch V., and Wagner, G. (1998) *Current Opinion in Structural Biology*, **8**, 619-623.
- FarmerII, B.T. and Venters, R. A. (1995) *J. Am. Chem. Soc.* **117**, 4187-4188.
- Fischer, D., Barret, C., Bryson, K., Elofsson, A., Godzik, A., Jones, D., Karplus, K.J., Kelley, L.A., Maccallum, R.M., Pawowski, K., Rost, B., Rychlewski, L. and Sternberg, M.J. (1999) *Proteins: Struc. Funct. and Gen.*, **3**, 209-217.
- Ferentz, A. E., Opperman, T., Walker, G. C. and Wagner, G. (1997) *Nat. Struct. Biol.* **4**, 979-983
- Folmer, R. H. A., Nilges, M., Konings, R. N. H. and Hilbers, C. W. (1995) *EMBO J.* **14**, 4132-4142
- Franzoni, L., Lücke, C., Perez, C., Cavazzini, D., Rademacher, M., Ludwig, C., Spisni, A., Rossi, G. L., and Rüterjans, H. (2002) *J. Biol. Chem.*, **277**, 21983-21997.
- Frank J.M. van de Ven: *Multidimensional NMR in Liquids*. VCH Publishers, New York, 1995.
- Gardener, K.H., Rosen, M.K. and Kay, E.L. (1997) *Biochemistry*, **36**, 1389-1401.
- Gardner, K. H., Rosen, M. K., Kay, L. E. (1997) *Biochemistry*, **36**, 1389-1401
- Grzesiek, S., Wingfield, P., Stahl, S., Kaufman, J. D. and Bax, A. (1995) *J. Am. Chem.*

- Soc.* **117**, 9594-9595.
- Grzesiek, S., and Bax, A. (1992) *J. Magn. Reson.*, **99**, 201-207.
- Grzesiek, S., and Bax, A. (1992) *J. Magn. Reson.*, **96**, 432-440.
- Handel, T. M., and Domaille, P. J. (1996) *Biochemistry*, **35**, 6569-6584.
- H. Friebolin: *Basic One- and Two-Dimensional NMR Spectroscopy*. Weinheim Wiley-VCH, 1998.
- Ikura, M., Kay, L. E., and Bax, A. (1990) *Biochemistry*, **29**, 4659-4667.
- 2Bertini, M. B. L. Janik, G. Liu, C. Luchinat, and A. Rosato. (2001) *J. Magn. Reson.* **148**, 23-30.
- J. Cavanagh, W. J. Fairbrother, A. G. Palmer III, N. J. Skelton: *Protein NMR Spectroscopy*. Academic Press, California, 1996.
- J. Linge, (2000). Ph.D. thesis, faculty of physics and astronomy at the Ruhr-University Germany.
- J. Patrick Loria, M. Rance, and Arthur G. Palmer, III. *J. Magnetic Resonance*, **141**, 180-184(1999).
- Krishna, N. R. and Berliner, L. J. Structure Computation and Dynamics in Protein NMR. *Biological Magnetic Resonance*, **17**, (1999) Kluwer Academic/Plenum Publishers.
- Laskowski, R. A., Rullmann, J. A. C., MacArthur, M. W., Kaptein, R., and Thornton, J. M. (1996) *J. Biomol. NMR*, **8**, 477-486.
- Lerche, M. H., Meissner, A., Poulsen, F. M., and Sørensen, O. W. (1999) *J. Magn. Reson.* **140**, 259-263.
- Liang, H., Petros, A. M., Meadows, R. P., Yoon, H. S., Egan, D. A., Walter, K., Holzman, T. F., Robins, T., and Fesik, S. W. (1996) *Biochemistry*, **35**, 2095-2103
- Lin, Y. J., Pfeiffer, S. Löhr, F., Klimmek, O. and Rüterjans, H. (2000) *J. Biomol. NMR*, **18**, 285-286
- Löhr, F., Pfeiffer, S., Lin, Y.-J., Hartleib, J., Klimmek, O. and Rüterjans, H. (2000), *J. Biomol. NMR*, **18**, 337-346.
- Manival, X., Yang, Y., Strub, M. P., Kochyan, M., Steinmetz, M., and Aymerich, S. (1997) *EMBO Journal*, **16**, 5019-5029.
- Melacini G. (2000) *J. Am. Chem. Soc.* **2000**, 122, 9735-9738
- Miura, T., Klaus, W., Ross, A., Güntert, P., and Senn, H. (2002) *J. Biomol. NMR*, **22**, 89-92.
- Mumenthaler, C. & Braun, W. (1995) *J. Mol. Biol.* **254**, 465-480.
- Nilges, M., S. I. O'Donoghue, Progress in Nuclear Resonance Spectroscopy 32 (1998) 107-139.
- Nilges, M.. Application of molecular modeling in NMR structure determination. 1-31

- Nilges, M. (1993) *Proteins*, **17**, 297-309.
- Nilges, M., O'Donoghue, S. I. (1998) *Progress in Nuclear Magnetic Resonance Spectroscopy* **32** 107-139
- Nilges, M. (1993) *proteins* **17**, 297-309
- Neri, D., Szyperski, T., Otting, G., Senn, H., and Wüthrich, K. (1989) *Biochemistry* **1989** 7510-7516
- Nomura, K. and Kainosho, M. (2002) *J. Magn. Reson.* **154**, 146-153.
- N. R. Krishna and L. J. Berliner. (1999) *Biological Magnetic Resonance* **17**.
- Klimmek, O., Kröger, A., Steudel, R. and Holdt, G. (1991) *Arch. Microbiol.*, **155**, 177-182.
- Klimmek, O., Kreis V., Klein, C., Simon, J., Wittershagen, A. and Kröger, A. (1998) *Eur. J. Biochem.*, **253**, 263-269.
- Klimmek, O., Stein, T., Pisa, R., Simon, J. and Kröger, A. (1999) *Eur. J. Biochem.*, **263**, 79-84.
- O'Donoghue, S. I., King, G. F., and Nilges, M. (1996) *J. Biomol. NMR*, **8**,193-206.
- Palmer, A. G., III, Fairbrother, W. J., Cavanagh, J., Wright, P. E., and Rance, M. J. (1992) *J. Biomol. NMR*, **2**,103-108.
- Pervushin, K., Riek, R., Wider, G. and Wüthrich, K. (1997) *Proc. Natl. Acad. Sci. USA.*, **94**, 12366-71.
- Pervushin, K., Riek, R., Wider, G. and Wüthrich, K. (1998) *J. Am. Chem. Soc.* **120**, 6394-6400.
- Pervushin, K., Riek, R., Wider, G. and Wüthrich, K. (1998) *J. Am. Chem. Soc.* **120**, 6394-6400.
- Pervushin, K., Riek, R., Wider, G. and Wüthrich, K. (1997) *Proc. Natl. Acad. Sci. U.S.A.* **94**, 12366-12371.
- P. Güntert, C. Mumenthaler and K. Wüthrich. (1997) *J. Mol. Biol.* **273**, 283-298.
- Prestegard, J.H. (1998) *Nature Struct. Biol.* **5** 517-522
- R. H.A. Folmer, C. W. Hilbers, R. N.H. Konings, and M. Nilges (1997) *J. Biomol. NMR*, **9**, 245-258.
- Rückert, M., and Otting, G. (2000) *J. Am. Chem. Soc.* **122**, 7793-7797.
- Salzmann, M., Wider, G., Pervushin, K., Senn, H. and Wüthrich, K. (1999) *J. Am. Chem. Soc.*, **121**, 844-848.
- S. I. O'Donoghue, G. F. King and M. Nilges. (1996) *J. Biomol. NMR*, **8**, 193-206.
- Sörbo, B. H. (1960) *Biochim. Biophys. Acta* **38**, 349-351.
- Stauffer, M. E., Skelton, N. J., and Fairbrother, W. J. (2002) *J. Biomol. NMR*, **23**, 57-61
- Tjandra, N. and Bax, A. (1997) *SCIENCE*, **278**, 1111-1113.
- Tsui, V., Zhu, L., Huang, T. H., Wright, P. E. and Case, D. A. (2000) *J. Biomol. NMR*,

**16**, 9-21.

Venters, R. A., Metzler, W. J., Spicer, L. D., Mueller, L. and FarmerII, B.T. (1995)

*J. Am. Chem. Soc.* **117**, 9592-9593.

Wider, G., Wüthrich, K. (1999) *Current Opinion in Structural Biology*, **9**, 594-601.

Wishart, D.S., Bigam, C.G., Yao, J., Abildgaard, F., Dyson, J., H.J., Oldfield, E.,

Markley, J.L. and Sykes, B.D. (1995) *J. Biomol. NMR*, **6**, 135-140.

Wishart, D.S., Watson, M.S., Boyko, R.F. and Sykes, B.D. (1997) *J. Biomol. NMR*,

**19**, 329-336.

Zhu, G., Xia, Y., Sze, K. H., and Yan, X. (1999) *J. Biomol. NMR*, **14**, 377-381.

## Appendix A.1

Amino acid sequence and chemical shift values [ppm] from SUD at pH 7.6 and 300K.

1	ALA	QB	1.540	6	LYS+	N	121.200	12	LYS+	QE	3.040
1	ALA	C	175.400	7	PHE	HN	8.375	12	LYS+	C	180.100
1	ALA	CA	54.800	7	PHE	HA	4.980	12	LYS+	CA	60.000
2	ASP-	HN	8.150	7	PHE	HB2	3.320	12	LYS+	CB	32.200
2	ASP-	HA	4.641	7	PHE	HB3	3.430	12	LYS+	N	118.200
2	ASP-	HB2	2.700	7	PHE	QD	7.460	13	ALA	HN	8.010
2	ASP-	HB3	2.760	7	PHE	QE	7.575	13	ALA	HA	4.120
2	ASP-	C	176.800	7	PHE	HZ	6.834	13	ALA	QB	1.535
2	ASP-	CA	54.000	7	PHE	C	179.100	13	ALA	C	181.000
2	ASP-	CB	41.300	7	PHE	CA	58.300	13	ALA	CA	55.000
2	ASP-	N	128.300	7	PHE	CB	37.800	13	ALA	CB	17.800
3	MET	HN	8.730	7	PHE	N	120.100	13	ALA	N	121.600
3	MET	HA	4.425	8	ASP-	HN	8.590	14	GLN	HN	8.535
3	MET	QB	1.676	8	ASP-	HA	4.780	14	GLN	HA	4.040
3	MET	QG	2.369	8	ASP-	QB	2.890	14	GLN	HB2	1.980
3	MET	QE	1.920	8	ASP-	C	177.600	14	GLN	HB3	2.460
3	MET	C	177.100	8	ASP-	CA	57.900	14	GLN	HG2	2.300
3	MET	CA	55.400	8	ASP-	CB	41.900	14	GLN	HG3	2.870
3	MET	CB	31.200	8	ASP-	N	120.100	14	GLN	HE21	6.890
3	MET	CG	32.200	9	ALA	HN	8.350	14	GLN	HE22	7.670
3	MET	CE	16.700	9	ALA	HA	4.120	14	GLN	C	180.100
3	MET	N	123.300	9	ALA	QB	1.610	14	GLN	CA	59.500
4	GLY	HN	8.625	9	ALA	C	181.600	14	GLN	CB	27.500
4	GLY	HA1	3.970	9	ALA	CA	55.400	14	GLN	CG	34.100
4	GLY	HA2	4.250	9	ALA	CB	17.800	14	GLN	N	120.700
4	GLY	C	175.800	9	ALA	N	120.100	14	GLN	NE2	113.200
4	GLY	CA	48.400	10	THR	HN	8.400	15	VAL	HN	8.420
4	GLY	N	108.800	10	THR	HA	3.890	15	VAL	HA	3.265
5	GLU-	HN	8.200	10	THR	HB	4.300	15	VAL	HB	1.720
5	GLU-	HA	4.190	10	THR	QG2	0.500	15	VAL	QG2	0.440
5	GLU-	QB	2.070	10	THR	C	175.600	15	VAL	QG1	0.770
5	GLU-	HG2	2.300	10	THR	CA	67.000	15	VAL	C	177.100
5	GLU-	HG3	2.390	10	THR	CB	68.800	15	VAL	CA	67.100
5	GLU-	C	179.300	10	THR	CG2	20.300	15	VAL	CB	31.900
5	GLU-	CA	59.200	10	THR	N	117.800	15	VAL	CG2	23.800
5	GLU-	CB	29.100	11	PHE	HN	8.425	15	VAL	CG1	21.100
5	GLU-	CG	36.300	11	PHE	HA	4.920	15	VAL	N	121.600
5	GLU-	N	119.900	11	PHE	HB2	3.360	16	LYS+	HN	7.830
6	LYS+	HN	7.790	11	PHE	HB3	3.580	16	LYS+	HA	3.790
6	LYS+	HA	4.200	11	PHE	QD	7.371	16	LYS+	QB	1.850
6	LYS+	QB	1.830	11	PHE	QE	7.178	16	LYS+	HG2	1.405
6	LYS+	HG2	1.370	11	PHE	HZ	7.028	16	LYS+	HG3	1.465
6	LYS+	HG3	1.460	11	PHE	C	177.200	16	LYS+	QD	1.676
6	LYS+	QD	1.610	11	PHE	CA	60.300	16	LYS+	QE	2.953
6	LYS+	QE	2.910	11	PHE	CB	38.800	16	LYS+	C	179.400
6	LYS+	C	180.100	11	PHE	N	124.200	16	LYS+	CA	60.100
6	LYS+	CA	59.100	12	LYS+	HN	8.785	16	LYS+	CB	32.500
6	LYS+	CB	31.600	12	LYS+	HA	3.420	16	LYS+	CG	24.700
6	LYS+	CG	24.700	12	LYS+	HB2	1.720	16	LYS+	CD	28.700
6	LYS+	CD	28.800	12	LYS+	HB3	1.830	16	LYS+	CE	41.900
6	LYS+	CE	41.900	12	LYS+	QD	1.610	16	LYS+	N	119.874



17	ALA	HN	7.930	23	VAL	C	175.800	28	LYS+	QB	1.720
17	ALA	HA	4.080	23	VAL	CA	62.300	28	LYS+	HG2	1.240
17	ALA	QB	1.420	23	VAL	CB	32.200	28	LYS+	HG3	1.500
17	ALA	C	180.100	23	VAL	CG2	20.300	28	LYS+	QD	1.610
17	ALA	CA	54.600	23	VAL	CG1	21.200	28	LYS+	QE	2.930
17	ALA	CB	17.800	23	VAL	N	118.800	28	LYS+	C	179.600
17	ALA	N	119.900	24	MET	HN	8.860	28	LYS+	CA	60.400
18	ALA	HN	7.940	24	MET	HA	5.220	28	LYS+	CB	31.900
18	ALA	HA	4.120	24	MET	QB	2.206	28	LYS+	CG	26.300
18	ALA	QB	1.420	24	MET	HG2	2.650	28	LYS+	CD	29.100
18	ALA	C	180.900	24	MET	HG3	2.910	28	LYS+	CE	41.900
18	ALA	CA	54.600	24	MET	QE	1.820	28	LYS+	N	113.700
18	ALA	CB	17.800	24	MET	C	176.400	29	ASP-	HN	7.640
18	ALA	N	120.500	24	MET	CA	52.300	29	ASP-	HA	4.510
19	LYS+	HN	8.455	24	MET	CB	29.000	29	ASP-	HB2	2.560
19	LYS+	HA	3.810	24	MET	CE	13.100	29	ASP-	HB3	2.950
19	LYS+	QB	1.828	24	MET	N	126.000	29	ASP-	C	179.100
19	LYS+	C	177.600	25	LEU	HN	8.915	29	ASP-	CA	57.000
19	LYS+	CA	60.300	25	LEU	HA	5.070	29	ASP-	CB	39.900
19	LYS+	CB	33.300	25	LEU	HB2	1.610	29	ASP-	N	120.800
19	LYS+	N	117.100	25	LEU	HB3	1.828	30	ALA	HN	9.065
20	ALA	HN	7.120	25	LEU	HG	1.676	30	ALA	HA	3.950
20	ALA	HA	4.190	25	LEU	QD1	0.580	30	ALA	QB	1.620
20	ALA	QB	1.480	25	LEU	QD2	0.940	30	ALA	C	178.200
20	ALA	C	177.900	25	LEU	C	176.200	30	ALA	CA	55.400
20	ALA	CA	53.900	25	LEU	CA	52.400	30	ALA	CB	16.900
20	ALA	CB	18.100	25	LEU	CB	46.300	30	ALA	N	125.700
20	ALA	N	117.100	25	LEU	CG	26.200	31	TYR	HN	8.760
21	ASP-	HN	7.250	25	LEU	CD1	26.700	31	TYR	HA	4.100
21	ASP-	HA	4.990	25	LEU	CD2	22.800	31	TYR	HB2	2.740
21	ASP-	HB2	2.520	25	LEU	N	124.000	31	TYR	HB3	2.880
21	ASP-	HB3	2.910	26	SER	HN	9.260	31	TYR	QD	7.090
21	ASP-	C	174.400	26	SER	HA	4.706	31	TYR	QE	6.856
21	ASP-	CA	53.500	26	SER	HB2	4.078	31	TYR	C	177.100
21	ASP-	CB	41.900	26	SER	HB3	4.313	31	TYR	CA	62.500
21	ASP-	N	116.100	26	SER	C	172.800	31	TYR	CB	38.100
22	MET	HN	7.680	26	SER	CA	57.000	31	TYR	CD1	132.800
22	MET	HA	4.810	26	SER	CB	62.200	31	TYR	CD2	132.800
22	MET	HB2	1.890	26	SER	N	119.200	31	TYR	CE1	117.600
22	MET	HB3	1.980	27	PRO	HA	4.560	31	TYR	CE2	117.600
22	MET	QG	2.520	27	PRO	HB2	1.640	31	TYR	N	117.700
22	MET	C	172.600	27	PRO	HB3	2.650	32	LYS+	HN	7.680
22	MET	CA	53.800	27	PRO	HG2	2.001	32	LYS+	HA	3.820
22	MET	CB	33.700	27	PRO	HG3	2.217	32	LYS+	QB	1.890
22	MET	CG	32.500	27	PRO	HD2	3.908	32	LYS+	HG2	1.265
22	MET	N	116.600	27	PRO	HD3	4.023	32	LYS+	HG3	1.440
23	VAL	HN	7.675	27	PRO	C	178.300	32	LYS+	QD	1.680
23	VAL	HA	4.270	27	PRO	CA	65.500	32	LYS+	QE	2.990
23	VAL	HB	2.040	27	PRO	CB	30.300	32	LYS+	C	177.600
23	VAL	QG2	0.830	28	LYS+	HN	8.266	32	LYS+	CA	59.500
23	VAL	QG1	1.070	28	LYS+	HA	3.750	32	LYS+	CB	32.500

32	LYS+	CG	23.800	36	GLU-	CG	36.300	41	THR	CB	70.300
32	LYS+	CD	28.800	36	GLU-	N	115.100	41	THR	CG2	21.500
32	LYS+	CE	41.900	37	ASN	HN	7.420	41	THR	N	123.100
32	LYS+	N	118.400	37	ASN	HA	5.260	42	LEU	HN	8.485
33	LEU	HN	7.850	37	ASN	HB2	2.620	42	LEU	HA	5.040
33	LEU	HA	3.880	37	ASN	HB3	2.900	42	LEU	HB2	1.500
33	LEU	HB2	1.440	37	ASN	HD21	7.480	42	LEU	HB3	1.680
33	LEU	HB3	1.740	37	ASN	HD22	8.240	42	LEU	HG	1.310
33	LEU	HG	1.220	37	ASN	C	172.200	42	LEU	QD1	0.250
33	LEU	QD2	0.060	37	ASN	CA	50.500	42	LEU	QD2	0.380
33	LEU	QD1	0.560	37	ASN	CB	40.000	42	LEU	C	173.400
33	LEU	C	179.800	37	ASN	ND2	116.400	42	LEU	CA	54.600
33	LEU	CA	58.100	37	ASN	N	116.400	42	LEU	CB	42.100
33	LEU	CB	42.100	38	PRO	HA	4.630	42	LEU	CG	27.500
33	LEU	CD2	25.600	38	PRO	HB2	1.990	42	LEU	CD1	25.600
33	LEU	CD1	23.200	38	PRO	HB3	2.350	42	LEU	CD2	25.600
33	LEU	N	119.440	38	PRO	QG	1.980	42	LEU	N	129.200
34	LEU	HN	7.980	38	PRO	HD2	3.560	43	ILE	HN	9.170
34	LEU	HA	3.860	38	PRO	HD3	3.840	43	ILE	HA	4.381
34	LEU	HB2	1.633	38	PRO	C	176.400	43	ILE	HB	1.570
34	LEU	HB3	1.870	38	PRO	CA	63.900	43	ILE	HG12	0.620
34	LEU	HG	1.740	38	PRO	CB	31.900	43	ILE	HG13	1.290
34	LEU	QD2	0.770	38	PRO	CG	26.600	43	ILE	QG2	0.500
34	LEU	QD1	0.940	38	PRO	CD	50.300	43	ILE	QD1	0.470
34	LEU	C	179.300	39	ASP-	HN	8.505	43	ILE	C	172.700
34	LEU	CA	57.600	39	ASP-	HA	4.490	43	ILE	CA	59.500
34	LEU	CB	40.900	39	ASP-	QB	2.690	43	ILE	CB	37.800
34	LEU	CD2	23.400	39	ASP-	C	175.700	43	ILE	CG1	27.000
34	LEU	CD1	27.500	39	ASP-	CA	54.500	43	ILE	CG2	17.200
34	LEU	N	117.700	39	ASP-	CB	40.000	43	ILE	CD1	13.700
35	GLN	HN	8.040	39	ASP-	N	115.600	43	ILE	N	127.900
35	GLN	HA	3.860	40	ILE	HN	7.750	44	ASP-	HN	8.420
35	GLN	HB2	1.852	40	ILE	HA	4.300	44	ASP-	HA	5.130
35	GLN	HB3	2.015	40	ILE	HB	1.850	44	ASP-	HB2	2.300
35	GLN	HG2	1.871	40	ILE	HG12	0.940	44	ASP-	HB3	2.930
35	GLN	HG3	1.979	40	ILE	HG13	1.720	44	ASP-	C	177.000
35	GLN	HE21	6.680	40	ILE	QG2	0.680	44	ASP-	CA	51.500
35	GLN	HE22	7.000	40	ILE	QD1	0.780	44	ASP-	CB	41.300
35	GLN	C	178.600	40	ILE	C	174.700	44	ASP-	N	128.100
35	GLN	CA	58.000	40	ILE	CA	61.800	45	VAL	HN	8.740
35	GLN	CB	29.600	40	ILE	CB	37.800	45	VAL	HA	5.630
35	GLN	N	116.800	40	ILE	CG1	26.900	45	VAL	HB	2.300
35	GLN	NE2	111.000	40	ILE	CG2	16.600	45	VAL	QG2	0.685
36	GLU-	HN	7.840	40	ILE	CD1	13.100	45	VAL	QG1	0.865
36	GLU-	HA	4.140	40	ILE	N	120.800	45	VAL	C	178.400
36	GLU-	HB2	1.940	41	THR	HN	7.140	45	VAL	CA	59.100
36	GLU-	HB3	2.030	41	THR	HA	4.230	45	VAL	CB	30.300
36	GLU-	QG	2.200	41	THR	HB	3.620	45	VAL	CG2	17.900
36	GLU-	C	176.300	41	THR	QG2	0.811	45	VAL	CG1	20.000
36	GLU-	CA	56.900	41	THR	C	173.000	45	VAL	N	115.500
36	GLU-	CB	30.300	41	THR	CA	62.300	46	ARG+	HN	7.640

46	ARG+	HA	4.122	51	LEU	N	119.900	56	LYS+	CD	29.100
46	ARG+	C	174.300	52	LYS+	HN	6.915	56	LYS+	N	114.900
46	ARG+	CA	57.200	52	LYS+	HA	4.010	57	PRO	HA	4.010
46	ARG+	N	121.600	52	LYS+	QB	1.820	57	PRO	HB2	0.250
47	ASP-	HN	9.330	52	LYS+	HG2	1.390	57	PRO	HB3	0.770
47	ASP-	HA	5.015	52	LYS+	HG3	1.480	57	PRO	HG2	0.196
47	ASP-	HB2	2.740	52	LYS+	QD	1.640	57	PRO	HG3	1.180
47	ASP-	HB3	3.170	52	LYS+	QE	2.920	57	PRO	QD	3.228
47	ASP-	C	177.000	52	LYS+	C	177.500	57	PRO	C	174.100
47	ASP-	CA	53.400	52	LYS+	CA	58.400	57	PRO	CA	62.500
47	ASP-	CB	40.300	52	LYS+	CB	32.200	57	PRO	CB	31.000
47	ASP-	N	122.300	52	LYS+	N	117.000	57	PRO	CG	26.600
48	PRO	HA	4.120	53	ALA	HN	7.550	57	PRO	CD	49.100
48	PRO	HB2	2.140	53	ALA	HA	4.260	58	ASP-	HN	8.015
48	PRO	HB3	2.600	53	ALA	QB	1.480	58	ASP-	HA	4.400
48	PRO	HG2	2.240	53	ALA	C	179.500	58	ASP-	HB2	1.760
48	PRO	HG3	2.560	53	ALA	CA	54.500	58	ASP-	HB3	2.780
48	PRO	HD2	3.750	53	ALA	CB	19.700	58	ASP-	C	174.300
48	PRO	HD3	3.970	53	ALA	N	118.600	58	ASP-	CA	52.500
48	PRO	C	178.200	54	MET	HN	8.305	58	ASP-	CB	39.700
48	PRO	CA	65.300	54	MET	HA	4.680	58	ASP-	N	122.500
48	PRO	CB	31.300	54	MET	HB2	1.960	59	VAL	HN	6.875
48	PRO	CG	28.200	54	MET	HB3	2.080	59	VAL	HA	4.680
48	PRO	CD	50.388	54	MET	HG2	2.530	59	VAL	HB	2.460
49	ASP-	HN	8.960	54	MET	HG3	2.800	59	VAL	QG2	0.680
49	ASP-	HA	4.300	54	MET	QE	1.480	59	VAL	QG1	1.010
49	ASP-	HB2	2.630	54	MET	C	176.500	59	VAL	C	175.800
49	ASP-	HB3	2.740	54	MET	CA	54.600	59	VAL	CA	58.400
49	ASP-	C	178.700	54	MET	CB	34.400	59	VAL	CB	34.400
49	ASP-	CA	56.200	54	MET	CG	32.800	59	VAL	CG2	18.800
49	ASP-	CB	38.100	54	MET	N	112.300	59	VAL	CG1	22.200
49	ASP-	N	115.400	55	GLY	HN	7.535	59	VAL	N	114.100
50	GLU-	HN	7.435	55	GLY	HA1	3.750	60	LYS+	HN	8.565
50	GLU-	HA	4.120	55	GLY	HA2	4.320	60	LYS+	HA	4.060
50	GLU-	C	177.800	55	GLY	C	173.300	60	LYS+	QB	1.830
50	GLU-	CA	59.000	55	GLY	CA	44.100	60	LYS+	HG2	1.420
50	GLU-	CB	30.300	55	GLY	N	106.300	60	LYS+	HG3	1.530
50	GLU-	N	123.100	56	LYS+	HN	8.325	60	LYS+	QD	1.680
51	LEU	HN	6.855	56	LYS+	HA	4.490	60	LYS+	QE	2.980
51	LEU	HA	3.797	56	LYS+	HB2	1.180	60	LYS+	C	177.600
51	LEU	HB2	1.309	56	LYS+	HB3	1.310	60	LYS+	CA	59.100
51	LEU	HB3	1.490	56	LYS+	HG2	0.950	60	LYS+	CB	32.500
51	LEU	HG	1.310	56	LYS+	HG3	1.130	60	LYS+	CG	24.700
51	LEU	QD2	0.250	56	LYS+	HD2	1.060	60	LYS+	CD	28.800
51	LEU	QD1	0.340	56	LYS+	HD3	1.180	60	LYS+	CE	41.900
51	LEU	C	180.100	56	LYS+	HE2	2.430	60	LYS+	N	121.600
51	LEU	CA	58.700	56	LYS+	HE3	2.610	61	ASN	HN	9.280
51	LEU	CB	41.600	56	LYS+	C	172.400	61	ASN	HA	4.940
51	LEU	CG	30.300	56	LYS+	CA	53.300	61	ASN	HB2	2.760
51	LEU	CD2	23.400	56	LYS+	CB	34.000	61	ASN	HB3	3.190
51	LEU	CD1	23.700	56	LYS+	CG	23.700	61	ASN	HD21	6.490

61	ASN	HD22	7.240	65	MET	C	171.400	72	PRO	C	179.000
61	ASN	C	172.500	65	MET	CA	53.800	72	PRO	CA	64.200
61	ASN	CA	51.900	65	MET	CB	35.600	72	PRO	CB	29.600
61	ASN	CB	36.900	65	MET	N	130.200	73	LEU	HN	7.595
61	ASN	N	119.500	66	SER	HN	7.650	73	LEU	HA	4.040
61	ASN	ND2	111.600	66	SER	HA	3.776	73	LEU	HB2	1.130
62	TYR	HN	7.970	66	SER	QB	4.180	73	LEU	HB3	1.806
62	TYR	HA	4.860	66	SER	C	176.600	73	LEU	QD1	0.660
62	TYR	QB	2.740	66	SER	CA	57.900	73	LEU	QD2	0.810
62	TYR	QD	6.744	66	SER	CB	63.100	73	LEU	C	180.300
62	TYR	QE	6.528	66	SER	N	117.300	73	LEU	CA	56.200
62	TYR	C	174.700	67	ARG+	HN	8.325	73	LEU	CB	41.900
62	TYR	CA	57.300	67	ARG+	HA	3.732	73	LEU	CD1	26.700
62	TYR	CB	42.500	67	ARG+	C	177.900	73	LEU	CD2	22.500
62	TYR	CD1	132.400	67	ARG+	CA	60.600	73	LEU	N	116.000
62	TYR	CD2	132.400	67	ARG+	CB	28.000	74	LEU	HN	7.725
62	TYR	CE1	118.000	67	ARG+	N	119.100	74	LEU	HA	3.480
62	TYR	CE2	118.000	68	GLY	HN	8.720	74	LEU	HB2	0.550
62	TYR	N	124.900	68	GLY	HA1	3.635	74	LEU	HB3	1.660
63	LYS+	HN	8.465	68	GLY	HA2	4.120	74	LEU	HG	1.500
63	LYS+	HA	4.250	68	GLY	C	173.800	74	LEU	QD1	-0.080
63	LYS+	HB2	1.350	68	GLY	CA	47.300	74	LEU	QD2	0.160
63	LYS+	HB3	1.431	68	GLY	N	105.300	74	LEU	C	180.800
63	LYS+	HG2	1.200	69	LYS+	HN	7.265	74	LEU	CA	58.800
63	LYS+	HG3	1.307	69	LYS+	HA	4.080	74	LEU	CB	40.100
63	LYS+	HD2	1.500	69	LYS+	C	175.100	74	LEU	CD1	24.700
63	LYS+	HD3	1.760	69	LYS+	CA	54.900	74	LEU	CD2	22.800
63	LYS+	QE	3.010	69	LYS+	CB	33.300	74	LEU	N	122.000
63	LYS+	C	172.800	69	LYS+	N	115.600	75	ALA	HN	8.275
63	LYS+	CA	55.000	70	LEU	HN	7.275	75	ALA	HA	4.545
63	LYS+	CB	36.500	70	LEU	HA	3.280	75	ALA	QB	1.655
63	LYS+	CG	25.000	70	LEU	HB2	1.430	75	ALA	C	178.700
63	LYS+	CD	28.700	70	LEU	HB3	1.665	75	ALA	CA	56.300
63	LYS+	N	128.600	70	LEU	HG	0.984	75	ALA	CB	18.700
64	HIS	HN	8.630	70	LEU	QD1	0.551	75	ALA	N	120.400
64	HIS	HA	5.030	70	LEU	QD2	0.638	76	LYS+	HN	7.490
64	HIS	HB2	2.965	70	LEU	C	176.200	76	LYS+	HA	4.680
64	HIS	HB3	3.300	70	LEU	CA	59.800	76	LYS+	HB2	1.660
64	HIS	HD2	7.023	70	LEU	CB	43.400	76	LYS+	HB3	2.130
64	HIS	HE1	7.988	70	LEU	CG	26.300	76	LYS+	HG2	1.390
64	HIS	C	175.200	70	LEU	CD1	23.400	76	LYS+	HG3	1.460
64	HIS	CA	54.700	70	LEU	CD2	26.400	76	LYS+	QE	2.990
64	HIS	CB	31.300	70	LEU	N	122.700	76	LYS+	C	177.400
64	HIS	CD2	119.300	71	GLU-	HN	10.215	76	LYS+	CA	55.000
64	HIS	N	124.200	71	GLU-	HA	3.330	76	LYS+	CB	31.900
65	MET	HN	7.980	71	GLU-	C	176.300	76	LYS+	CG	25.000
65	MET	HA	3.776	71	GLU-	CA	62.200	76	LYS+	N	114.700
65	MET	HB2	1.330	71	GLU-	CB	25.200	77	SER	HN	7.880
65	MET	HB3	1.503	71	GLU-	N	112.900	77	SER	HA	4.080
65	MET	HG2	1.850	72	PRO	HA	3.290	77	SER	QB	3.660
65	MET	HG3	2.174	72	PRO	QB	1.660	77	SER	C	175.500

77	SER	CA	61.300	83	LYS+	HB3	2.110	87	VAL	N	121.400
77	SER	CB	64.400	83	LYS+	HG2	1.370	88	PHE	HN	8.165
77	SER	N	116.200	83	LYS+	HG3	1.530	88	PHE	HA	5.500
78	GLY	HN	8.955	83	LYS+	C	174.500	88	PHE	HB2	2.455
78	GLY	HA1	3.800	83	LYS+	CA	53.100	88	PHE	HB3	2.845
78	GLY	HA2	4.110	83	LYS+	CB	32.200	88	PHE	QD	6.931
78	GLY	C	174.800	83	LYS+	CG	24.700	88	PHE	QE	6.695
78	GLY	CA	45.700	83	LYS+	N	120.500	88	PHE	C	174.300
78	GLY	N	111.400	84	PRO	HA	5.100	88	PHE	CA	57.300
79	LEU	HN	7.825	84	PRO	HB2	1.892	88	PHE	CB	42.200
79	LEU	HA	4.260	84	PRO	HB3	2.430	88	PHE	N	121.400
79	LEU	HG	1.407	84	PRO	HG2	2.032	89	CYS	HN	7.200
79	LEU	QD1	0.750	84	PRO	HG3	2.189	89	CYS	HA	4.944
79	LEU	QD2	0.880	84	PRO	HD2	3.361	89	CYS	C	180.700
79	LEU	C	175.500	84	PRO	HD3	4.142	89	CYS	CA	58.100
79	LEU	CA	55.200	84	PRO	C	174.700	89	CYS	N	122.900
79	LEU	CB	43.200	84	PRO	CA	62.300	91	THR	HN	8.380
79	LEU	CD1	25.700	84	PRO	CB	31.900	91	THR	N	125.200
79	LEU	CD2	22.800	84	PRO	CD	50.652	92	ALA	CA	55.300
79	LEU	N	120.091	85	VAL	HN	7.785	95	ALA	HA	3.711
80	ASP-	HN	8.605	85	VAL	HA	5.260	95	ALA	QB	1.135
80	ASP-	HA	5.010	85	VAL	HB	1.960	95	ALA	C	177.800
80	ASP-	HB2	2.630	85	VAL	QG2	0.776	95	ALA	CA	54.600
80	ASP-	HB3	2.910	85	VAL	QG1	1.050	95	ALA	CB	17.800
80	ASP-	C	176.800	85	VAL	C	174.500	96	ALA	HN	7.570
80	ASP-	CA	49.600	85	VAL	CA	58.300	96	ALA	HA	3.840
80	ASP-	CB	42.200	85	VAL	CB	35.900	96	ALA	QB	1.438
80	ASP-	N	121.000	85	VAL	CG2	18.800	96	ALA	C	178.700
81	PRO	HA	3.560	85	VAL	CG1	23.100	96	ALA	CA	54.600
81	PRO	HB2	0.900	85	VAL	N	109.000	96	ALA	CB	18.300
81	PRO	HB3	1.720	86	VAL	HN	8.760	96	ALA	N	120.300
81	PRO	HD2	3.700	86	VAL	HA	4.840	97	LEU	HN	7.185
81	PRO	HD3	4.103	86	VAL	HB	1.890	97	LEU	HA	3.890
81	PRO	C	176.400	86	VAL	QG1	0.770	97	LEU	HB2	1.690
81	PRO	CA	64.100	86	VAL	QG2	0.845	97	LEU	HB3	1.940
81	PRO	CB	30.200	86	VAL	C	176.000	97	LEU	QD2	0.720
81	PRO	CD	50.388	86	VAL	CA	59.700	97	LEU	QD1	1.010
82	GLU-	HN	8.310	86	VAL	CB	33.300	97	LEU	C	180.000
82	GLU-	HA	4.120	86	VAL	CG1	23.100	97	LEU	CA	57.800
82	GLU-	HB2	1.910	86	VAL	CG2	19.000	97	LEU	CB	38.600
82	GLU-	HB3	2.140	86	VAL	N	121.400	97	LEU	CD2	21.000
82	GLU-	HG2	2.110	87	VAL	HN	9.140	97	LEU	CD1	24.700
82	GLU-	HG3	2.340	87	VAL	HA	4.900	97	LEU	N	116.000
82	GLU-	C	177.700	87	VAL	HB	1.850	98	ALA	HN	8.865
82	GLU-	CA	56.700	87	VAL	QG2	0.780	98	ALA	HA	4.450
82	GLU-	CB	29.400	87	VAL	QG1	0.846	98	ALA	QB	1.330
82	GLU-	CG	35.900	87	VAL	C	175.500	98	ALA	C	179.300
82	GLU-	N	117.300	87	VAL	CA	61.100	98	ALA	CA	54.100
83	LYS+	HN	8.005	87	VAL	CB	32.800	98	ALA	CB	18.700
83	LYS+	HA	4.860	87	VAL	CG2	20.900	98	ALA	N	122.300
83	LYS+	HB2	1.910	87	VAL	CG1	20.600	99	GLY	HN	8.850

99	GLY	QA	3.540	104	GLU-	HA	4.140	109	THR	CB	69.400
99	GLY	C	174.900	104	GLU-	HB2	2.109	109	THR	CG2	21.900
99	GLY	CA	47.100	104	GLU-	HB3	2.693	109	THR	N	118.800
99	GLY	N	106.300	104	GLU-	HG2	2.304	110	ILE	HN	8.065
100	LYS+	HN	7.693	104	GLU-	HG3	2.585	110	ILE	HA	4.560
100	LYS+	HA	4.080	104	GLU-	C	178.000	110	ILE	HB	1.655
100	LYS+	HB2	1.936	104	GLU-	CA	59.100	110	ILE	HG12	1.310
100	LYS+	HB3	2.196	104	GLU-	CB	28.400	110	ILE	QG2	0.790
100	LYS+	HG2	1.395	104	GLU-	N	121.400	110	ILE	QD1	0.770
100	LYS+	HG3	1.547	105	TYR	HN	8.095	110	ILE	C	174.400
100	LYS+	C	179.000	105	TYR	HA	4.340	110	ILE	CA	60.100
100	LYS+	CA	60.000	105	TYR	HB2	3.080	110	ILE	CB	40.300
100	LYS+	CB	31.633	105	TYR	HB3	3.490	110	ILE	CG1	26.900
100	LYS+	N	124.900	105	TYR	QD	7.444	110	ILE	CG2	18.600
101	THR	HN	7.810	105	TYR	QE	6.970	110	ILE	CD1	14.100
101	THR	HA	4.080	105	TYR	C	175.100	110	ILE	N	126.600
101	THR	HB	4.230	105	TYR	CA	60.000	111	TYR	HN	9.095
101	THR	QG2	1.180	105	TYR	CB	38.800	111	TYR	HA	5.770
101	THR	C	176.700	105	TYR	N	119.000	111	TYR	HB2	2.890
101	THR	CA	67.300	106	GLY	HN	7.810	111	TYR	HB3	3.020
101	THR	CB	68.400	106	GLY	HA1	3.700	111	TYR	QD	6.975
101	THR	CG2	21.900	106	GLY	HA2	4.360	111	TYR	QE	6.702
101	THR	N	119.200	106	GLY	C	174.800	111	TYR	C	174.400
102	LEU	HN	8.725	106	GLY	CA	45.200	111	TYR	CA	55.500
102	LEU	HA	3.800	106	GLY	N	105.000	111	TYR	CB	41.600
102	LEU	HB2	0.780	107	PHE	HN	8.350	111	TYR	CD1	133.300
102	LEU	HB3	1.790	107	PHE	HA	4.706	111	TYR	CD2	133.300
102	LEU	HG	1.570	107	PHE	HB2	2.650	111	TYR	CE1	117.200
102	LEU	QD2	-0.100	107	PHE	HB3	2.932	111	TYR	CE2	117.200
102	LEU	QD1	0.160	107	PHE	QD	7.571	111	TYR	N	126.800
102	LEU	C	180.100	107	PHE	QE	7.084	112	ASN	HN	8.810
102	LEU	CA	58.400	107	PHE	C	176.600	112	ASN	HA	5.400
102	LEU	CG	25.600	107	PHE	CA	59.200	112	ASN	HB2	2.660
102	LEU	CD2	21.900	107	PHE	CB	37.500	112	ASN	HB3	3.490
102	LEU	CD1	25.900	107	PHE	N	120.700	112	ASN	HD21	5.740
102	LEU	N	119.200	108	LYS+	HN	7.610	112	ASN	HD22	6.430
103	ARG+	HN	8.175	108	LYS+	HA	4.275	112	ASN	C	174.800
103	ARG+	HA	4.560	108	LYS+	QB	1.830	112	ASN	CA	51.400
103	ARG+	HB2	2.000	108	LYS+	HG2	1.400	112	ASN	CB	41.300
103	ARG+	HB3	2.110	108	LYS+	HG3	1.590	112	ASN	N	118.900
103	ARG+	HG2	1.740	108	LYS+	QE	2.930	112	ASN	ND2	127.700
103	ARG+	HG3	1.890	108	LYS+	C	177.900	113	SER	HN	7.250
103	ARG+	HD2	3.290	108	LYS+	CA	57.600	113	SER	HA	4.740
103	ARG+	HD3	3.360	108	LYS+	CB	34.700	113	SER	HB2	3.386
103	ARG+	C	181.100	108	LYS+	N	121.600	113	SER	HB3	4.446
103	ARG+	CA	59.600	109	THR	HN	9.130	113	SER	C	174.600
103	ARG+	CB	29.100	109	THR	HA	4.320	113	SER	CA	58.300
103	ARG+	CG	26.600	109	THR	HB	3.710	113	SER	CB	64.000
103	ARG+	CD	42.500	109	THR	QG2	1.030	113	SER	N	120.300
103	ARG+	N	121.800	109	THR	C	172.100	114	GLU-	HN	9.975
104	GLU-	HN	8.065	109	THR	CA	62.700	114	GLU-	HA	3.860

114	GLU-	HB2	1.810	119	LYS+	HD3	1.700	122	GLU-	HG2	2.260
114	GLU-	HB3	2.000	119	LYS+	QE	2.990	122	GLU-	HG3	2.445
114	GLU-	HG2	2.110	119	LYS+	C	177.300	122	GLU-	C	178.700
114	GLU-	HG3	2.220	119	LYS+	CA	57.500	122	GLU-	CA	59.900
114	GLU-	C	177.800	119	LYS+	CB	32.800	122	GLU-	CB	30.000
114	GLU-	CA	58.200	119	LYS+	N	120.100	122	GLU-	CG	36.300
114	GLU-	CB	29.700	120	TRP	HN	8.495	122	GLU-	N	122.900
114	GLU-	CG	35.700	120	TRP	HA	3.800	123	GLU-	HN	8.160
114	GLU-	N	106.800	120	TRP	QB	3.450	123	GLU-	HA	4.230
115	GLY	HN	8.550	120	TRP	HE1	9.804	123	GLU-	HB2	1.763
115	GLY	HA1	3.754	120	TRP	HD1	6.588	123	GLU-	HB3	2.055
115	GLY	HA2	4.080	120	TRP	HE3	7.618	123	GLU-	C	176.600
115	GLY	C	174.400	120	TRP	HZ2	7.033	123	GLU-	CA	56.500
115	GLY	CA	46.000	120	TRP	HH2	6.840	123	GLU-	CB	29.100
115	GLY	N	116.600	120	TRP	HZ3	7.033	123	GLU-	N	115.100
116	GLY	HN	8.010	120	TRP	C	178.000	124	GLY	HN	7.785
116	GLY	HA1	3.130	120	TRP	CA	61.600	124	GLY	HA1	3.710
116	GLY	HA2	3.440	120	TRP	CB	29.400	124	GLY	HA2	3.840
116	GLY	C	174.000	120	TRP	N	123.300	124	GLY	C	174.900
116	GLY	CA	45.500	120	TRP	NE1	129.400	124	GLY	CA	45.900
116	GLY	N	105.800	120	TRP	CD1	125.800	124	GLY	N	107.700
117	MET	HN	8.915	120	TRP	CZ2	112.900	125	LEU	HN	7.330
117	MET	HA	4.340	120	TRP	CH2	123.000	125	LEU	HA	3.860
117	MET	C	176.800	120	TRP	CZ3	121.600	125	LEU	QB	2.261
117	MET	CA	56.500	121	LEU	HN	8.555	125	LEU	HG	0.680
117	MET	CB	32.200	121	LEU	HA	4.280	125	LEU	QD1	-0.210
117	MET	N	126.400	121	LEU	HB2	1.500	125	LEU	QD2	0.120
118	ASP-	HN	9.085	121	LEU	HB3	2.140	125	LEU	C	174.400
118	ASP-	HA	4.400	121	LEU	HG	1.790	125	LEU	CA	53.100
118	ASP-	QB	2.910	121	LEU	QD2	1.006	125	LEU	CB	36.700
118	ASP-	C	179.500	121	LEU	QD1	1.025	125	LEU	CG	26.900
118	ASP-	CA	58.000	121	LEU	C	182.100	125	LEU	CD1	25.300
118	ASP-	CB	39.100	121	LEU	CA	57.100	125	LEU	CD2	23.000
118	ASP-	N	119.000	121	LEU	CB	42.100	125	LEU	N	122.300
119	LYS+	HN	7.440	121	LEU	CD2	22.500	126	PRO	HA	4.400
119	LYS+	HA	4.300	121	LEU	CD1	26.200	126	PRO	HB2	2.200
119	LYS+	HB2	1.810	121	LEU	N	114.400	126	PRO	HB3	2.430
119	LYS+	HB3	1.980	122	GLU-	HN	7.830	126	PRO	HG2	1.975
119	LYS+	QG	1.410	122	GLU-	HA	3.990	126	PRO	HG3	2.177
119	LYS+	HD2	1.630	122	GLU-	QB	2.260	126	PRO	HD2	2.501
126	PRO	HD3	3.283	127	SER	N	120.300	128	LEU	CG	26.900
126	PRO	C	177.700	128	LEU	HN	9.045	128	LEU	CD1	25.400
126	PRO	CA	64.500	128	LEU	HA	4.660	128	LEU	CD2	23.100
126	PRO	CG	27.800	128	LEU	HB2	1.320	128	LEU	N	121.400
126	PRO	CD	49.900	128	LEU	HB3	1.370	129	ASP-	HN	8.625
127	SER	HN	8.920	128	LEU	HG	1.180	129	ASP-	HA	4.380
127	SER	HA	5.140	128	LEU	QD1	0.640	129	ASP-	HB2	2.672
127	SER	QB	3.690	128	LEU	QD2	0.700	129	ASP-	HB3	2.780
127	SER	C	172.200	128	LEU	C	176.100	129	ASP-	C	175.800
127	SER	CA	57.600	128	LEU	CA	53.600	129	ASP-	CA	54.600
127	SER	CB	66.900	128	LEU	CB	44.700	129	ASP-	CB	39.900

129	ASP-	N	118.600
130	ARG+	HN	8.220
130	ARG+	HA	4.170
130	ARG+	HB2	1.630
130	ARG+	HB3	1.740
130	ARG+	QG	1.460
130	ARG+	HD2	3.070
130	ARG+	HD3	3.150
130	ARG+	C	176.300
130	ARG+	CA	56.100
130	ARG+	CB	30.000
130	ARG+	CG	26.600
130	ARG+	CD	43.100
130	ARG+	N	118.400
131	SER	HN	8.390
131	SER	HA	4.320
131	SER	QB	3.810
131	SER	C	174.500
131	SER	CA	58.700
131	SER	CB	64.000



## Appendix A.2

Missing <sup>1</sup>H chemical shifts of SUD protein

	Residue	missin shifts							
		g							
1	ALA	HA							
6	LYS+	QZ							
10	THR	HG1							
12	LYS+	QG	QZ						
16	LYS+	QZ							
19	LYS+	QG	QD	QE	QZ				
22	MET	QE							
26	SER	HG							
28	LYS+	QZ							
31	TYR	HH							
32	LYS+	QZ							
41	THR	HG1							
46	ARG+	QB	QG	QD	HE	QH1	QH2		
50	GLU-	QB	QG						
52	LYS+	QZ							
56	LYS+	QZ							
60	LYS+	QZ							
62	TYR	HH							
63	LYS+	QZ							
64	HIS	HD1							
65	MET	QE							
66	SER	HG							
67	ARG+	QB	QG	QD	HE	QH1	QH2		
69	LYS+	QB	QG	QD	QE	QZ			
71	GLU-	QB	QG						
72	PRO	QG	QD						
73	LEU	HG							
76	LYS+	QD	QZ						
77	SER	HG							
79	LEU	QB							
81	PRO	QG							
83	LYS+	QD	QE	QZ					
88	PHE	HZ							
89	CYS	QB	HG						
90	LYS+	HN	HA	QB	QG	QD	QE	QZ	
91	THR	HA	HB	QG2	HG1				
92	ALA	HN	HA	QB					
93	ALA	HN	HA	QB					
94	ARG+	HN	HA	QB	QG	QD	HE	QH1	QH2
95	ALA	HN							
97	LEU	HG							

100	LYS+	QD	QE	QZ
101	THR	HG1		
103	ARG+	HE	QH1	QH2
105	TYR	HH		
107	PHE	HZ		
108	LYS+	QD	QZ	
109	THR	HG1		
110	ILE	HG13		
111	TYR	HH		
113	SER	HG		
117	MET	QB	QG	QE
119	LYS+	QZ		
123	GLU-	QG		
127	SER	HG		
130	ARG+	HE	QH1	QH2
131	SER	HG		

73.9% assigned, 111 missing <sup>1</sup>H chemical shifts

### Appendix A.3

Hydrogen bond restraints (Å) of SUD protein

monomer	residue	atom	monomer	residue	atom	lower limit	upper limit
A	25	HN	A	112	O	1,8	2,2
A	43	HN	A	86	O	1,8	2,2
A	44	HN	A	63	O	1,8	2,2
A	63	HN	A	42	O	1,8	2,2
A	65	HN	A	44	O	1,8	2,2
A	85	HN	A	109	O	1,8	2,2
A	86	HN	A	41	O	1,8	2,2
A	87	HN	A	111	O	1,8	2,2
A	88	HN	A	43	O	1,8	2,2
A	111	HN	A	85	O	1,8	2,2
A	112	HN	A	23	O	1,8	2,2
A	23	HN	A	110	O	1,8	2,2
A	42	HN	A	61	O	1,8	2,2
A	41	HN	A	84	O	1,8	2,2
A	23	N	A	110	O	2,7	3,2
A	42	N	A	61	O	2,7	3,2
A	41	N	A	84	O	2,7	3,2
A	25	N	A	112	O	2,7	3,2
A	43	N	A	86	O	2,7	3,2
A	44	N	A	63	O	2,7	3,2
A	63	N	A	42	O	2,7	3,2
A	65	N	A	44	O	2,7	3,2
A	85	N	A	109	O	2,7	3,2
A	86	N	A	41	O	2,7	3,2
A	87	N	A	111	O	2,7	3,2
A	88	N	A	43	O	2,7	3,2
A	111	N	A	85	O	2,7	3,2
A	112	N	A	23	O	2,7	3,2
B	23	HN	B	110	O	1,8	2,2
B	42	HN	B	61	O	1,8	2,2
B	41	HN	B	84	O	1,8	2,2
B	23	N	B	110	O	2,7	3,2
B	42	N	B	61	O	2,7	3,2
B	41	N	B	84	O	2,7	3,2
B	25	HN	B	112	O	1,8	2,2
B	43	HN	B	86	O	1,8	2,2
B	44	HN	B	63	O	1,8	2,2
B	63	HN	B	42	O	1,8	2,2
B	65	HN	B	44	O	1,8	2,2

B	85	HN	B	109	O	1,8	2,2
B	86	HN	B	41	O	1,8	2,2
B	87	HN	B	111	O	1,8	2,2
B	88	HN	B	43	O	1,8	2,2
B	111	HN	B	85	O	1,8	2,2
B	112	HN	B	23	O	1,8	2,2
B	25	N	B	112	O	2,7	3,2
B	43	N	B	86	O	2,7	3,2
B	44	N	B	63	O	2,7	3,2
B	63	N	B	42	O	2,7	3,2
B	65	N	B	44	O	2,7	3,2
B	85	N	B	109	O	2,7	3,2
B	86	N	B	41	O	2,7	3,2
B	87	N	B	111	O	2,7	3,2
B	88	N	B	43	O	2,7	3,2
B	111	N	B	85	O	2,7	3,2
B	112	N	B	23	O	2,7	3,2

## Appendix A.4

Manually assigned NOEs between NH-NH. The NOE-derived distance restraints were set to 6 Å for upper limit and 4 Å for lower limit .

A 6	HN	A 7	HN	A 15	HN	A 16	HN	A 28	HN	A 32	HN
A 6	HN	A 8	HN	A 15	HN	A 17	HN	A 29	HN	A 26	HN
A 7	HN	A 6	HN	A 16	HN	A 12	HN	A 29	HN	A 28	HN
A 8	HN	A 10	HN	A 16	HN	A 13	HN	A 29	HN	A 30	HN
A 8	HN	A 6	HN	A 18	HN	A 19	HN	A 29	HN	A 31	HN
A 9	HN	A 10	HN	A 18	HN	A 20	HN	A 29	HN	A 32	HN
A 9	HN	A 11	HN	A 18	HN	A 21	HN	A 30	HN	A 28	HN
A 9	HN	A 12	HN	A 19	HN	A 16	HN	A 30	HN	A 29	HN
A 10	HN	A 11	HN	A 19	HN	A 17	HN	A 30	HN	A 31	HN
A 10	HN	A 12	HN	A 19	HN	A 18	HN	A 30	HN	A 32	HN
A 10	HN	A 13	HN	A 19	HN	A 20	HN	A 31	HN	A 28	HN
A 10	HN	A 8	HN	A 19	HN	A 21	HN	A 31	HN	A 29	HN
A 10	HN	A 9	HN	A 19	HN	A 22	HN	A 31	HN	A 30	HN
A 11	HN	A 10	HN	A 20	HN	A 17	HN	A 31	HN	A 32	HN
A 11	HN	A 12	HN	A 20	HN	A 18	HN	A 32	HN	A 28	HN
A 11	HN	A 13	HN	A 20	HN	A 19	HN	A 32	HN	A 29	HN
A 11	HN	A 14	HN	A 20	HN	A 21	HN	A 32	HN	A 30	HN
A 11	HN	A 15	HN	A 20	HN	A 22	HN	A 32	HN	A 31	HN
A 11	HN	A 8	HN	A 21	HN	A 18	HN	A 32	HN	A 33	HN
A 11	HN	A 9	HN	A 21	HN	A 19	HN	A 32	HN	A 35	HN
A 12	HN	A 10	HN	A 21	HN	A 20	HN	A 33	HN	A 32	HN
A 12	HN	A 11	HN	A 21	HN	A 22	HN	A 35	HN	A 32	HN
A 12	HN	A 13	HN	A 22	HN	A 19	HN	A 35	HN	A 36	HN
A 12	HN	A 14	HN	A 22	HN	A 20	HN	A 35	HN	A 37	HN
A 12	HN	A 15	HN	A 22	HN	A 21	HN	A 36	HN	A 35	HN
A 12	HN	A 16	HN	A 23	HN	A 110	HN	A 36	HN	A 37	HN
A 12	HN	A 9	HN	A 23	HN	A 112	HN	A 37	HN	A 35	HN
A 13	HN	A 10	HN	A 23	HN	A 24	HN	A 37	HN	A 36	HN
A 13	HN	A 11	HN	A 24	HN	A 112	HN	A 37	HN	A 39	HN
A 13	HN	A 12	HN	A 24	HN	A 23	HN	A 39	HN	A 37	HN
A 13	HN	A 14	HN	A 24	HN	A 25	HN	A 39	HN	A 40	HN
A 13	HN	A 15	HN	A 25	HN	A 113	HN	A 39	HN	A 41	HN
A 13	HN	A 16	HN	A 25	HN	A 24	HN	A 39	HN	A 61	HD2
A 14	HN	A 12	HN	A 25	HN	A 26	HN				2
A 14	HN	A 13	HN	A 26	HN	A 114	HN	A 40	HN	A 39	HN
A 14	HN	A 15	HN	A 26	HN	A 25	HN	A 40	HN	A 41	HN
A 14	HN	A 16	HN	A 26	HN	A 28	HN	A 40	HN	A 61	HD2
A 14	HN	A 17	HN	A 26	HN	A 29	HN				1
A 15	HN	A 11	HN	A 28	HN	A 26	HN	A 41	HN	A 39	HN
A 15	HN	A 12	HN	A 28	HN	A 29	HN	A 41	HN	A 40	HN
A 15	HN	A 13	HN	A 28	HN	A 30	HN	A 41	HN	A 61	HD2
A 15	HN	A 14	HN	A 28	HN	A 31	HN				1

A	41	HN	A	61	HD2	A	59	HN	A	120	HE1	A	74	HN	A	71	HN
					2	A	59	HN	A	58	HN	A	74	HN	A	73	HN
A	45	HN	A	46	HN	A	59	HN	A	60	HN	A	74	HN	A	75	HN
A	46	HN	A	45	HN	A	59	HN	A	61	HN	A	74	HN	A	76	HN
A	47	HN	A	49	HN	A	60	HN	A	59	HN	A	74	HN	A	77	HN
A	47	HN	A	50	HN	A	60	HN	A	61	HN	A	75	HN	A	73	HN
A	47	HN	A	51	HN	A	61	HD2	A	40	HN	A	75	HN	A	74	HN
A	49	HN	A	47	HN			1				A	75	HN	A	76	HN
A	49	HN	A	50	HN	A	61	HD2	A	41	HN	A	75	HN	A	77	HN
A	49	HN	A	51	HN			1				A	76	HN	A	74	HN
A	49	HN	A	52	HN	A	61	HD2	A	39	HN	A	76	HN	A	75	HN
A	49	HN	A	53	HN			2				A	76	HN	A	77	HN
A	50	HN	A	47	HN	A	61	HD2	A	41	HN	A	76	HN	A	79	HN
A	50	HN	A	49	HN			2				A	77	HN	A	74	HN
A	50	HN	A	51	HN	A	61	HN	A	59	HN	A	77	HN	A	75	HN
A	50	HN	A	52	HN	A	61	HN	A	60	HN	A	77	HN	A	76	HN
A	50	HN	A	53	HN	A	61	HN	A	62	HN	A	77	HN	A	79	HN
A	51	HN	A	47	HN	A	62	HN	A	61	HN	A	78	HN	A	79	HN
A	51	HN	A	49	HN	A	62	HN	A	63	HN	A	79	HN	A	76	HN
A	51	HN	A	50	HN	A	63	HN	A	62	HN	A	79	HN	A	77	HN
A	51	HN	A	52	HN	A	63	HN	A	64	HN	A	79	HN	A	80	HN
A	51	HN	A	53	HN	A	64	HN	A	63	HN	A	80	HN	A	82	HN
A	51	HN	A	54	HN	A	65	HN	A	64	HN	A	80	HN	A	83	HN
A	51	HN	A	55	HN	A	65	HN	A	66	HN	A	82	HN	A	80	HN
A	52	HN	A	49	HN	A	66	HN	A	65	HN	A	82	HN	A	83	HN
A	52	HN	A	50	HN	A	66	HN	A	67	HN	A	83	HN	A	80	HN
A	52	HN	A	51	HN	A	67	HN	A	66	HN	A	83	HN	A	82	HN
A	52	HN	A	53	HN	A	67	HN	A	68	HN	A	89	HN	A	117	HN
A	52	HN	A	54	HN	A	67	HN	A	69	HN	A	96	HN	A	100	HN
A	52	HN	A	55	HN	A	67	HN	A	70	HN	A	96	HN	A	97	HN
A	53	HN	A	49	HN	A	68	HN	A	67	HN	A	96	HN	A	98	HN
A	53	HN	A	50	HN	A	68	HN	A	69	HN	A	96	HN	A	99	HN
A	53	HN	A	51	HN	A	68	HN	A	70	HN	A	97	HN	A	100	HN
A	53	HN	A	52	HN	A	68	HN	A	71	HN	A	97	HN	A	96	HN
A	53	HN	A	54	HN	A	69	HN	A	67	HN	A	97	HN	A	98	HN
A	53	HN	A	55	HN	A	69	HN	A	68	HN	A	97	HN	A	99	HN
A	54	HN	A	51	HN	A	69	HN	A	70	HN	A	98	HN	A	100	HN
A	54	HN	A	52	HN	A	69	HN	A	71	HN	A	98	HN	A	101	HN
A	54	HN	A	53	HN	A	70	HN	A	67	HN	A	98	HN	A	96	HN
A	54	HN	A	55	HN	A	70	HN	A	68	HN	A	98	HN	A	97	HN
A	55	HN	A	51	HN	A	70	HN	A	69	HN	A	98	HN	A	99	HN
A	55	HN	A	52	HN	A	70	HN	A	71	HN	A	99	HN	A	100	HN
A	55	HN	A	53	HN	A	71	HN	A	68	HN	A	99	HN	A	101	HN
A	55	HN	A	54	HN	A	71	HN	A	69	HN	A	99	HN	A	96	HN
A	55	HN	A	56	HN	A	71	HN	A	70	HN	A	99	HN	A	97	HN
A	56	HN	A	55	HN	A	71	HN	A	73	HN	A	99	HN	A	98	HN
A	56	HN	A	58	HN	A	71	HN	A	74	HN	A	100	HN	A	101	HN
A	58	HN	A	127	HN	A	73	HN	A	71	HN	A	100	HN	A	102	HN
A	58	HN	A	56	HN	A	73	HN	A	74	HN	A	100	HN	A	103	HN
A	58	HN	A	59	HN	A	73	HN	A	75	HN	A	100	HN	A	97	HN

A 100	HN	A 98	HN	A 114	HN	A 115	HN	A 125	HN	A 122	HN
A 100	HN	A 99	HN	A 114	HN	A 116	HN	A 125	HN	A 123	HN
A 101	HN	A 100	HN	A 114	HN	A 26	HN	A 125	HN	A 124	HN
A 101	HN	A 102	HN	A 115	HN	A 114	HN	A 127	HN	A 120	HE1
A 101	HN	A 103	HN	A 115	HN	A 116	HN	A 127	HN	A 128	HN
A 101	HN	A 98	HN	A 116	HN	A 114	HN	A 127	HN	A 58	HN
A 101	HN	A 99	HN	A 116	HN	A 115	HN	A 128	HN	A 120	HE1
A 102	HN	A 100	HN	A 117	HN	A 118	HN	A 128	HN	A 127	HN
A 102	HN	A 101	HN	A 117	HN	A 119	HN	B 6	HN	B 7	HN
A 102	HN	A 103	HN	A 117	HN	A 89	HN	B 6	HN	B 8	HN
A 102	HN	A 104	HN	A 118	HN	A 117	HN	B 7	HN	B 6	HN
A 103	HN	A 100	HN	A 118	HN	A 119	HN	B 8	HN	B 10	HN
A 103	HN	A 101	HN	A 118	HN	A 120	HN	B 8	HN	B 6	HN
A 103	HN	A 102	HN	A 118	HN	A 121	HN	B 9	HN	B 10	HN
A 103	HN	A 104	HN	A 118	HN	A 122	HN	B 9	HN	B 11	HN
A 103	HN	A 107	HN	A 119	HN	A 117	HN	B 9	HN	B 12	HN
A 104	HN	A 103	HN	A 119	HN	A 118	HN	B 10	HN	B 11	HN
A 104	HN	A 105	HN	A 119	HN	A 120	HN	B 10	HN	B 12	HN
A 104	HN	A 106	HN	A 119	HN	A 121	HN	B 10	HN	B 13	HN
A 104	HN	A 107	HN	A 119	HN	A 122	HN	B 10	HN	B 8	HN
A 105	HN	A 104	HN	A 120	HE1	A 127	HN	B 10	HN	B 9	HN
A 105	HN	A 106	HN	A 120	HE1	A 128	HN	B 11	HN	B 10	HN
A 105	HN	A 107	HN	A 120	HE1	A 59	HN	B 11	HN	B 12	HN
A 106	HN	A 104	HN	A 120	HN	A 118	HN	B 11	HN	B 13	HN
A 106	HN	A 105	HN	A 120	HN	A 119	HN	B 11	HN	B 14	HN
A 106	HN	A 107	HN	A 120	HN	A 121	HN	B 11	HN	B 15	HN
A 107	HN	A 103	HN	A 120	HN	A 122	HN	B 11	HN	B 8	HN
A 107	HN	A 104	HN	A 121	HN	A 118	HN	B 11	HN	B 9	HN
A 107	HN	A 105	HN	A 121	HN	A 119	HN	B 12	HN	B 10	HN
A 107	HN	A 106	HN	A 121	HN	A 120	HN	B 12	HN	B 11	HN
A 108	HN	A 109	HN	A 121	HN	A 122	HN	B 12	HN	B 13	HN
A 109	HN	A 108	HN	A 121	HN	A 123	HN	B 12	HN	B 14	HN
A 109	HN	A 110	HN	A 121	HN	A 124	HN	B 12	HN	B 15	HN
A 110	HN	A 109	HN	A 121	HN	A 125	HN	B 12	HN	B 16	HN
A 110	HN	A 23	HN	A 122	HN	A 118	HN	B 12	HN	B 9	HN
A 112	HD2	A 96	HN	A 122	HN	A 119	HN	B 13	HN	B 10	HN
	1			A 122	HN	A 120	HN	B 13	HN	B 11	HN
A 112	HD2	A 97	HN	A 122	HN	A 121	HN	B 13	HN	B 12	HN
	1			A 122	HN	A 123	HN	B 13	HN	B 14	HN
A 112	HD2	A 97	HN	A 122	HN	A 124	HN	B 13	HN	B 15	HN
	2			A 122	HN	A 125	HN	B 13	HN	B 16	HN
A 112	HN	A 113	HN	A 123	HN	A 121	HN	B 14	HN	B 12	HN
A 112	HN	A 114	HN	A 123	HN	A 122	HN	B 14	HN	B 13	HN
A 112	HN	A 23	HN	A 123	HN	A 124	HN	B 14	HN	B 15	HN
A 112	HN	A 24	HN	A 123	HN	A 125	HN	B 14	HN	B 16	HN
A 113	HN	A 112	HN	A 124	HN	A 121	HN	B 14	HN	B 17	HN
A 113	HN	A 114	HN	A 124	HN	A 122	HN	B 15	HN	B 11	HN
A 113	HN	A 25	HN	A 124	HN	A 123	HN	B 15	HN	B 12	HN
A 114	HN	A 112	HN	A 124	HN	A 125	HN	B 15	HN	B 13	HN
A 114	HN	A 113	HN	A 125	HN	A 121	HN	B 15	HN	B 14	HN

B 15	HN	B 16	HN	B 30	HN	B 31	HN	B 50	HN	B 53	HN
B 15	HN	B 17	HN	B 30	HN	B 32	HN	B 51	HN	B 47	HN
B 16	HN	B 12	HN	B 31	HN	B 28	HN	B 51	HN	B 49	HN
B 16	HN	B 13	HN	B 31	HN	B 29	HN	B 51	HN	B 50	HN
B 18	HN	B 19	HN	B 31	HN	B 30	HN	B 51	HN	B 52	HN
B 18	HN	B 20	HN	B 31	HN	B 32	HN	B 51	HN	B 53	HN
B 18	HN	B 21	HN	B 32	HN	B 28	HN	B 51	HN	B 54	HN
B 19	HN	B 16	HN	B 32	HN	B 29	HN	B 51	HN	B 55	HN
B 19	HN	B 17	HN	B 32	HN	B 30	HN	B 52	HN	B 49	HN
B 19	HN	B 18	HN	B 32	HN	B 31	HN	B 52	HN	B 50	HN
B 19	HN	B 20	HN	B 32	HN	B 33	HN	B 52	HN	B 51	HN
B 19	HN	B 21	HN	B 32	HN	B 35	HN	B 52	HN	B 53	HN
B 19	HN	B 22	HN	B 33	HN	B 32	HN	B 52	HN	B 54	HN
B 20	HN	B 17	HN	B 35	HN	B 32	HN	B 52	HN	B 55	HN
B 20	HN	B 18	HN	B 35	HN	B 36	HN	B 53	HN	B 49	HN
B 20	HN	B 19	HN	B 35	HN	B 37	HN	B 53	HN	B 50	HN
B 20	HN	B 21	HN	B 36	HN	B 35	HN	B 53	HN	B 51	HN
B 20	HN	B 22	HN	B 36	HN	B 37	HN	B 53	HN	B 52	HN
B 21	HN	B 18	HN	B 37	HN	B 35	HN	B 53	HN	B 54	HN
B 21	HN	B 19	HN	B 37	HN	B 36	HN	B 53	HN	B 55	HN
B 21	HN	B 20	HN	B 37	HN	B 39	HN	B 54	HN	B 51	HN
B 21	HN	B 22	HN	B 39	HN	B 37	HN	B 54	HN	B 52	HN
B 22	HN	B 19	HN	B 39	HN	B 40	HN	B 54	HN	B 53	HN
B 22	HN	B 20	HN	B 39	HN	B 41	HN	B 54	HN	B 55	HN
B 22	HN	B 21	HN	B 39	HN	B 61	HD2	B 55	HN	B 51	HN
B 23	HN	B 110	HN				2	B 55	HN	B 52	HN
B 23	HN	B 112	HN	B 40	HN	B 39	HN	B 55	HN	B 53	HN
B 23	HN	B 24	HN	B 40	HN	B 41	HN	B 55	HN	B 54	HN
B 24	HN	B 112	HN	B 40	HN	B 61	HD2	B 55	HN	B 56	HN
B 24	HN	B 23	HN				1	B 56	HN	B 55	HN
B 24	HN	B 25	HN	B 41	HN	B 39	HN	B 56	HN	B 58	HN
B 25	HN	B 113	HN	B 41	HN	B 40	HN	B 58	HN	B 127	HN
B 25	HN	B 24	HN	B 41	HN	B 61	HD2	B 58	HN	B 56	HN
B 25	HN	B 26	HN				1	B 58	HN	B 59	HN
B 26	HN	B 114	HN	B 41	HN	B 61	HD2	B 59	HN	B 120	HE1
B 26	HN	B 25	HN				2	B 59	HN	B 58	HN
B 26	HN	B 28	HN	B 45	HN	B 46	HN	B 59	HN	B 60	HN
B 26	HN	B 29	HN	B 46	HN	B 45	HN	B 59	HN	B 61	HN
B 28	HN	B 26	HN	B 47	HN	B 49	HN	B 60	HN	B 59	HN
B 28	HN	B 29	HN	B 47	HN	B 50	HN	B 60	HN	B 61	HN
B 28	HN	B 30	HN	B 47	HN	B 51	HN	B 61	HD2	B 40	HN
B 28	HN	B 31	HN	B 49	HN	B 47	HN		1		
B 28	HN	B 32	HN	B 49	HN	B 50	HN	B 61	HD2	B 41	HN
B 29	HN	B 26	HN	B 49	HN	B 51	HN		1		
B 29	HN	B 28	HN	B 49	HN	B 52	HN	B 61	HD2	B 39	HN
B 29	HN	B 30	HN	B 49	HN	B 53	HN		2		
B 29	HN	B 31	HN	B 50	HN	B 47	HN	B 61	HD2	B 41	HN
B 29	HN	B 32	HN	B 50	HN	B 49	HN		2		
B 30	HN	B 28	HN	B 50	HN	B 51	HN	B 61	HN	B 59	HN
B 30	HN	B 29	HN	B 50	HN	B 52	HN	B 61	HN	B 60	HN



B 61	HN	B 62	HN	B 77	HN	B 79	HN	B 104	HN	B 103	HN
B 62	HN	B 61	HN	B 78	HN	B 79	HN	B 104	HN	B 105	HN
B 62	HN	B 63	HN	B 79	HN	B 76	HN	B 104	HN	B 106	HN
B 63	HN	B 62	HN	B 79	HN	B 77	HN	B 104	HN	B 107	HN
B 63	HN	B 64	HN	B 79	HN	B 80	HN	B 105	HN	B 104	HN
B 64	HN	B 63	HN	B 80	HN	B 82	HN	B 105	HN	B 106	HN
B 65	HN	B 64	HN	B 80	HN	B 83	HN	B 105	HN	B 107	HN
B 65	HN	B 66	HN	B 82	HN	B 80	HN	B 106	HN	B 104	HN
B 66	HN	B 65	HN	B 82	HN	B 83	HN	B 106	HN	B 105	HN
B 66	HN	B 67	HN	B 83	HN	B 80	HN	B 106	HN	B 107	HN
B 67	HN	B 66	HN	B 83	HN	B 82	HN	B 107	HN	B 103	HN
B 67	HN	B 68	HN	B 89	HN	B 117	HN	B 107	HN	B 104	HN
B 67	HN	B 69	HN	B 96	HN	B 100	HN	B 107	HN	B 105	HN
B 67	HN	B 70	HN	B 96	HN	B 97	HN	B 107	HN	B 106	HN
B 68	HN	B 67	HN	B 96	HN	B 98	HN	B 108	HN	B 109	HN
B 68	HN	B 69	HN	B 96	HN	B 99	HN	B 109	HN	B 108	HN
B 68	HN	B 70	HN	B 97	HN	B 100	HN	B 109	HN	B 110	HN
B 68	HN	B 71	HN	B 97	HN	B 96	HN	B 110	HN	B 109	HN
B 69	HN	B 67	HN	B 97	HN	B 98	HN	B 110	HN	B 23	HN
B 69	HN	B 68	HN	B 97	HN	B 99	HN	B 112	HD2	B 96	HN
B 69	HN	B 70	HN	B 98	HN	B 100	HN		1		
B 69	HN	B 71	HN	B 98	HN	B 101	HN	B 112	HD2	B 97	HN
B 70	HN	B 67	HN	B 98	HN	B 96	HN		1		
B 70	HN	B 68	HN	B 98	HN	B 97	HN	B 112	HD2	B 97	HN
B 70	HN	B 69	HN	B 98	HN	B 99	HN		2		
B 70	HN	B 71	HN	B 99	HN	B 100	HN	B 112	HN	B 113	HN
B 71	HN	B 68	HN	B 99	HN	B 101	HN	B 112	HN	B 114	HN
B 71	HN	B 69	HN	B 99	HN	B 96	HN	B 112	HN	B 23	HN
B 71	HN	B 70	HN	B 99	HN	B 97	HN	B 112	HN	B 24	HN
B 71	HN	B 73	HN	B 99	HN	B 98	HN	B 113	HN	B 112	HN
B 71	HN	B 74	HN	B 100	HN	B 101	HN	B 113	HN	B 114	HN
B 73	HN	B 71	HN	B 100	HN	B 102	HN	B 113	HN	B 25	HN
B 73	HN	B 74	HN	B 100	HN	B 103	HN	B 114	HN	B 112	HN
B 73	HN	B 75	HN	B 100	HN	B 97	HN	B 114	HN	B 113	HN
B 74	HN	B 71	HN	B 100	HN	B 98	HN	B 114	HN	B 115	HN
B 74	HN	B 73	HN	B 100	HN	B 99	HN	B 114	HN	B 116	HN
B 74	HN	B 75	HN	B 101	HN	B 100	HN	B 114	HN	B 26	HN
B 74	HN	B 76	HN	B 101	HN	B 102	HN	B 115	HN	B 114	HN
B 74	HN	B 77	HN	B 101	HN	B 103	HN	B 115	HN	B 116	HN
B 75	HN	B 73	HN	B 101	HN	B 98	HN	B 116	HN	B 114	HN
B 75	HN	B 74	HN	B 101	HN	B 99	HN	B 116	HN	B 115	HN
B 75	HN	B 76	HN	B 102	HN	B 100	HN	B 117	HN	B 118	HN
B 75	HN	B 77	HN	B 102	HN	B 101	HN	B 117	HN	B 119	HN
B 76	HN	B 74	HN	B 102	HN	B 103	HN	B 117	HN	B 89	HN
B 76	HN	B 75	HN	B 102	HN	B 104	HN	B 118	HN	B 117	HN
B 76	HN	B 77	HN	B 103	HN	B 100	HN	B 118	HN	B 119	HN
B 76	HN	B 79	HN	B 103	HN	B 101	HN	B 118	HN	B 120	HN
B 77	HN	B 74	HN	B 103	HN	B 102	HN	B 118	HN	B 121	HN
B 77	HN	B 75	HN	B 103	HN	B 104	HN	B 118	HN	B 122	HN
B 77	HN	B 76	HN	B 103	HN	B 107	HN	B 119	HN	B 117	HN

B 119 HN B 118 HN  
B 119 HN B 120 HN  
B 119 HN B 121 HN  
B 119 HN B 122 HN  
B 120 HE1 B 127 HN  
B 120 HE1 B 128 HN  
B 120 HE1 B 59 HN  
B 120 HN B 118 HN  
B 120 HN B 119 HN  
B 120 HN B 121 HN  
B 120 HN B 122 HN  
B 121 HN B 118 HN  
B 121 HN B 119 HN  
B 121 HN B 120 HN  
B 121 HN B 122 HN  
B 121 HN B 123 HN  
B 121 HN B 124 HN  
B 121 HN B 125 HN  
B 122 HN B 118 HN  
B 122 HN B 119 HN  
B 122 HN B 120 HN  
B 122 HN B 121 HN  
B 122 HN B 123 HN  
B 122 HN B 124 HN  
B 122 HN B 125 HN  
B 123 HN B 121 HN  
B 123 HN B 122 HN  
B 123 HN B 124 HN  
B 123 HN B 125 HN  
B 124 HN B 121 HN  
B 124 HN B 122 HN  
B 124 HN B 123 HN  
B 124 HN B 125 HN  
B 125 HN B 121 HN  
B 125 HN B 122 HN  
B 125 HN B 123 HN  
B 125 HN B 124 HN  
B 127 HN B 120 HE1  
B 127 HN B 128 HN  
B 127 HN B 58 HN  
B 128 HN B 120 HE1  
B 128 HN B 127 HN

## Appendix A.5

Inter-monomer distance restraints (Å) of SUD protein

monomer	residue	atom	monomer	residue	atom	lower limit	upper limit
A	7	hd%	B	75	hb%	0	6
A	8	ha	B	75	hb%	0	6
A	8	hb%	B	75	hb%	0	6
A	10	hg2%	B	105	he%	0	6
A	11	hn	B	105	he%	0	6
A	12	hn	B	105	he%	0	6
A	8	hn	B	75	hb%	0	6
A	8	hn	B	75	hb%	0	6
B	7	hd%	A	75	hb%	0	6
B	8	ha	A	75	hb%	0	6
B	8	hb%	A	75	hb%	0	6
B	10	hg2%	A	105	he%	0	6
B	11	hn	A	105	he%	0	6
B	12	hn	A	105	he%	0	6
B	8	hn	A	75	hb%	0	6
B	8	hn	A	75	hb%	0	6

## Appendix A.6

### Manually stereospecific assignments of Val and Leu residues of SUD protein

atoms	stereo	QG1 of Val	15	23	45	59	85	86	87						
atoms	stereo	QD1 of Leu	25	33	34	42	51	70	74	79	97	102	121	125	128

## Appendix A.7

### Dihedral angle restraints (degree) of SUD protein

3	PHI	-100,8	-77,4	29	PSI	-46,8	-35,7
3	PSI	-8,8	17,6	30	PHI	-69,1	-58,8
5	PHI	-69,8	-56,3	30	PSI	-45,8	-31,7
5	PSI	-52,2	-39,9	31	PHI	-66,5	-51,5
6	PHI	-69,6	-54,9	31	PSI	-49,9	-35,4
6	PSI	-49,7	-34,9	32	PHI	-67,2	-55,4
7	PHI	-79	-55	32	PSI	-48,1	-38,3
7	PSI	-48,2	-31,2	33	PHI	-68,9	-59,2
8	PHI	-67	-58,9	33	PSI	-48	-34,9
8	PSI	-50,2	-36,1	34	PHI	-70,4	-55,9
9	PHI	-67,6	-58	34	PSI	-47,9	-33,2
9	PSI	-50,1	-35,2	35	PHI	-68	-52,9
10	PHI	-69,6	-60,9	35	PSI	-45,9	-26,9
10	PSI	-48,1	-30,4	36	PHI	-89,6	-59,4
11	PHI	-65,4	-57,1	36	PSI	-34,9	-4
11	PSI	-43,9	-34,4	37	PHI	-143,1	-90,1
12	PHI	-66,7	-62,7	37	PSI	98,4	158
12	PSI	-49,4	-35,6	40	PHI	-112	-65,2
13	PHI	-69,4	-59,9	40	PSI	103,5	149,8
13	PSI	-44,4	-35	41	PHI	-113,2	-95,8
14	PHI	-67,4	-60,6	41	PSI	113,6	134,3
14	PSI	-44,5	-35,8	42	PHI	-116,6	-89
15	PHI	-69,7	-60,4	42	PSI	116,6	131,2
15	PSI	-49,5	-39,8	43	PHI	-126,4	-96,3
16	PHI	-64,7	-52,4	43	PSI	110,9	137,9
16	PSI	-49,2	-35,5	44	PHI	-129	-82,3
17	PHI	-65,4	-55,1	44	PSI	119	155,5
17	PSI	-51,1	-34,9	45	PHI	-115,3	-83,8
18	PHI	-68,3	-57,7	45	PSI	118,9	154,5
18	PSI	-47,3	-38,1	46	PHI	-158,4	-79,7
19	PHI	-68,1	-58	46	PSI	115,6	171,3
19	PSI	-47,9	-33,3	48	PHI	-70,6	-52,8
20	PHI	-88,1	-51,7	48	PSI	-44,5	-28,2
20	PSI	-47,1	-5,6	49	PHI	-70,3	-55,1
22	PHI	-136,8	-82,7	49	PSI	-49,8	-38,4
22	PSI	98,6	159,2	50	PHI	-69,3	-61,9
23	PHI	-117,6	-81,9	50	PSI	-47,1	-35,6
23	PSI	106,7	128,6	51	PHI	-68,3	-60
24	PHI	-119,5	-83,9	51	PSI	-42,8	-37,6
24	PSI	114,4	141,4	52	PHI	-71	-55,6
25	PHI	-144,9	-123,3	52	PSI	-45,2	-33,8
25	PSI	135,3	172	53	PHI	-82,7	-54,2
26	PHI	-138,1	-83,1	53	PSI	-38,8	-21
26	PSI	97,6	159	54	PHI	-108,3	-80,7
28	PHI	-66,6	-53,6	54	PSI	-16,8	14,6
28	PSI	-50,5	-37,8	56	PHI	-150,8	-83,9
29	PHI	-70,7	-56,1	56	PSI	136,9	167,5

59	PHI	-146,5	-98,8	62	PSI	114,1	134,7
59	PSI	140,3	168	63	PHI	-139,3	-97,6
61	PHI	-117,8	-79	63	PSI	122,5	149
61	PSI	87,6	142,5	64	PHI	-111,6	-81,7
62	PHI	-118,7	-81,4	64	PSI	121,7	140,6
65	PHI	-127,5	-81,4	111	PHI	-124,5	-103,3
65	PSI	112,7	150,9	111	PSI	126,4	154,5
68	PHI	-86,5	-61,6	112	PHI	-140,2	-106,9
68	PSI	-30	-2,2	112	PSI	125,3	151,8
71	PHI	-65,4	-52,9	113	PHI	-135,2	-100,3
71	PSI	-52,6	-25	113	PSI	110,4	132,5
72	PHI	-78	-54,1	117	PHI	-72,1	-57,9
72	PSI	-45,2	-27,5	117	PSI	-47,3	-31,4
74	PHI	-69,4	-55,5	118	PHI	-66,1	-57,6
74	PSI	-46,5	-34,8	118	PSI	-47,2	-31,3
75	PHI	-69,8	-55,6	119	PHI	-69,2	-60,4
75	PSI	-38,7	-17,8	119	PSI	-47,5	-38,2
80	PHI	-121,4	-93,8	120	PHI	-70,8	-56
80	PSI	113,3	162,4	120	PSI	-48,8	-40
85	PHI	-151,9	-127,8	121	PHI	-68,2	-58,1
85	PSI	142,4	164,8	121	PSI	-44,9	-37,6
93	PHI	-69,5	-60,1	122	PHI	-68	-54,5
93	PSI	-47,2	-34,6	122	PSI	-45,2	-37,4
95	PHI	-71,1	-60,2	123	PHI	-110,9	-82,2
95	PSI	-48,3	-18,5	123	PSI	-8,7	16,5
96	PHI	-69	-57,8	125	PHI	-130,1	-72,6
96	PSI	-44,3	-34,6	125	PSI	106,4	156,3
97	PHI	-70,6	-56,9	128	PHI	-144,7	-89,5
97	PSI	-52,5	-32,8	128	PSI	128,4	180,5
98	PHI	-67,8	-54,9				
98	PSI	-51,5	-37,3				
100	PHI	-69,6	-59,9				
100	PSI	-50,6	-33,8				
101	PHI	-67,5	-59,8				
101	PSI	-49,4	-41				
102	PHI	-67,1	-56				
102	PSI	-47,3	-33,4				
103	PHI	-68,3	-57				
103	PSI	-42,5	-32,7				
104	PHI	-72,2	-60,9				
104	PSI	-46,3	-22,7				
105	PHI	-96,5	-64,7				
105	PSI	-34,5	11,3				
109	PHI	-120,1	-87,9				
109	PSI	112,6	137,8				
110	PHI	-119,9	-93				
110	PSI	119	138,5				

## Appendix A.8

### Residual dipolar coupling restraints (Hz) of SUD protein

monomer	residue	atom	monomer	residue	atom	coupling
A	4	N	A	4	HN	-6,805
A	5	N	A	5	HN	-17,285
A	6	N	A	6	HN	-22,47
A	8	N	A	8	HN	-11,15
A	9	N	A	9	HN	-9,145
A	10	N	A	10	HN	-20,685
A	11	N	A	11	HN	-7,945
A	13	N	A	13	HN	-28,57
A	14	N	A	14	HN	-13,97
A	15	N	A	15	HN	-10,43
A	19	N	A	19	HN	2,355
A	20	N	A	20	HN	-33,875
A	21	N	A	21	HN	-12,18
A	22	N	A	22	HN	6,88
A	25	N	A	25	HN	-16,885
A	26	N	A	26	HN	-18,025
A	28	N	A	28	HN	10,15
A	29	N	A	29	HN	-7,875
A	30	N	A	30	HN	4,345
A	31	N	A	31	HN	6,955
A	34	N	A	34	HN	8,355
A	35	N	A	35	HN	8,4
A	36	N	A	36	HN	3,375
A	39	N	A	39	HN	-18,62
A	40	N	A	40	HN	-22,57
A	43	N	A	43	HN	14,83
A	45	N	A	45	HN	-2,48
A	47	N	A	47	HN	7,83
A	49	N	A	49	HN	4,01
A	50	N	A	50	HN	12,89
A	51	N	A	51	HN	-13,115
A	52	N	A	52	HN	-19,89
A	53	N	A	53	HN	2,09
A	54	N	A	54	HN	0,145
A	55	N	A	55	HN	-31,88
A	56	N	A	56	HN	6,06
A	59	N	A	59	HN	-27,135
A	60	N	A	60	HN	-15,815
A	61	N	A	61	HN	-1,015
A	62	N	A	62	HN	19,28
A	63	N	A	63	HN	15,63
A	65	N	A	65	HN	2,09

A	66	N	A	66	HN	12,82
A	68	N	A	68	HN	20,435
A	70	N	A	70	HN	6,47
A	71	N	A	71	HN	-4,31
A	73	N	A	73	HN	6,655
A	75	N	A	75	HN	-25,55
A	76	N	A	76	HN	-7,275
A	77	N	A	77	HN	8,765
A	78	N	A	78	HN	-13,205
A	80	N	A	80	HN	-6,645
A	82	N	A	82	HN	13,35
A	87	N	A	87	HN	14,86
A	89	N	A	89	HN	-18,18
A	96	N	A	96	HN	7,87
A	97	N	A	97	HN	19,335
A	98	N	A	98	HN	15,315
A	99	N	A	99	HN	8,795
A	100	N	A	100	HN	9,545
A	105	N	A	105	HN	8,05
A	106	N	A	106	HN	6,095
A	109	N	A	109	HN	12,625
A	110	N	A	110	HN	24,28
A	112	N	A	112	HN	-0,35
A	113	N	A	113	HN	-16,37
A	114	N	A	114	HN	-24,17
A	115	N	A	115	HN	8,69
A	116	N	A	116	HN	13,88
A	118	N	A	118	HN	-3,67
A	119	N	A	119	HN	3,285
A	120	N	A	120	HN	-27,98
A	121	N	A	121	HN	-28,26
A	122	N	A	122	HN	-6,155
A	123	N	A	123	HN	-10,4
A	125	N	A	125	HN	-12,125
A	127	N	A	127	HN	12,205
A	128	N	A	128	HN	9,41
A	130	N	A	130	HN	-15,655
B	4	N	B	4	HN	-6,805
B	5	N	B	5	HN	-17,285
B	6	N	B	6	HN	-22,47
B	8	N	B	8	HN	-11,15
B	9	N	B	9	HN	-9,145
B	10	N	B	10	HN	-20,685
B	11	N	B	11	HN	-7,945
B	13	N	B	13	HN	-28,57
B	14	N	B	14	HN	-13,97
B	15	N	B	15	HN	-10,43
B	19	N	B	19	HN	2,355
B	20	N	B	20	HN	-33,875
B	21	N	B	21	HN	-12,18
B	22	N	B	22	HN	6,88



B	25	N	B	25	HN	-16,885
B	26	N	B	26	HN	-18,025
B	28	N	B	28	HN	10,15
B	29	N	B	29	HN	-7,875
B	30	N	B	30	HN	4,345
B	31	N	B	31	HN	6,955
B	34	N	B	34	HN	8,355
B	35	N	B	35	HN	8,4
B	36	N	B	36	HN	3,375
B	39	N	B	39	HN	-18,62
B	40	N	B	40	HN	-22,57
B	43	N	B	43	HN	14,83
B	45	N	B	45	HN	-2,48
B	47	N	B	47	HN	7,83
B	49	N	B	49	HN	4,01
B	50	N	B	50	HN	12,89
B	51	N	B	51	HN	-13,115
B	52	N	B	52	HN	-19,89
B	53	N	B	53	HN	2,09
B	54	N	B	54	HN	0,145
B	55	N	B	55	HN	-31,88
B	56	N	B	56	HN	6,06
B	59	N	B	59	HN	-27,135
B	60	N	B	60	HN	-15,815
B	61	N	B	61	HN	-1,015
B	62	N	B	62	HN	19,28
B	63	N	B	63	HN	15,63
B	65	N	B	65	HN	2,09
B	66	N	B	66	HN	12,82
B	68	N	B	68	HN	20,435
B	70	N	B	70	HN	6,47
B	71	N	B	71	HN	-4,31
B	73	N	B	73	HN	6,655
B	75	N	B	75	HN	-25,55
B	76	N	B	76	HN	-7,275
B	77	N	B	77	HN	8,765
B	78	N	B	78	HN	-13,205
B	80	N	B	80	HN	-6,645
B	82	N	B	82	HN	13,35
B	87	N	B	87	HN	14,86
B	89	N	B	89	HN	-18,18
B	96	N	B	96	HN	7,87
B	97	N	B	97	HN	19,335
B	98	N	B	98	HN	15,315
B	99	N	B	99	HN	8,795
B	100	N	B	100	HN	9,545
B	105	N	B	105	HN	8,05
B	106	N	B	106	HN	6,095
B	109	N	B	109	HN	12,625
B	110	N	B	110	HN	24,28
B	112	N	B	112	HN	-0,35

B	113	N	B	113	HN	-16,37
B	114	N	B	114	HN	-24,17
B	115	N	B	115	HN	8,69
B	116	N	B	116	HN	13,88
B	118	N	B	118	HN	-3,67
B	119	N	B	119	HN	3,285
B	120	N	B	120	HN	-27,98
B	121	N	B	121	HN	-28,26
B	122	N	B	122	HN	-6,155
B	123	N	B	123	HN	-10,4
B	125	N	B	125	HN	-12,125
B	127	N	B	127	HN	12,205
B	128	N	B	128	HN	9,41
B	130	N	B	130	HN	-15,655

## Lebenslauf

Lin, Yi-Jan

geboren am 20. September 1970 in Kaohsiung, Taiwan

- |                                  |   |
|----------------------------------|---|
| 1989                             | Abschluss der "Taiwan Provincial Tainan First Senior High School"   |
| 09.1990-06.1994                  | Beginn des Studiums der Chemie an der Kaohsiung Medical College in Taiwan   |
| 06.1994                          | Bachelor of Science in Chemistry  |
| 08.1994-06.1996                  | Wehrdienst in Taiwan  |
| 10.1996-03.1997                  | Deutschkurs an der Universität Bielefeld  |
| 04.1997                          | Erfolgreiche "Prüfung zum Nachweis Deutscher Sprachkenntnisse" an der TH Aachen   |
| 04.1997-09.1998                  | Biochemiestudium an der Medizinische Hochschule Hannover und Universität Hannover   |
| 10.1998                          | Beginn der vorliegenden Dissertation unter Anleitung von Herrn Prof. Dr. Rüterjans an der J. W. Goethe Universität in Frankfurt am Main   |
| August 20-25, 2000               | Teilnahme an der "XIX International Conference on Magnetic Resonance in Biological System" (ICMRBS) in Florenz, Italien und Posterpräsentation                                    |
| 12.2000                          | Assistent des NMR-Praktikums (Resonanzzuordnung)  |
| 09.2001                          | Teilnahme an dem EMBO Kurs: "Structure determination of biological macromolecules by solution NMR" an der European Molecular Biology Laboratory (EMBL) in Heidelberg, Deutschland |
| 11.2001                          | Teilnahme an dem "5 <sup>th</sup> User Meeting of the European Large-Scale Facilities for NMR" in Frankfurt, Deutschland  |
| 12.2001                          | Assistent des NMR-Praktikums (Resonanzzuordnung)  |
| August 25-30, 2002               | Teilnahme an der "XX International Conference on Magnetic Resonance in Biological System"(ICMRBS) in Toronto, Kanada und Posterpräsentation                                       |
| September 17-<br>Oktober 4, 2002 | Zusatzausbildung durch Herrn Dr. Peter Güntert in Riken, Japan  |
| Publikationen                    | Journal of Biomolecular NMR, 18: 285-286, 2000<br>Journal of Biomolecular NMR, 18: 337-346, 2000  |